Paleoclimatic variability and extreme events since the last deglaciation in Peru : sedimentary record and model simulations

Marco Yseki

Sorbonne Université

École doctorale des Sciences de l'Environnement d'Ile de France (ED129)

Laboratoire d'Océanographie et du Climat: Expérimentation et Approches Numériques.

Variabilité paléoclimatique et événements extrêmes depuis la dernière déglaciation au Pérou : enregistrement sédimentaire et simulations de modèles

Par Marco Yseki

Thèse de doctorat de Paléocéanographie

Dirigée par Bruno Turcq

Co-Dirigée par Dimitri Gutiérrez

Présentée et soutenue publiquement le 30 mai 2022

Devant un jury composé de :

Rapporteur	Cristhophe Colin	Université Paris-Saclay
Rapporteur	Jorge Valdez	Universidad de Antofagasta
Exameniteur	Abdel Sifeddine	IRD-Sorbone Université
Examinatrice	Charlotte Skonieczny	Université Paris-Saclay
Examinatrice	Valentina Flores	Universidad de Chile
Directeur de thèse	Bruno Turcq	IRD-Sorbone Université
Co-Directeur de thése	Dimitri Gutiérrez	Universidad Peruana Cayetano Heredia

Acknowledgments

This research was funded by a PhD fellowship from the “Institut de Recherche pour le Developpement (IRD)”. I would like to specially acknowledge to my advisor Bruno Turcq, for their invaluable academic support and patience in the development of this thesis. Also, thanks to Dimitri Gutierrez, Sandrine Caquineau, Renato Salvatteci and Matthieu Carré for their support during the preparation of the thesis. Agradecer también a mi familia (Luisa y Liz) por su apoyo durante estos años. Finalmente, agradecer a todos los que han hecho posible este trabajo.

Table of Contents

1. General Introduction

The response of the Peruvian Upwelling System (PUS) to future global warming is uncertain. Since high productivity in the PUS supports one of the most abundant fisheries in the world, the anchovy fishery (Pauly and Christensen, 1995), how the wind and upwelling dynamic in PUS would respond to climate change is of great interest to a wide range of scientists and stakeholders. Bakun (1990) proposed an increase in alongshore wind stress and coastal upwelling in EBUSs, including the PUS, due to an enhanced pressure gradient between the coast and the adjacent ocean due to global warming. In fact, Gutiérrez et al. (2011) found a negative sea surface temperature (SST) trend in central-southern Peru during 1950-2010 possibly explained by an increase in coastal upwelling. A recent study using a high-resolution regional model indicates that summer winds decrease weakly (0-5%) while winter wind increase weakly (0-10%) under IPCC RCP 8.5 scenario (Chamorro et al., 2021). However, this increase is driven by the alongshore pressure gradient and intensification of the South Pacific Subtropical High (SPSH) (Chamorro et al., 2021) and not by the pressure gradient between land and ocean as proposed by Bakun. (1990).

Additional uncertainties are related to the response of El Niño Southern Oscillation (ENSO) to global warming and its possible impacts through teleconnections in PUS. During El Niño events, especially those with high SST anomalies in the Eastern Pacific (EP), strong thunderstorms and precipitation occur on the coast of Peru (Lagos et al., 2008; Lavado-Casimiro y Espinoza, 2014; Sanabria et al 2018, Sulca et al 2018). These events produce catastrophic flash floods and large discharge of sediments during a few days (Morera et al., 2017; Takahashi and Martinez, 2017; Guzmán et al., 2020). How increasing greenhouse gases influence ENSO is still unclear. While CMIP5 and CMIP6 models together tend to suggest an increased ENSO variability with increasing atmospheric CO2 concentrations (Cai et al., 2014, 2015, 2018), two recent studies found that ENSO is weakening with increasing CO2 when using simulations on millennial time scales that reduce the noise due to the internal variability of the system (Callahan et al., 2021) or when model biases are minimized with an ultra-high-resolution model (Wengel et al., 2021).

Paleoceanographic studies allow to estimate the influence of past climatic variations and provide a better understanding of the mechanisms involved, favoring a

better assessment of future changes. The Peruvian margin is a region with favorable conditions for the preservation of paleoceanographic records, due to the presence of an Oxygen Minimum Zone (OMZ), high sedimentation rates and favorable topographic conditions (e.g., Reinhardt et al., 2002; Rein et al., 2005; Gutiérrez et al., 2006, 2009; Sifeddine et al., 2008; Mollier-Vogel et al., 2013; Salvatteci et al., 2014, 2016, 2019; Fleury et al., 2015,2016; Briceño-Zuluaga et al., 2016). The last deglaciation (18-11 kyr BP) and Mid-Holocene (8-4 kyr BP) were periods of rapid global warming (Wanner et al., 2008; Clark et al., 2012; Shakun et al., 2012; Fischer et al., 2018; Kaufman et al., 2020) and offer natural experimental conditions to observe the behavior of wind and upwelling dynamic in PUS and ENSO in a context of global warming.

The objectives of this thesis are: 1) To reconstruct the millennial variability of fluvial and aeolian inputs and to infer the changes in precipitation and winds during the last deglaciation in the central-southern Peruvian margin. 2) To reconstruct the interannual variability of fluvial inputs and precipitation and infer ENSO variability during the last deglaciation in the central-southern Peruvian margin and 3) To reconstruct the millennial variability of aeolian inputs and winds during the Holocene in southern Peru. For this reason, grain-size distribution and X-Ray Fluorescence analysis were performed in sediments core collected in central-southern Peruvian margin (M77/2-005-3, Callao, 12º05 S, 77º40,07 W, 214 m water depth; G14, Pisco, 14.38ºS, 76.42ºW, 390 m depth and M135-004-3, Ilo, 17º2 S, 71º4 W, 229 m water depth).

1.1. Regional setting

The PUS, located off Peru, is one of the most productive Eastern Boundary Upwelling Systems (EBUSs) in terms of fisheries (Chavez et al., 2008) (Fig 1a and 1b). High biological productivity is linked to the upwelling of subsurface nutrient-rich waters driven by surface wind stress (Pennington et al., 2006). Another of the most important particularities of this system is the presence of a ZMO product of the decomposition and sinking of biological production and poor ventilation (Hellin and Levin, 2004). In PUS, upwelling-favorable winds occur throughout the year, being more intense during the austral winter, which is regionally linked to the seasonal movements of the Intertropical Convergence Zone (ITCZ) and the South Pacific Subtropical High (SPSH) (Strub et al., 1998; Karstensen and Ulloa, 2009). In addition, along the coast of Peru, semi-permanent low-pressure zones associated with the arid regions located on the coast of the upwelling

centers are found, especially at Pisco (14ºS), which coincides with the Ica desert. Enhanced winds resulting from the land-sea temperature gradient produce an upwelling that reinforces the temperature and pressure difference along the coast.

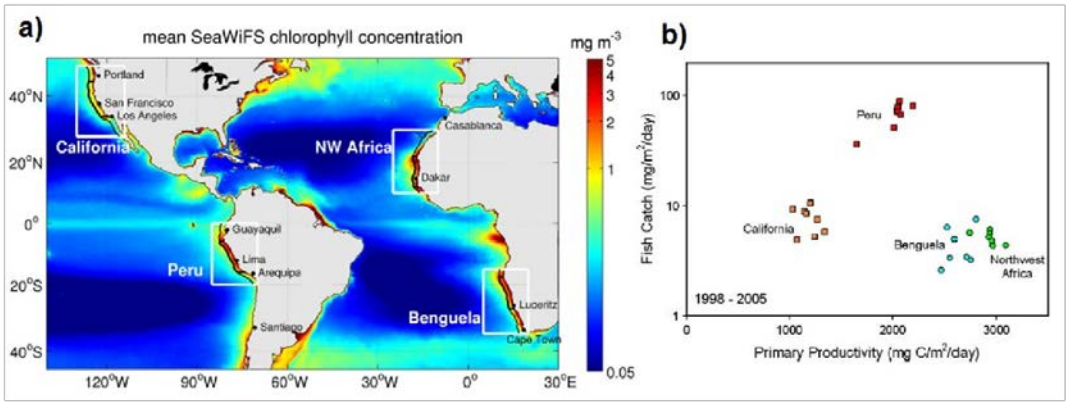

Figure 1. The four Eastern Boundary Upwelling Systems (a). The figure was adapted from Messié and Chavez (2015). Fish catch vs. primary productivity between 1998 and 2005 in the four major EBUS (b). The figure was adapted from Chavez et al. (2008).

1.1.1. Present-day atmospheric and oceanographic conditions

The climate of the Eastern Tropical Pacific is closely linked to a regional atmospheric circulation resulting from the connections between the SPSH, the ITCZ and the Walker Circulation.

SPSH extends over the entire South Pacific Ocean basin and is the dominant climatic forcing of the PUS (Strub et al., 1998). The limits of the south Pacific High are the ITCZ in the north and the polar front in the south (Strub et al., 1998). At, seasonal scale, the SPSH causes favorable-upwelling winds during the winter in PUS (Strub et al., 1998; Karstensen and Ulloa, 2009) (Fig 2).

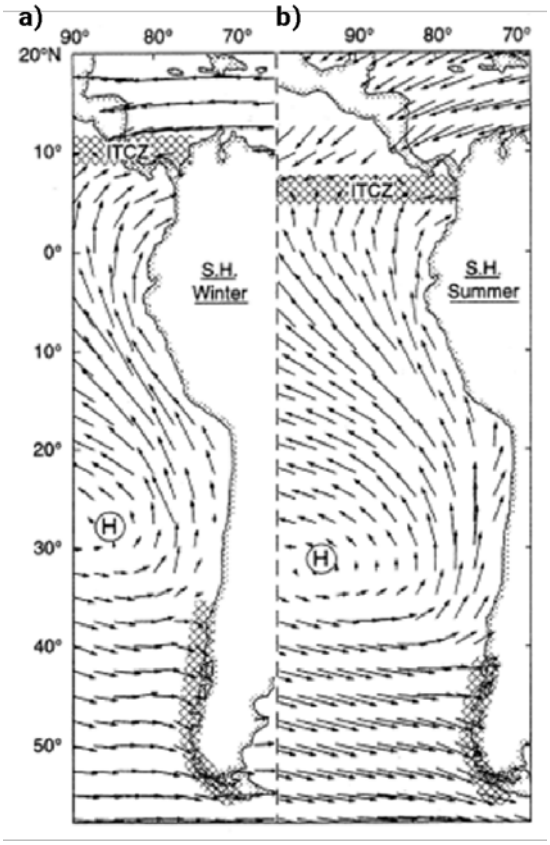

Figure 2. Climatologically wind during austral winter (a) and summer (b). The figure was adapted from Strub et al. (1998).

The ITCZ is the region of the globe where the trade winds of the Northern Hemisphere converge with the trade winds of the Southern Hemisphere. The ITCZ is a belt of low pressure near the equator that shapes climate and society in the tropics and shows an annual latitudinal shift from ~10ºN during the austral winter to 2-5ºN in austral summer, producing a seasonality in the intensity and spatial distribution of precipitation in the tropics (Strub et al., 1998) (Fig. 3).

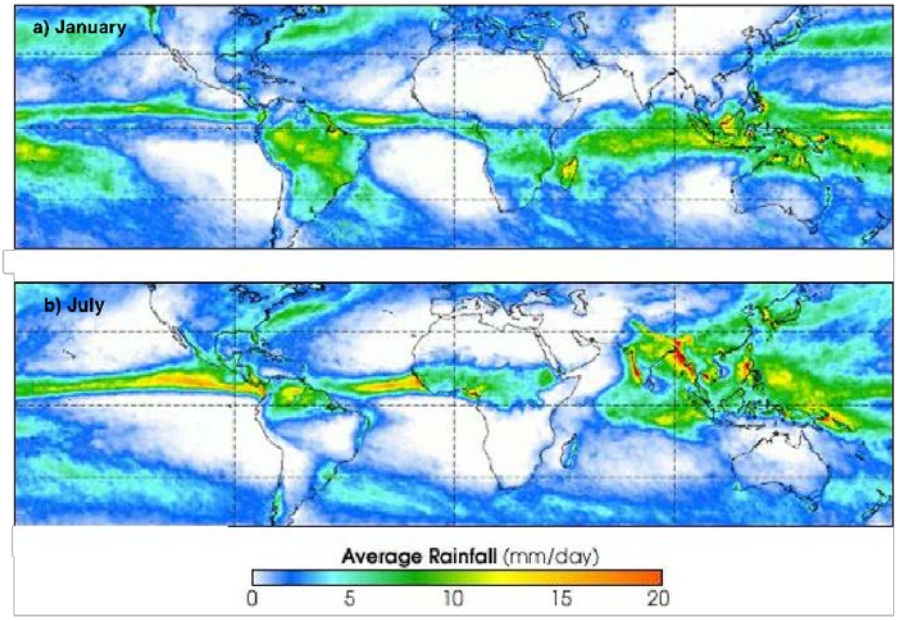

Figure 3. Position of the ITCZ in January and July (1998-2020) marked by intense rainfalls on the oceans. Figures modified from the NASA/GSFC

The Walker Circulation is a major component of the global atmospheric circulation. In the Pacific Ocean, the Walker cell generates a zonal sea surface temperature gradient, with cold temperatures in the East and a heat accumulation in the West Pacific, supported by a thermocline inclination of the Equatorial Pacific (Bjerknes 1969). Due to this East-West temperature gradient, warm air rises above through the West Pacific Warm Pool, diverging in all directions in the upper troposphere and then converging over the East Pacific Cold Tongue (Gill, 1980). This atmospheric circulation is strongly affected by ENSO (Cane, 2005). During the warm phase of ENSO (El Niño), the weakening of the trade winds causes a displacement of warm air and surface water masses from the Western Pacific to the Central Pacific, causing an increase in precipitation in northern Peru, which can generate coastal flooding. During the cold phase (La Niña), the trade winds strengthen, producing an increase in temperature and humidity in the Western Pacific and an expansion of the Cold Tongue towards the Central Pacific, along with drier conditions along the Peruvian coast (Fig. 4).

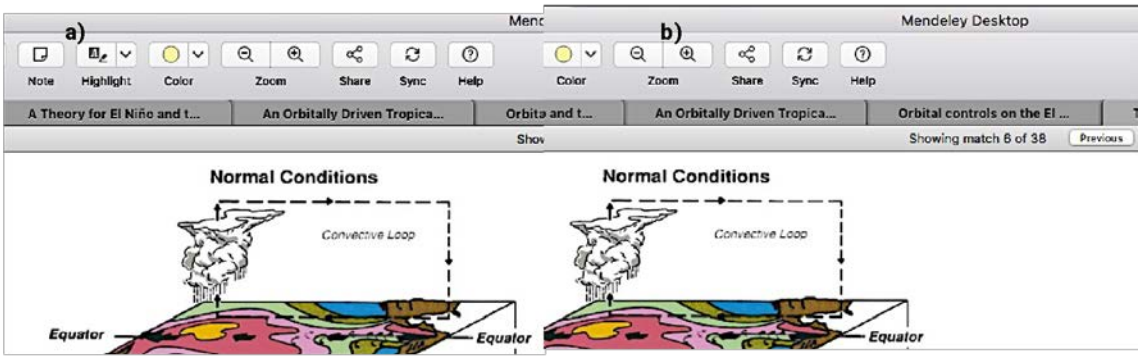

Figure 4. Schematics of Normal Conditions (a) and El Niño Conditions (b) in the equatorial Pacific Ocean and atmosphere. Figure modified from Cane (2005).

The coastal currents in the PUS are similar as those observed in other EBUE and is composed by two currents systems: The Equatorial Current System (ECS) and the Peruvian Current System (PCS) (Fig. 5) (Ishida et al., 2005; Kessler 2006, Penven et al., 2005; Montes et al., 2010; Chaigneau et al., 2013). The ECS is composed by the by the Surface Equatorial Current (SEC), the subsurface Equatorial Undercurrent (EUC) and the Southern Subsuperficial Countercurrents (SSCC).

At the surface, two equator currents dominate the PCS: The Peru Coastal Current (PCC) and the Peru Oceanic Current (POC). The PCC is found within 100 km from the coast and between surface and ~ 50 m and transports cold and nutrient- rich waters due to coastal upwelling (Penven et al., 2005; Pietri et al., 2014). The PCC present a velocity range from 5 to 15 cm.s $^{-1}$ and the maximum PCC flow occurs in phase with the seasonal cycle of the trade wind during austral winter (Strub et al., 1998). The offshore POC flows northward, farther than 180 km from the coast and up to 500 m depth (Chaigneau et al., 2013). At subsurface, the Peru-Chile Undercurrent (PCUC) flows poleward until 48ºS and dominates the subsuperficial circulation on the Peruvian shelf between 100 and 200 m depth (Brockman et al., 1980; Brinck et al., 1983). According to Chaigneau et al. (2013), the PCUC intensifies from 8°S to 16°S and decreases south of 16°S. Finally, Last, the poleward Peru-Chile Countercurrent (PCCC) is found further from the coast than the PCUC and spans between 5°S – 35°S (Strub et al., 1998).

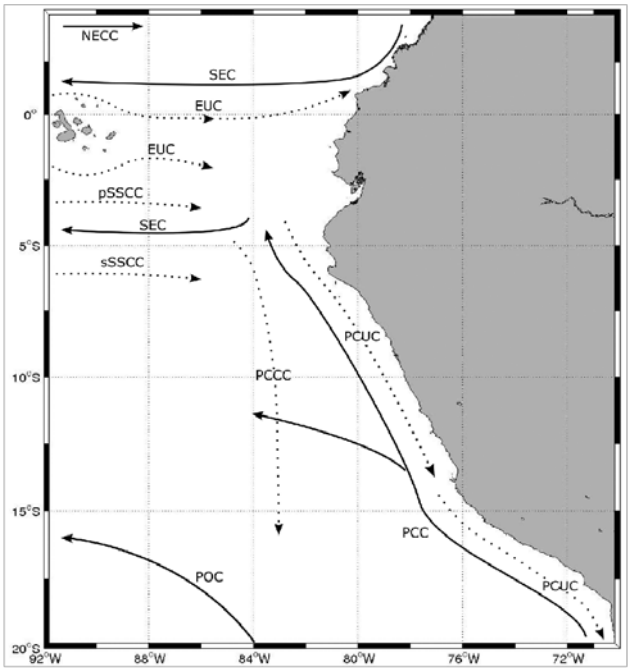

Figure 5. Oceanic circulation scheme for the eastern tropical Pacific. Figure obtained from Montes et al (2010).

1.1.2. Terrigenous material transport to the Peruvian margin

We focus on the central-southern part (12-17ºS) of the Peruvian margin. Callao (12ºS), Pisco (14ºS) and Ilo (17ºS) are located onshore of the Lima Basin (Suess et al., 1987). This basin exhibits high productivity and anoxic conditions favored by an intense Oxygen Minimum Zone. Sediments are composed of fine grains, are rich in organic matter and contain abundant diatoms. The general absence of bioturbation in some areas and during some time periods due to the low oxygen level allows the preservation of laminations and therefore the use of these sediments as palaeoceanographic records (e.g., Rein et al., 2005; Sifeddine et al., 2008; Gutiérrez et al., 2006, 2009, 2011; Briceño-Zuluaga et al., 2016; Salvatteci et al., 2014, 2016, 2019). In Callao, muddy laminated areas are reported (Reinhardt et al., 2002), but sedimentary records collected in the OMZ core, off Pisco and Ilo, show more continuous laminations than the records collected off Callao (e.g., Salvatteci et al., 2016, 2019).

According to Scheidegger and Krissek (1982), he main transport of the detrital fraction of coarse silt and sand to the hemipelagic sediments in the Peruvian margin is by the action of winds. In contrast to Callao, Pisco and Ilo are characterized by the presence of large coastal deserts, extreme aridity and dust storms (Fig. 6). During these sporadic sand storms wind velocities can exceed 10-15 m/s (Briceño-Zuluaga et al., 2017). These

storms are produced by a local intensification of alongshore surface wind and by alongshore pressure gradients (Briceño-Zuluaga et al., 2017). Also, in Pisco, an intense coastal upwelling linked to strong alongshore surface wind occurs (Dewitte et al., 2011; Gutiérrez et al., 2011; Rahn and Garreaud, 2013). The intensity of alongshore surface winds presents a seasonal variability, with stronger winds during winter and weaker winds during summer. This seasonality is linked regionally to the displacements of the ITCZ-SPSH system and locally to continental-oceanic and alongshore pressure gradients (Strub et al., 1998; Gutiérrez et al., 2011; Chamorro et al., 2018).

In contrast to the fine sands transported by winds, quartz-rich silt and clays are transported by rivers to the continental shelf (Scheidegger and Krissek, 1982). The central-southern Peruvian coast is characterized by very low annual precipitations (Callao,14 mm y^{-1}, Pisco, 2 mm y^{-1} and Ilo, 26 mm y^{-1}) and scarce flows of coastal rivers (Lagos et al., 2008). However, during summer there is an increase in river discharges associated with increased monsoon precipitation in the Andes (Garreaud et al., 2009; Vuille et al., 2012). Occasional floods occur and higher sediment discharges are associated with intense precipitation during extreme El Niño events (Bourrel et al., 2015; Morera et al., 2017; Rau et al., 2016; Guzman et al., 2020).

Once in the water column, dispersion patterns of clays (< 4 μm) and fine silts (8-11 μm) coincide with the surface and subsurface currents, while the fine sands present limited dispersion near the coast (Scheidegger and Krissek, 1982). Likewise, near-bottom processes and bottom topography exert considerable control over the dispersal of hemipelagic sediments on the Peruvian margin (Scheidegger and Krissek, 1982, Erdem et al., 2016).

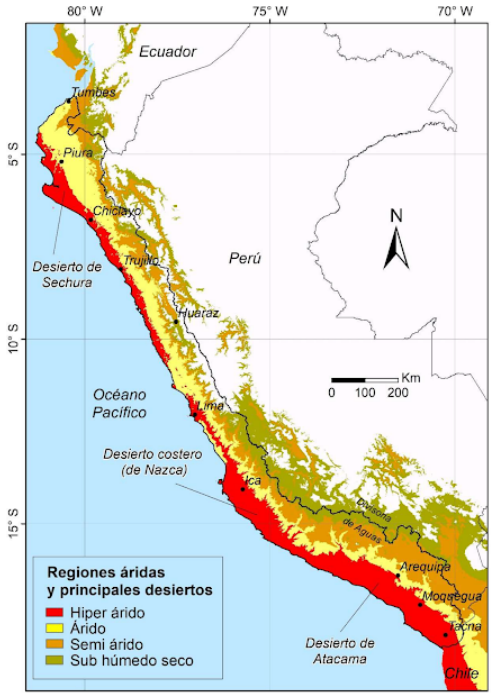

Figure 6. Aridity map and main deserts in Peru. Figure obtained from Rau (2019).

1.2. Summary of climatic changes in South America during the last deglaciation and Mid-Holocene.

The last deglaciation, a period of global warming from the end of the Last Glacial Maximum (LGM, ~ 19 kyr BP) to the early Holocene (11 kyr BP), is an outstanding period in Earth's history that allows us a better understanding of the mechanisms regulating regional climatic conditions under rapid global warming (Clark et al., 2012; Shakun et al., 2012). During the last deglaciation, the most important millennial-scale events in the northern hemisphere are: Heinrich Stadial 1 (HS1, ~18-15 kyr BP) in which two distinct stages of discharge of ice stream occurred (H1.1, ~16.2 kyr BP and H1.2, ~15.1 kyr BP) (Heinrich, 1988; Bard et al., 2020; Hodell et al., 2017), the Bølling-Allerød warm period (BA, ~14.7-12.9 kyr BP) (Buizert et al., 2014; Ivanovic et al., 2018) and the Younger Dryas cold event (YD, ~12.9-11.5 kyr BP) (Alley, 2000). Whereas, in the southern hemisphere, the most notorious event was the Antarctic Cold Reversal cold period (ACR, ~15-13 kyr BP) (Pedro et al., 2015).

During HS1 (~18-15 kyr BP), a decrease in temperature is recorded in the Greenland and other Northern Hemisphere records (Johnsen et al., 2001; Waelbroeck et

al., 2001). During this period the Heinrich event occurred, this event was characterized by an increase in freshwater flux due to iceberg collapse and evidenced by the presence of ice drift debris in marine cores (Heinrich, 1998; Álvarez-Solas et al., 2011). The decrease in temperature during Heinrich events in the Northern Hemisphere is explained by a reduction in heat transport, due to the increase in freshwater flux in the North Atlantic, producing changes in temperature, salinity and density of surface waters, causing a weakening of the Atlantic Meridional Overturning Circulation (Stanford et al., 2011; McManus et al., 2004; Ng et al., 2018). In South America, an increase in terrigenous input is observed in Northern Peru (Mollier-Vogel et al., 2013) and wetter conditions are recorded in the Southeast and Northeast of Brazil (Turcq et al., 1997; Arz et al. 1998, Cruz et al., 2005; Montade et al., 2015; Stríkis et al., 2015; Zhang et al 2015, Novello et al., 2017; Mulitza et al., 2017). In addition, the highest lake level of Titicaca lake has been recorded between 16.5 and 15 ka (Blard et al. 2011). On the other hand, a decrease in terrigenous input in Cariaco Basin (Venezuela) was reported (Peterson et al., 2000; Deplazes et al., 2013). Higher precipitations in Northeast Brazil and lower in northern South America suggest a shift of the ITCZ and an intensification of the South American Monsoon System during that period.

Subsequent to the HS1, a period characterized by a global temperature increase called the Bølling-Allerød occurred (14.7-12.9 kyr BP) (Buizert et al., 2014; Ivanovic et al., 2018). This temperature increment coincided with a very marked melt and marine transgression event ("Meltwater pulse 1a") centered at ~14.6 ka, marking the termination of the last glacial period (Weaver et al., 2003). In the southern hemisphere, a cold period called the Antarctic Cold Reversal, is observed at the same time, in which the warming trend is stopped. (Pedro et al., 2015). This period corresponds to a maximum of glacier advance in the tropical Andes, which would be linked to cold SST in the southern hemisphere (Jomelli et al., 2014). During the BA, a northern shift of the ITCZ is recorded (Peterson et al., 2000; Haug et al., 2001; Deplazes et al., 2013), causing a reduction of terrigenous input in northern Peru (Mollier-Vogel et al., 2013) and dry conditions in southeastern and northeastern Brazil (Arz et al. 1998, Cruz et al., 2005; Montade et al., 2015; Stríkis et al., 2015; Zhang et al 2015, Novello et al., 2017, Mulitza et al., 2017). However, this reduction in terrigenous input during the BA was not registered until now in the center of the Peruvian margin (Rein et al., 2005).

Finally, subsequent to the BA and the ACR, a climatic cooling phase of millennial duration occurs in the northern hemisphere, called the Younger Dryas Dryas (12.9-11.5

kyr BP) (Alley, 2000). In the Peruvian margin, at the beginning of the YD, there were an increase in primary productivity and minimum values of terrigenous content, which increase towards the end of the period in central Peru (Rein et al., 2005). In northern Peru, a slight increase in the terrigenous input (Mollier-Vogel et al., 2013) was recorded coinciding with the increase in humidity in southeastern and northeastern Brazil Cruz et al., 2005; Montade et al., 2015; Stríkis et al., 2015; Zhang et al 2015; Novello et al., 2017), in Titicaca lake (Baker et al., 2001; Blard et al., 2011) and in Andean ice cores (Thompson et al., 2000). These results suggest a southern shift of the ITCZ and intensification of the South American Monsoon in the Southeast region of Brazil during the YD.

The Early Holocene (11.5-8 kyr BP) is poorly represented in the Peruvian margin cores, probably because of the occurrence of erosional events that may be due to an enhancement of bottom currents (Peru-Chile Undercurrent) or internal waves (Erdem et al., 2016; Salvatteci et al., 2016). On the continent it appears as a warmer and/or drier period in ice cores, lakes and speleothems (Thomson, 2000; Van Broekelen et al., 2008, Bird et al., 2011).

The Mid-Holocene (MH, ~8-4 ka BP) was a warm period in the Northern Hemisphere due to orbital variations and insolation changes (Kaufman et al., 2004, 2020; Renssen et al., 2009; Wanner et al., 2008; Fischer et al., 2018). The MH was characterized by an increase (decrease) in summer insolation in the Northern Hemisphere (Southern Hemisphere) in comparison with present-day conditions. The change in insolation was due to the nearly 101° difference between the longitude of the MH and the current perihelion longitude (Prado et al., 2013). Multiple evidences during the MH suggest a strong SST Pacific zonal gradient and thus an intensified Walker Circulation (Koutavas and Joanides, 2012) also known as La Niña-type conditions in the tropical Pacific (Carré et al., 2012). During this key period, a northern shift of the ITCZ (Haug et al., 2001; McGee et al., 2014) is also recorded during boreal summer and autumn in response to Northern Hemisphere summer insolation increase due to change in precession while in boreal winter and spring the ITCZ was shifted to the south (Cruz et al. 2009; Silva Dias et al., 2009). In addition, alkenone-derived temperature record (Salvatteci et al., 2019) and isotopic data from fossil mollusk (Carré et al., 2012) suggest a strong cooling in PUS during the MH maybe due to an increase of coastal upwelling linked to an intensification of the SPSH (Carré et al., 2012; Salvatteci et al., 2019).

1.3. References

Alley, R.B., 2000. The Younger Dryas cold interval as viewed from central Greenland. Quaternary science reviews, 19(1-5), pp.213-226.

Álvarez-Solas, J., Montoya, M., Ritz, C., Ramstein, G., Charbit, S., Dumas, C., Nisancioglu, K., Dokken, T. and Ganopolski, A., 2011. Heinrich event 1: an example of dynamical ice-sheet reaction to oceanic changes. Climate of the Past, 7(4), pp.1297-1306.

Arz, H. W., J. P tzold, and G. Wefer,1998. Correlated millennial-scale changes in surface hydrography and terrigenous sediment yield inferred from last-glacial marine deposits off northeastern Brazil, Quat. Res., 50(2), 157–166,

Baker, P.A., Seltzer, G.O., Fritz, S.C., Dunbar, R.B., Grove, M.J., Tapia, P.M., Cross, S.L., Rowe, H.D. and Broda, J.P., 2001. The history of South American tropical precipitation for the past 25,000 years. science, 291(5504), pp.640-643.

Bard, E., Rostek, F., Turon, J. L., and Gendreau, S., 2000. Hydrological impact of Heinrich events in the subtropical Northeast Atlantic. *Science*, *289*(5483), 1321–1324.

Bakun, A., 1990. Global climate change and intensification of coastal ocean upwelling. Science, 247(4939), pp.198-201.

Bird, B. W., Abbott, M. B., Rodbell, D. T., and Vuille, M.,2011. Holocene tropical South American hydroclimate revealed from a decadally resolved lake sediment δ18O record. *Earth and Planetary Science Letters*, *310*(3–4), 192–202.

Bjerknes, J., 1969. Atmospheric teleconnections from the equatorial Pacific. *Monthly weather review*, *97*(3), pp.163-172.

Blard, P.H., Sylvestre, F., Tripati, A.K., Claude, C., Causse, C., Coudrain, A., Condom, T., Seidel, J.L., Vimeux, F., Moreau, C. and Dumoulin, J.P., 2011. Lake highstands on the Altiplano (Tropical Andes) contemporaneous with Heinrich 1 and the Younger Dryas: new insights from 14C, U–Th dating and δ18O of carbonates. Quaternary Science Reviews, 30(27-28), pp.3973-3989.

Briceño-Zuluaga, F., Castagna, A., Rutllant, J.A., Flores-Aqueveque, V., Caquineau, S., Sifeddine, A., Velazco, F., Gutierrez, D. and Cardich, J., 2017. Paracas dust storms: sources, trajectories and associated meteorological conditions. Atmospheric Environment, 165, pp.99-110.

Briceño-Zuluaga, F.J., Sifeddine, A., Caquineau, S., Cardich, J., Salvatteci, R., Gutierrez, D., Ortlieb, L., Velazco, F., Boucher, H. and Machado, C., 2016. Terrigenous material supply to the Peruvian central continental shelf (Pisco, 14° S) during the last 1000 years: paleoclimatic implications. Climate of the Past, 12(3), pp.787-798.

Brink, K.H., Halpern, D., Huyer, A. and Smith, R.L., 1983. The physical environment of the Peruvian upwelling system. Progress in Oceanography, 12(3), pp.285-305.

Brockmann, C., Fahrbach, E., Huyer, A. and Smith, R.L., 1980. The poleward undercurrent along the Peru coast: 5 to 15 S. Deep Sea Research Part A. Oceanographic Research Papers, 27(10), pp.847-856.

Buizert, C., Gkinis, V., Severinghaus, J.P., He, F., Lecavalier, B.S., Kindler, P., Leuenberger, M., Carlson, A.E., Vinther, B., Masson-Delmotte, V. and White, J.W., 2014. Greenland temperature response to climate forcing during the last deglaciation. Science, 345(6201), pp.1177-1180.

Cai, W., Borlace, S., Lengaigne, M., Van Rensch, P., Collins, M., Vecchi, G., Timmermann, A., Santoso, A., McPhaden, M.J., Wu, L. and England, M.H., 2014. Increasing frequency of extreme El Niño events due to greenhouse warming. *Nature climate change*, *4*(2), pp.111-116.

Cai, W., Santoso, A., Wang, G., Yeh, S.W., An, S.I., Cobb, K.M., Collins, M., Guilyardi, E., Jin, F.F., Kug, J.S. and Lengaigne, M., 2015. ENSO and greenhouse warming. *Nature Climate Change*, *5*(9), pp.849-859.

Cai, W., Wang, G., Dewitte, B., Wu, L., Santoso, A., Takahashi, K., Yang, Y., Carréric, A. and McPhaden, M.J., 2018. Increased variability of eastern Pacific El Niño under greenhouse warming. *Nature*, *564*(7735), pp.201-206.

Callahan, C.W., Chen, C., Rugenstein, M., Bloch-Johnson, J., Yang, S. and Moyer, E.J., 2021. Robust decrease in El Niño/Southern Oscillation amplitude under long-term warming. *Nature Climate Change*, *11*(9), pp.752-757.

Cane, M.A., 2005. The evolution of El Niño, past and future. Earth and Planetary Science Letters, 230(3-4), pp.227-240.

Carré, M., Azzoug, M., Bentaleb, I., Chase, B.M., Fontugne, M., Jackson, D., Ledru, M.P., Maldonado, A., Sachs, J.P. and Schauer, A.J., 2012. Mid-Holocene mean climate in the south eastern Pacific and its influence on South America. Quaternary International, 253, pp.55-66.

Chaigneau, A., Dominguez, N., Eldin, G., Vasquez, L., Flores, R., Grados, C. and Echevin, V., 2013. Near-coastal circulation in the Northern Humboldt Current System from shipboard ADCP data. Journal of Geophysical Research: Oceans, 118(10), pp.5251-5266.

Chamorro, A., Echevin, V., Colas, F., Oerder, V., Tam, J. and Quispe-Ccalluari, C., 2018. Mechanisms of the intensification of the upwelling-favorable winds during El Niño 1997–1998 in the Peruvian upwelling system. Climate Dynamics, 51(9), pp.3717-3733.

Chamorro, A., Echevin, V., Dutheil, C., Tam, J., Gutiérrez, D. and Colas, F., 2021. Projection of upwelling-favorable winds in the Peruvian upwelling system under the RCP8. 5 scenario using a high-resolution regional model. Climate Dynamics, 57(1), pp.1-16.

Chavez, F.P., Bertrand, A., Guevara-Carrasco, R., Soler, P. and Csirke, J., 2008. The northern Humboldt Current System: Brief history, present status and a view towards the future. Progress in Oceanography, 79(2-4), pp.95-105.

Clark, P.U., Shakun, J.D., Baker, P.A., Bartlein, P.J., Brewer, S., Brook, E., Carlson, A.E., Cheng, H., Kaufman, D.S., Liu, Z. and Marchitto, T.M., 2012. Global climate evolution during the last deglaciation. *Proceedings of the National Academy of Sciences*, *109*(19), pp.E1134-E1142.

Cruz, F.W., Burns, S.J., Karmann, I., Sharp, W.D., Vuille, M., Cardoso, A.O., Ferrari, J.A., Silva Dias, P.L. and Viana, O., 2005. Insolation-driven changes in atmospheric circulation over the past 116,000 years in subtropical Brazil. Nature, 434(7029), pp.63-66.

Cruz, F. W., Vuille, M., Burns, S. J., Wang, X., Cheng, H., Werner, M., Lawrence Edwards, R., Karmann, I., Auler, A. S., & Nguyen, H., 2009. Orbitally driven east-west antiphasing of South American precipitation. *Nature Geoscience*, *2*(3), 210–214.

Deplazes, G., Lückge, A., Peterson, L.C., Timmermann, A., Hamann, Y., Hughen, K.A., Röhl, U., Laj, C., Cane, M.A., Sigman, D.M. and Haug, G.H., 2013. Links between tropical rainfall and North Atlantic climate during the last glacial period. Nature Geoscience, 6(3), pp.213-217.

Dewitte, B., Illig, S., Renault, L., Goubanova, K., Takahashi, K., Gushchina, D., Mosquera, K. and Purca, S., 2011. Modes of covariability between sea surface temperature and wind stress intraseasonal anomalies along the coast of Peru from satellite observations (2000–2008). *Journal of Geophysical Research: Oceans*, *116*(C4).

Erdem, Z., Schönfeld, J., Glock, N., Dengler, M., Mosch, T., Sommer, S., Elger, J. and Eisenhauer, A., 2016. Peruvian sediments as recorders of an evolving hiatus for the last 22 thousand years. *Quaternary Science Reviews*, *137*, pp.1-14.

Fischer, H., Meissner, K.J., Mix, A.C., Abram, N.J., Austermann, J., Brovkin, V., Capron, E., Colombaroli, D., Daniau, A.L., Dyez, K.A. and Felis, T., 2018. Palaeoclimate constraints on the impact of 2◦ C anthropogenic warming and beyond, Nat. Geosci., 11, 474–485

Fleury, S., Crosta, X., Schneider, R., Blanz, T., Ther, O. and Martinez, P., 2016. Centennial-scale variations in diatom productivity off Peru over the last 3000 years. *The Holocene*, *26*(4), pp.520-531.

Fleury, S., Martinez, P., Crosta, X., Charlier, K., Billy, I., Hanquiez, V., Blanz, T. and Schneider, R.R., 2015. Pervasive multidecadal variations in productivity within the Peruvian Upwelling System over the last millennium. *Quaternary Science Reviews*, *125*, pp.78-90.

Garreaud, R.D., Vuille, M., Compagnucci, R. and Marengo, J., 2009. Present-day south american climate. *Palaeogeography, Palaeoclimatology, Palaeoecology*, *281*(3-4), pp.180-195.

Gill, A.E., 1980. Some simple solutions for heat-induced tropical circulation. *Quarterly Journal of the Royal Meteorological Society*, *106*(449), pp.447-462.

Gutiérrez, D., Bouloubassi, I., Sifeddine, A., Purca, S., Goubanova, K., Graco, M., Field, D., Méjanelle, L., Velazco, F., Lorre, A. and Salvatteci, R., 2011. Coastal cooling and increased productivity in the main upwelling zone off Peru since the mid-twentieth century. Geophysical Research Letters, 38(7).

Gutiérrez, D., Sifeddine, A., Field, D.B., Ortlieb, L., Vargas, G., Chavez, F.P., Velazco, F., Ferreira, V., Tapia, P., Salvatteci, R. and Boucher, H., 2009. Rapid reorganization in ocean biogeochemistry off Peru towards the end of the Little Ice Age. Biogeosciences, 6(5), pp.835-848.

Gutiérrez, D., Sifeddine, A., Reyss, J.L., Vargas, G., Velazco, F., Salvatteci, R., Ferreira, V., Ortlieb, L., Field, D., Baumgartner, T. and Boussafir, M., 2006. Anoxic sediments off Central Peru record interannual to multidecadal changes of climate and upwelling ecosystem during the last two centuries. Advances in Geosciences, 6, pp.119-125.

Guzman, E., Ramos, C. and Dastgheib, A., 2020. Influence of the El Niño Phenomenon on Shoreline Evolution. Case Study: Callao Bay, Perú. *Journal of Marine Science and Engineering*, *8*(2), p.90.

Haug, G.H., Hughen, K.A., Sigman, D.M., Peterson, L.C. and Rohl, U., 2001. Southward migration of the intertropical convergence zone through the Holocene. Science, 293(5533), pp.1304-1308.

Heinrich, H., 1988. Origin and consequences of cyclic ice rafting in the northeast Atlantic Ocean during the past 130,000 years. *Quaternary research*, *29*(2), pp.142-152.

Helly, J.J. and Levin, L.A., 2004. Global distribution of naturally occurring marine hypoxia on continental margins. *Deep Sea Research Part I: Oceanographic Research Papers*, *51*(9), pp.1159-1168.

Hodell, D.A., Nicholl, J.A., Bontognali, T.R., Danino, S., Dorador, J., Dowdeswell, J.A., Einsle, J., Kuhlmann, H., Martrat, B., Mleneck-Vautravers, M.J. and Rodríguez-Tovar, F.J., 2017. Anatomy of Heinrich Layer 1 and its role in the last deglaciation. Paleoceanography, 32(3), pp.284-303.

Ishida, A., Mitsudera, H., Kashino, Y. and Kadokura, T., 2005. Equatorial Pacific subsurface countercurrents in a high-resolution global ocean circulation model. *Journal of Geophysical Research: Oceans*, *110*(C7).

Ivanovic, R.F., Gregoire, L.J., Wickert, A.D. and Burke, A., 2018. Climatic effect of Antarctic meltwater overwhelmed by concurrent Northern hemispheric melt. Geophysical Research Letters, 45(11), pp.5681-5689.

Johnsen, S.J., Dahl-Jensen, D., Gundestrup, N., Steffensen, J.P., Clausen, H.B., Miller, H., Masson-Delmotte, V., Sveinbjörnsdottir, A.E. and White, J., 2001. Oxygen isotope and palaeotemperature records from six Greenland ice-core stations: Camp Century, Dye-3, GRIP, GISP2, Renland and NorthGRIP. Journal of Quaternary Science: Published for the Quaternary Research Association, 16(4), pp.299-307.

Jomelli, V., Favier, V., Vuille, M., Braucher, R., Martin, L., Colose, C., Brunstein, D., He, F., Khodri, M., Leanni, L., Rinterknecht, V., Grancher, D., Francou, B., Ceballos, J. L., Fonseca, H., Liu, Z., & Bourles, D. Leanni L. L., Rinterknecht V., Grancher D., Francou B., Ceballos J. L., Fonseca H., Liu Z. and Otto-Bliesner B. L. 2014. A major advance of tropical glaciers during the Antarctic cold reversal. *Nature*, *513*, 224–228.

Karstensen, J., & Ulloa, O., 2009. Peru-Chile current system. In J. H. Steele, S. A. Thorpe, & K. K. Turekian (Eds.), Ocean currents (2nd ed., pp. 385–392). London: Academic Press.

Kaufman, D., McKay, N., Routson, C., Erb, M., Dätwyler, C., Sommer, P.S., Heiri, O. and Davis, B., 2020. Holocene global mean surface temperature, a multi-method reconstruction approach. Scientific data, 7(1), pp.1-13.

Kaufman, D.S., Ager, T.A., Anderson, N.J., Anderson, P.M., Andrews, J.T., Bartlein, P.J., Brubaker, L.B., Coats, L.L., Cwynar, L.C., Duvall, M.L. and Dyke, A.S., 2004. Holocene thermal maximum in the western Arctic (0–180 W). Quaternary Science Reviews, 23(5-6), pp.529-560.

Kesler, W.S., 2006. The circulation of the eastern tropical Pacific. *A Review Progress in Oceanography*, *69*(2-4), pp.181-217.

Koutavas, A. and Joanides, S., 2012. El Niño–Southern oscillation extrema in the holocene and last glacial maximum. Paleoceanography, 27(4).

Lagos, P., Silva, Y., Nickl, E. and Mosquera, K., 2008. El Niño–related precipitation variability in Perú. Advances in Geosciences, 14, pp.231-237.

Lavado-Casimiro, W. and Espinoza, J.C., 2014. Impactos de El Niño y La Niña en las lluvias del Perú (1965-2007). *Revista Brasileira de Meteorologia*, *29*, pp.171-182.

McGee, D., Donohoe, A., Marshall, J. and Ferreira, D., 2014. Changes in ITCZ location and cross-equatorial heat transport at the Last Glacial Maximum, Heinrich Stadial 1, and the mid-Holocene. Earth and Planetary Science Letters, 390, pp.69-79.

McManus, J.F., Francois, R., Gherardi, J.M., Keigwin, L.D. and Brown-Leger, S., 2004. Collapse and rapid resumption of Atlantic meridional circulation linked to deglacial climate changes. *nature*, *428*(6985), pp.834-837.

Mollier-Vogel, E., Leduc, G., Böschen, T., Martinez, P. and Schneider, R.R., 2013. Rainfall response to orbital and millennial forcing in northern Peru over the last 18 ka. *Quaternary Science Reviews*, *76*, pp.29-38.

Montade, V., Kageyama, M., Combourieu-Nebout, N., Ledru, M.P., Michel, E., Siani, G. and Kissel, C., 2015. Teleconnection between the Intertropical Convergence Zone and southern westerly winds throughout the last deglaciation. *Geology*, *43*(8), pp.735-738.

Montes, I., Colas, F., Capet, X. and Schneider, W., 2010. On the pathways of the equatorial subsurface currents in the eastern equatorial Pacific and their contributions to the Peru-Chile Undercurrent. *Journal of Geophysical Research: Oceans*, *115*(C9).

Morera, S.B., Condom, T., Crave, A., Steer, P. and Guyot, J.L., 2017. The impact of extreme El Niño events on modern sediment transport along the western Peruvian Andes (1968–2012). *Scientific Reports*, *7*(1), pp.1-14.

Mulitza, S., Chiessi, C. M., Schefuß, E., Lippold, J., Wichmann, D., Antz, B., Mackensen, A., Paul, A., Prange, M., Rehfeld, K., Werner, M., Bickert, T., Frank, N., Kuhnert, H., Lynch-Stieglitz, J., Portilho-Ramos, R. C., Sawakuchi, A. O., Schulz, M., Schwenk, T., … Zhang, Y. 2017. Synchronous and proportional deglacial changes in Atlantic meridional overturning and northeast Brazilian precipitation. *Paleoceanography*, *32*(6), 622–633.

Ng, H.C., Robinson, L.F., McManus, J.F., Mohamed, K.J., Jacobel, A.W., Ivanovic, R.F., Gregoire, L.J. and Chen, T., 2018. Coherent deglacial changes in western Atlantic Ocean circulation. *Nature communications*, *9*(1), pp.1-10.

Novello, V.F., Cruz, F.W., Vuille, M., Stríkis, N.M., Edwards, R.L., Cheng, H., Emerick, S., De Paula, M.S., Li, X., Barreto, E.D.S. and Karmann, I., 2017. A high-resolution history of the South American Monsoon from Last Glacial Maximum to the Holocene. *Scientific reports*, *7*(1), pp.1-8.

Pauly, D. and Christensen, V., 1995. Primary production required to sustain global fisheries. *Nature*, *374*(6519), pp.255-257.

Pedro, J.B., Bostock, H.C., Bitz, C.M., He, F., Vandergoes, M.J., Steig, E.J., Chase, B.M., Krause, C.E., Rasmussen, S.O., Markle, B.R. and Cortese, G., 2016. The spatial extent and dynamics of the Antarctic Cold Reversal. Nature Geoscience, 9(1), pp.51-55.

Pennington, J.T., Mahoney, K.L., Kuwahara, V.S., Kolber, D.D., Calienes, R. and Chavez, F.P., 2006. Primary production in the eastern tropical Pacific: A review. Progress in oceanography, 69(2-4), pp.285-317.

Penven, P., Echevin, V., Pasapera, J., Colas, F. and Tam, J., 2005. Average circulation, seasonal cycle, and mesoscale dynamics of the Peru Current System: A modeling approach. *Journal of Geophysical Research: Oceans*, *110*(C10).

Peterson, L.C., Haug, G.H., Hughen, K.A. and Rohl, U., 2000. Rapid changes in the hydrologic cycle of the tropical Atlantic during the last glacial. Science, 290(5498), pp.1947-1951.

Pietri, A., Echevin, V., Testor, P., Chaigneau, A., Mortier, L., Grados, C. and Albert, A., 2014. Impact of a coastal-trapped wave on the near-coastal circulation of the Peru upwelling system from glider data. Journal of Geophysical Research: Oceans, 119(3), pp.2109-2120.

Prado, L.F., Wainer, I., Chiessi, C.M., Ledru, M.P. and Turcq, B., 2013. A mid-Holocene climate reconstruction for eastern South America. *Climate of the Past*, *9*(5), pp.2117-2133.

Rahn, D. and Garreaud, R.: A synoptic climatology of the near-surface wind along the west coast of South America, International Journal of Climatology, 34(3), 780-792, doi:10.1002/joc.3724, 2013.

Rau, P., Bourrel, L., Labat, D., Melo, P., Dewitte, B., Frappart, F., Lavado, W. and Felipe, O., 2017. Regionalization of rainfall over the Peruvian Pacific slope and coast. *International Journal of Climatology*, *37*(1), pp.143-158.

Rau P. 2019. Aportes en ingeniería hidrológica de zonas áridas. Casos aplicados a la vertiente del Pacífico peruano. VII Congreso internacional de Hidráulica, Hidrología, Saneamiento y Medio Ambiente. ICG. 1 Noviembre. Lima.

Rein, B., Lückge, A., Reinhardt, L., Sirocko, F., Wolf, A. and Dullo, W.C., 2005. El Niño variability off Peru during the last 20,000 years. *Paleoceanography*, *20*(4).

Reinhardt, L., Kudrass, H.R., Lückge, A., Wiedicke, M., Wunderlich, J. and Wendt, G., 2002. High-resolution sediment echosounding off Peru: Late Quaternary depositional sequences and sedimentary structures of a current-dominated shelf. Marine Geophysical Researches, 23(4), pp.335-351.

Renssen, H., Seppä, H., Crosta, X., Goosse, H. and Roche, D.M., 2012. Global characterization of the Holocene thermal maximum. Quaternary Science Reviews, 48, pp.7-19.

Salvatteci, R., Gutiérrez, D., Field, D., Sifeddine, A., Ortlieb, L., Bouloubassi, I., Boussafir, M., Boucher, H. and Cetin, F., 2014. The response of the Peruvian Upwelling Ecosystem to centennial-scale global change during the last two millennia. *Climate of the Past*, *10*(2), pp.715-731.

Salvatteci, R., Gutiérrez, D., Sifeddine, A., Ortlieb, L., Druffel, E., Boussafir, M. and Schneider, R., 2016. Centennial to millennial-scale changes in oxygenation and productivity in the Eastern Tropical South Pacific during the last 25,000 years. Quaternary Science Reviews, 131, pp.102-117.

Salvatteci, R., Schneider, R.R., Blanz, T. and Mollier-Vogel, E., 2019. Deglacial to Holocene ocean temperatures in the Humboldt Current System as indicated by alkenone paleothermometry. Geophysical Research Letters, 46(1), pp.281-292.

Sanabria, J., Bourrel, L., Dewitte, B., Frappart, F., Rau, P., Solis, O. and Labat, D., 2018. Rainfall along the coast of Peru during strong El Niño events. *International Journal of Climatology*, *38*(4), pp.1737-1747.

Scheidegger, K.F. and Krissek, L.A., 1982. Dispersal and deposition of eolian and fluvial sediments off Peru and northern Chile. Geological Society of America Bulletin, 93(2), pp.150-162.

Shakun, J.D., Clark, P.U., He, F., Marcott, S.A., Mix, A.C., Liu, Z., Otto-Bliesner, B., Schmittner, A. and Bard, E., 2012. Global warming preceded by increasing carbon dioxide concentrations during the last deglaciation. *Nature*, *484*(7392), pp.49-54.

Sifeddine, A., Gutiérrez, D., Ortlieb, L., Boucher, H., Velazco, F., Field, D., Vargas, G., Boussafir, M., Salvatteci, R., Ferreira, V. and García, M., 2008. Laminated sediments from the central Peruvian continental slope: A 500 year record of upwelling system productivity, terrestrial runoff and redox conditions. Progress in Oceanography, 79(2-4), pp.190-197.

Silva Dias P.L., Turcq B., Silva Dias, M.A.F., Braconnot, P., Jorgetti, T., 2009. Evaluation of Model Simulation of 6ka BP and Present Climate in Tropical South America. In: F. Vimeux et al. edts Past climate variability from the Last Glacial Maximum to the Holocene in South America an Surrounding regions. *Developments in Paleoenvironmental Research Series (DPER) Vol. 14*, Springer Verlag, p. 259-281.

Stanford, J.D., Rohling, E.J., Bacon, S., Roberts, A.P., Grousset, F.E. and Bolshaw, M., 2011. A new concept for the paleoceanographic evolution of Heinrich event 1 in the North Atlantic. Quaternary Science Reviews, 30(9-10), pp.1047-1066.

Stríkis, N.M., Chiessi, C.M., Cruz, F.W., Vuille, M., Cheng, H., de Souza Barreto, E.A., Mollenhauer, G., Kasten, S., Karmann, I., Edwards, R.L. and Bernal, J.P., 2015. Timing and structure of Mega-SACZ events during Heinrich Stadial 1. Geophysical Research Letters, 42(13), pp.5477-5484A.

Strub, P. T., Mesias, J. M., Montecino, V., Rutllant, J., & Salinas, S., 1998. Coastal ocean circulation off Western South America. Coastal segment (6,E). In A. Robinson & K. Brink (Eds.), The sea (Vol. 11, pp. 273–313). New York: John Wiley & Sons, Inc.

Suess, E., Kulm, L.D. and Killingley, J.S., 1987. Coastal upwelling and a history of organic-rich mudstone deposition off Peru. Geological Society, London, Special Publications, 26(1), pp.181-197.

Sulca, J., Takahashi, K., Espinoza, J.C., Vuille, M. and Lavado-Casimiro, W., 2018. Impacts of different ENSO flavors and tropical Pacific convection variability (ITCZ, SPCZ) on austral summer rainfall in South America, with a focus on Peru. *International Journal of Climatology*, *38*(1), pp.420-435.

Takahashi, K. and Martínez, A.G., 2019. The very strong coastal El Niño in 1925 in the far-eastern Pacific. Climate Dynamics, 52(12), pp.7389-7415.

Thompson, L.G., Mosley-Thompson, E. and Henderson, K.A., 2000. Ice-core palaeoclimate records in tropical South America since the Last Glacial Maximum. *Journal of Quaternary Science: Published for the Quaternary Research Association*, *15*(4), pp.377-394.

Turcq, B., Pressinnoti, M.M.N. and Martin, L.,1997. Paleohydrology and paleoclimate of the past 33,000 years at the Tamanduá River, Central Brazil. *Quaternary Research*, 1997, 47 p. 284-294.

Waelbroeck, C. et Duplessy, J.C., Michel, E., Labeyrie, L. Paillard, D. and Duprat, J., The timing of the last deglaciation in North Atlantic climate records. 2001. *Nature*, vol. 412,, p. 724-727

Van Breukelen, M.R., Vonhof, H.B., Hellstrom, J.C., Wester, W.C.G. and Kroon, D., 2008. Fossil dripwater in stalagmites reveals Holocene temperature and rainfall variation in Amazonia. *Earth and Planetary Science Letters*, *275*(1-2), pp.54-60.

Wanner, H., Beer, J., Bütikofer, J., Crowley, T.J., Cubasch, U., Flückiger, J., Goosse, H., Grosjean, M., Joos, F., Kaplan, J.O. and Küttel, M., 2008. Mid-to Late Holocene climate change: an overview. Quaternary Science Reviews, 27(19-20), pp.1791-1828.

Weaver, A.J., Saenko, O.A., Clark, P.U. and Mitrovica, J.X., 2003. Meltwater pulse 1A from Antarctica as a trigger of the Bølling-Allerød warm interval. Science, 299(5613), pp.1709-1713.

Wengel, C., Lee, S.S., Stuecker, M.F., Timmermann, A., Chu, J.E. and Schloesser, F., 2021. Future high-resolution El Niño/Southern Oscillation dynamics. Nature Climate Change, 11(9), pp.758-765.

Zhang, Y., Chiessi, C.M., Mulitza, S., Zabel, M., Trindade, R.I., Hollanda, M.H.B., Dantas, E.L., Govin, A., Tiedemann, R. and Wefer, G., 2015. Origin of increased terrigenous supply to the NE South American continental margin during Heinrich Stadial 1 and the Younger Dryas. Earth and Planetary Science Letters, 432, pp.493-500.

2. Millennial variability of terrigenous transport to the central-southern Peruvian margin during the last deglaciation (18-13 kyr BP)

Marco Yseki[1], Bruno Turcq[1], Sandrine Caquineau[1], Renato Salvatteci[2], José Solis[3], C. Gregory Skilbeck[4] & Dimitri Gutiérrez[3,5]

[1]LOCEAN-IPSL, Laboratoire d'Océanographie et du Climat: Expérimentation et Approches Numériques, Sorbonne Université, CNRS, IRD, MNHN, Paris, France.
[2]Center for Ocean and Society, Kiel University, Kiel, 24105, Germany.
[3]Laboratorio de Ciencias del Mar, Facultad de Ciencias y Filosofía, Universidad Peruana Cayetano Heredia, Lima, Peru.
[4]Faculty of Science, University of Technology Sydney. PO Box 123 Broadway, Sydney NSW. 2007.
[5]Dirección General de Investigaciones Oceanográficas y de Cambio Climático, Instituto del Mar del Perú, Callao. Peru.

Chapter I focuses on objective 1 of the thesis, which is to reconstruct millennial variability of fluvial and aeolian transports and to infer changes in precipitation and winds respectively in the central-southern Peruvian margin during the last deglaciation. The grain-size distribution of Peruvian margin sediments is typically polymodal and for that reason provides information on sediment transport mechanisms and/or sediment sources. Grain-size distributions on surface sediments and sediments cores (M77/2-005-3, Callao and G14, Pisco) were measured and end-member analysis was used to deconvolved them into sub-populations. Using this methodology allows us to discriminate the different sources of terrigenous input, reconstructing the variations of fluvial and aeolian inputs dependent on changes in precipitation and winds intensity. This chapter was submitted to *Climate of the past* on January 07 2022 and is now under revision.

2.1. Abstract

Reconstructing precipitation and wind from the geological record could help to understand the potential changes in precipitation and wind dynamics in response to climate change in Peru. The last deglaciation offers natural experimental conditions to test precipitation and wind dynamics response to high latitude forcing. While considerable research has been done to reconstruct precipitation variability during the last deglaciation in the Atlantic sector of South America, the Pacific sector of South America has received little attention. This work aims to fill this gap by reconstructing types of terrigenous transport to the central-southern Peruvian margin (12°S and 14ºS) during the last deglaciation (18-13 kyr BP). For this purpose, we used grain-size distribution in sediments of marine core M77/2-005-3 (Callao, 12ºS) and G14 (Pisco, 14ºS). We analyzed end-members (EM) to identify grain-size components and reconstruct potential sources and transport processes of terrigenous material across time. We identified four end-members for both Callao and Pisco sediments. In Callao, we propose that changes in EM4 (101 μm) and EM2 (58 μm) contribution mainly reflect hydrodynamic energy and diffuse sources, respectively, while EM3 (77 um) and EM1 (11 μm) variations reflect changes in aeolian and fluvial inputs, respectively. In Pisco, changes in the contribution of EM1 (10 μm) reflect changes in river inputs while EM2 (52 μm), EM3 (75 μm) and EM4 (94 μm) reflect an aeolian origin linked to surface winds. At millennial-scale, our record shows an increase of the fluvial inputs during the last part of Heinrich Stadial 1 (~ 16-14.7 kyr BP) at both locations. This increase was linked to higher precipitation in Andes related to a reduction of the Atlantic Meridional Overturning Circulation and meltwater discharge in North Atlantic. In contrast, during Bølling-Allerød (~ 14.7-13 kyr BP), there was an aeolian input increase, associated with stronger winds and lower precipitation that indicate an expansion of the South Pacific Subtropical High. These conditions would correspond to a northern displacement of the Intertropical Convergence Zone-South Subtropical High system associated with a stronger Walker circulation. Our results suggest that variations in river discharge and changes in surface wind intensity in the western margin of South America during the last deglaciation were sensitive to Atlantic Meridional Overturning Circulation variations and Walker circulation on millennial timescales. In the context of global warming, large-scale precipitation and fluvial discharge increases in the Andes related to Atlantic Meridional Overturning

Circulation decline and southward displacement of the Intertropical Convergence Zone should be considered.

2.2. Introduction

The last deglaciation, a period of global warming from the end of the Last Glacial Maximum (LGM, ~ 19 kyr BP) to the early Holocene (11.7 kyr BP), is an outstanding period in Earth's history that allows us a better understanding of the mechanisms regulating regional climatic conditions under global warming (Clark et al., 2012; Shakun et al., 2012). During the last deglaciation, variations in meltwater discharge in the North Atlantic and their consequent impact on the intensity of the Atlantic Meridional Overturing Circulation (AMOC) generated abrupt climatic changes on a millennial-scale (McManus et al., 2004; Mulitza et al., 2017; Ng et al., 2018). The latter resulted in changes in the meridional-oceanic temperature gradient and a meridional shift of the mean annual position of the Intertropical Convergence Zone (ITCZ) (Cheng et al., 2012; Deplazes et al., 2013; Mcgee et al., 2014).

Numerous studies based on continental and marine records have evaluated the effects of meltwater discharge and temperature variations in the North Atlantic on precipitation in Tropical South America, TSA (e.g., Mollier-Vogel et al., 2013; Novello et al., 2017; Mulitza et al., 2017; Stríkis et al., 2015, Bahr et al., 2018). Most studies suggest wetter conditions in this region during cold events in North Hemisphere such as Heinrich Stadial 1 (HS1, ~ 18-14.7 kyr BP) and the Younger Dryas (YD, ~ 12.9-11 kyr BP) linked to a southern displacement of the ITCZ (e.g., Mollier-Vogel et al., 2013; Mulitza et al., 2017; Bahr et al., 2018) and an intensification of the South American Monsoon in its southern domain (Novello et al., 2017; Stríkis et al., 2015) in response to the weakening of the AMOC and increased meltwater discharges into the North Atlantic. Conversely, during the Bølling-Allerød (B-A, 14.7-12.9 kyr BP), a warm period in North Hemisphere, dry conditions developed in TSA (e.g., Mollier-Vogel et al., 2013; Novello et al., 2017; Mulitza et al., 2017) associated with a strong AMOC, a more northerly position of the ITCZ and a weakening of the South American Monsoon.

However, most records covering the last deglaciation come from Eastern South America (e.g., Cruz et al., 2005; Stríkis et al., 2015; Montade et al., 2015; Zhang et al., 2015; Bahr et al., 2018; Novello et al., 2017, Mulitza et al., 2017; Stríkis et al., 2018), while records from the western slope of the Andes (e.g., Baker et al., 2001a, 2001b) and

the Peruvian margin are scarce (e.g., Rein et al., 2005; Mollier-Vogel et al., 2013). Previous attempts to reconstruct changes in precipitation in the western flank of the Andes using marine sediment records show contrasting results. In northern Peru (4ºS), Mollier-Vogel et al. (2013) based on Titanium (Ti) to Calcium (Ca) ratios, suggested an increase in fluvial inputs during HS1 and YD and reduced precipitation during the B-A. However off Callao (12ºS), no difference in fluvial inputs, based on lithic content, between HS1 and BA was reported (Rein et al., 2005). The difference between both records could be due to changes in sediment transport at the two sites and/or to the interpretation of proxies used in these studies. In both studies, Ti/Ca at 4ºS (Mollier-Vogel et al., 2013) and lithic content at 12ºS (Rein et al., 2005) are interpreted as indicators of fluvial inputs. The latter, is generally true in northern Peru, 4ºS, where rainfall can reach 466 mm y-1 (Lagos et al., 2008). However, other processes can be invoked in more arid regions such as central-southern Peru where rainfall is scarce (less than 20 mm y-1) (Lagos et al., 2008). Indeed, Briceño-Zuluaga et al. (2016) showed that, during the last millennium, part of the detrital fraction of marine sediments collected off Pisco was also of aeolian origin. According to Briceño-Zuluaga et al. (2016) aeolian inputs off Pisco can contribute up to almost 50% of the terrigenous fraction during some climatic periods (e.g., the Medieval Climatic Anomaly). These results are based on the grain size distributions of terrigenous components in the sediment.

The grain-size distribution of Peruvian margin sediments is typically polymodal and for that reason provides information on sediment transport mechanisms and/or sediment sources (Briceño-Zuluaga et al., 2016). Aeolian particles diameters are relatively coarser than fluvial ones and if wind intensification occurs, the aeolian flow and the frequency of coarse particles (>36 μm) would increase. Thus, the relative abundance of fluvial particles (6-14 μm) would reflect the precipitation and continental runoff (e.g., Stuut et al., 2002; Stuut and Lamy 2004; Pichevin et al., 2005; Briceño-Zuluaga, et al., 2016; Beuscher et al., 2017). Mathematical methods are used to identify grain-size components of polymodal sediments. For instance, End Member Analysis (EMA) has been widely used to infer changes in fluvial and/or aeolian inputs (e.g., Stuut et al., 2002, 2004, 2007, 2014; Weltje y Prins, 2003; 2007; Pichevin et al., 2005; Holz et al., 2007; Just et al., 2012; Beuscher et al., 2017; Humphries et al., 2017; Jiang et al., 2017).

The aim of this work is to reconstruct at millennial-scale the transport (fluvial and aeolian) and sedimentation of the terrigenous inputs off central-southern Peru (Callao and

Pisco) during the last deglaciation. For this purpose, grain size distributions on surface sediments and sediments cores (M77/2-005-3, Callao and G14, Pisco) were measured and EMA was used to deconvolved them into sub-populations. Using this methodology allows us to discriminate the different sources of terrigenous input, reconstructing the variations of fluvial and aeolian inputs dependent on changes in precipitation and winds intensity. On other hand, surface sediments were collected for grain size analyses during normal conditions and during the 2017 Coastal El Niño (April 2017), the latter characterized by increased river discharges (Guzman et al., 2020) and variations of surface winds in Peru (Echevin et al., 2018). These observations allow us to understand the effect of changes in precipitation and winds on grain-size distribution during periods of different climatic conditions. In addition, we used as a proxy for fluvial vs aeolian inputs the Titanium/Zirconium (Ti/Zr) record from X-Ray Fluorescence (XRF) analysis of the 106KL core collected off Callao and described by Rein et al. (2005). We postulate that changes in the AMOC intensity have modulated the variability of winds and precipitation in the Western TSA, as inferred by changes in the grain size distribution of marine sediment particles, at millennial time-scales. Our work provides new information on sedimentation, types of transport and sources of terrigenous inputs on the Peruvian margin during the last deglaciation, offering the possibility to better understand the mechanisms modulating these processes during past periods of global warming.

2.2.1. Regional setting

We focus on the central-southern part (12-14ºS) of the Peruvian margin. Callao and Pisco are located onshore of the Lima Basin (Suess et al., 1987). This basin exhibits high productivity and anoxic conditions favored by an intense Oxygen Minimum Zone; hence sediments are composed of fine grains, are rich in organic matter and contain abundant diatoms. The general absence of bioturbation in some areas and during some time periods allows the preservation of laminations and therefore their use as palaeoceanographic records (e.g., Rein et al., 2005; Sifeddine et al., 2008; Gutiérrez et al., 2006, 2009, 2011; Briceño-Zuluaga et al., 2016; Salvatteci et al., 2014a, 2016, 2019). In Callao, muddy laminated areas are reported (Reinhardt et al., 2002), but sedimentary records collected in the OMZ core, off Pisco, show more continuous laminations than the records collected off Callao (e.g., Salvatteci et al., 2016, 2019).

The main transport of the detrital fraction of coarse silt and sand to the hemipelagic sediments in the Peruvian margin is by the action of winds (Scheidegger and Krissek, 1982). In contrast to Callao, Pisco is characterized by the presence of large coastal deserts, extreme aridity and dust storms known as Paracas winds. During these sporadic sand storms wind velocities can exceed 10-15 m/s (Briceño-Zuluaga et al., 2017). These storms are produced by a local intensification of alongshore surface wind and by alongshore pressure gradients (Briceño-Zuluaga et al., 2017). Also, in Pisco, an intense coastal upwelling linked to strong alongshore surface wind occurs (Dewitte et al., 2011; Gutiérrez et al., 2011; Rahn and Garreaud, 2013). The intensity of alongshore surface winds presents a seasonal variability, with stronger winds during winter and weaker winds during summer (Fig. 1). This seasonality is linked regionally to the displacements of the ITCZ-South Pacific Subtropical High (SPSH) system and locally to continental-oceanic and alongshore pressure gradients (Strub et al., 1998; Gutiérrez et al., 2011; Chamorro et al., 2018). In contrast to the coarser particles transported by winds, large quantities of quartz-rich silt and clays are transported by rivers to the continental shelf (Scheidegger and Krissek, 1982). The central-southern Peruvian coast is characterized by very low annual precipitations (Callao,14 mm y-1 and Pisco, 2 mm y-1) and scarce flows of coastal rivers (Lagos et al., 2008). However, during summer there is an increase in river discharges associated with increased monsoon precipitation in the Andes (Garreaud et al., 2009; Vuille et al., 2012). Occasional floods occur and higher sediment discharges are associated with intense precipitation during extreme El Niño events (Bourrel et al., 2015; Morera et al., 2017; Rau et al., 2016; Guzman et al., 2020).

Aeolian clays and silts are transported offshore by trade winds (Saukel et al., 2011), while coarser particles (e.g., > 40 μm) settle in the ocean on the continental shelf (Scheidegger and Krissek, 1982). Once in the water column, dispersion patterns of clays (< 4 μm) and fine silts (8-11 μm) coincide with the surface and subsurface currents, while the coarser fraction presents limited dispersion near the coast (Scheidegger and Krissek, 1982). Likewise, near-bottom processes and bottom topography exert considerable control over the dispersal of hemipelagic sediments on the Peruvian margin (Scheidegger and Krissek, 1982).

2.3. Materials and methods

2.3.1. Surface sediments, marine core and age model

Surface sediments (0-0.5 cm) were collected in front of Callao and Pisco by the Instituto del Mar del Peru during the years 2015 (December), 2016 (August and December) and 2017 (February, April and August) along transects perpendicular to the coast (Fig. S1). Details on the sampling sites are given in Table S1. Samples collected in April 2017 coincided with the occurrence of a coastal El Niño event, and will be considered as representative of "Coastal El Niño" conditions hereafter. All the other samples will represent "normal" conditions.

The core M77/2-005-3, was retrieved from the Southeast Pacific continental slope (12º05 S, 77º40,07 W, 214 m water depth, 1336 cm long) during the M77-2 expedition in 2008 (Fig. 1). Because we focus on the last deglaciation period, we worked with the section from 0 to 700 cm core depth. A first depth-age model based on four ^{14}C ages was built in Salvatteci et al. (2019). In this study, we added twenty-two ^{14}C ages and developed a new age depth-model (Table S2). Radiocarbon measurements were performed on bulk sediment at the Laboratoire de Mesures du Carbone-14 (LMC14, Gif-sur Yvette, France). Ortlieb et al. (2011) reported a regional reservoir effect (ΔR) of 511 ± 278 years for Early Holocene (10.4-6.8 kyr) and in the absence of ΔR data for older period we use this value to calibrated the ^{14}C measurements for the last deglaciation as in Salvatteci et al. (2016, 2019). In order to construct the age model, we used the maximum probability ages obtained from the CALIB 8.1 software. The chronological model indicates that the examined section (0-700 cm) of core M77/2-005-3 (Fig. S2) recorded the LGM and the last deglaciation (22-13 kyr BP; 95-700 cm). Core M77/2-005-3 presents a hiatus at 94 cm and thus great part of the Holocene is missing.

Core G14 (14ºS, 76ºW, 390 m water depth) was retrieved during the Galathea-3 expedition in 2007 (Salvatteci et al., 2016). Radiocarbon dates of G14 were published in Salvatteci et al. (2016). For this study, a new depth-age model was developed with an updated calibration using the CALIB 8.1 software. The upper part of sediment layers was not recovered in G14 which ranges from 13.4 to 24.6 kyr BP (Fig. S2).

The lithological description of M77/2-005-3 and G14 is available in Salvatteci et al. (2016, 2019). M77/2-005-3 and G14 cores show laminated and banded sediments with no evident signs of major discontinuities during the last deglaciation (Salvatteci et al.,

2016, 2019). G14 core presents more continuous laminated packaged in comparison to M72/2-005-3 core. (Salvatteci et al., 2016, 2019).

In order to compare our new data from cores M77/2-005-3 and G14 with previously published records in the area we modified the age model of core 106 KL (Rein et al., 2005). Core 106 KL (12°030S, 77°39.80W, 184 m water depth) was retrieved during cruise SONNE 147 (Rein et al., 2004, 2005). Chronology model and lithology were fully described in Rein et al. (2004, 2005). A new depth-age model was developed with an updated calibration using the CALIB 8.1 software (Fig. S2) and we only used the sections covering the last deglaciation.

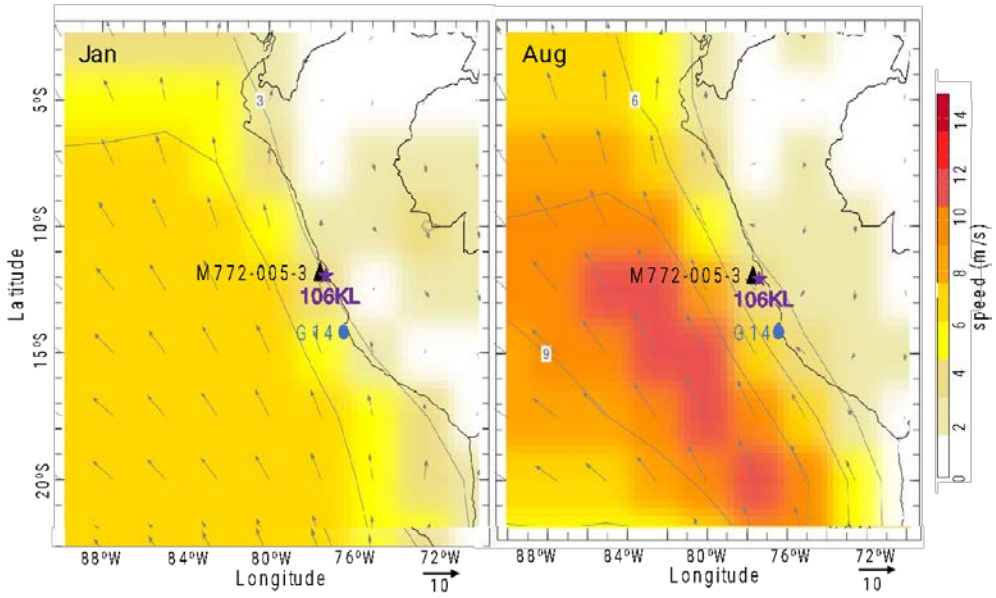

Figure 1. (A) Location of the sampling of the sediment cores M77/2-005-3, 106Kl and G14 core. Average wind speed (m/s) at 1000 hPa in January and August (http://iridl.ldeo.columbia.edu).

2.3.2. Grain-size distribution and end-member analysis

In order to reduce the effect of resuspension of particles that can produce artificial results, only laminated and banded sequences were subsampled for grain-size distribution analysis. Reworked sediments are widespread in the marine sediment records off Peru and can be distinguished from well-preserved sediments using X-ray images (Salvatteci et al., 2014b). For both surface and core sediment samples, in order to isolate the terrigenous fraction, we followed the procedure described in Briceño-Zuluaga et al. (2016). Organic matter, calcium carbonates and biogenic silica were successively removed with hydrogen peroxide (H_2O_2 30% at 60ºC for 3 to 4 days), hydrochloric acid

(HCl 10% for 12h) and sodium carbonate (Na_2CO_3, 1M at 90ºC for 3h), respectively. The grain size distribution was then measured using an automated image analysis system (model FPIA3000, Malvern Instruments) with a measurement range of 0.5-200 μm. Further details on the FPIA3000 are described in Flores-Aqueveque et al. (2014) and Briceño-Zuluaga et al. (2016). Given that only particles smaller than 200 μm can be measured under the analytical conditions applied in this work, all samples were sieved with a 200 μm mesh before being analyzed. Particles larger than 200 μm were not recovered in any sample, thus we consider that our analysis covers the full range of grain size present in the surface and cores sediments.

AnalySize modelling algorithm (Paterson and Heslop, 2015), which is based on the unmixing performed in hyperspectral image analysis, was used to unmix the grain-size distribution. The algorithm claims to establish a physical mixing model that transforms the measured grain-size distribution to a limited number of unimodal grain-size end members. The coefficient of determination (r^2) which represents the proportion of the variance of each grain size class is calculated to estimate the minimum number of end members necessary. More specific details are available from Paterson and Heslop (2015).

2.3.3. XRF analysis

The piston core KL 106 was analyzed with an Avaatech XRF Core Scanner at the Marum Center (Bremen). Here XRF scanning was done for 19 elements at 2-mm intervals. Ti is an aluminum/silicate-related element and is associated with clay minerals transported from the continent to the ocean through river discharges (Jansen et al., 1998; Yarincik et al., 2000). For this reason, Ti is employed as a proxy for river discharge (e.g., Haug et al., 2001). In contrast, Zr is predominantly enriched in heavy mineral species, in particular zircon. The latter is broadly distributed in natural sediments and typically has relatively coarse grain size (Pettijohn, 1941). Zr has been widely used in studies such proxy of mean depositional grain-size variations (e.g., Dypvik and Harris, 2001; Wu et al., 2020). Therefore, Zr-rich sand can be used as a potential proxy for aeolian input. As a consequence of the above, we used the logarithm of the ratio of Ti to Zr intensity (counts per second) as a potential proxy for fluvial versus aeolian input.

2.4. Results

2.4.1. Grain-size distribution of the surface sediments

The grain-size distribution of all surface samples collected at the stations in Callao and Pisco are shown in Figure 2. In Callao and Pisco, during normal conditions, the abundance of fine particles (< 10 µm) is higher at the deepest and furthest off shore station than at coastal stations, while, coarse particles (60-120 µm) are more abundant close to the coast (Fig. 2). Coarser particles are deposited mainly on the inner continental shelf due to their weight. During the 2017 Coastal El Niño, a strong increase in fine particles (< 10 µm) abundance was found only at station E2 (Fig. 2a) in Callao. On the other hand, the abundance of the coarse fraction (50-100 µm) in the sediments from the most distant stations (E12 and E11) increased in Pisco (Fig. 2d and 2e).

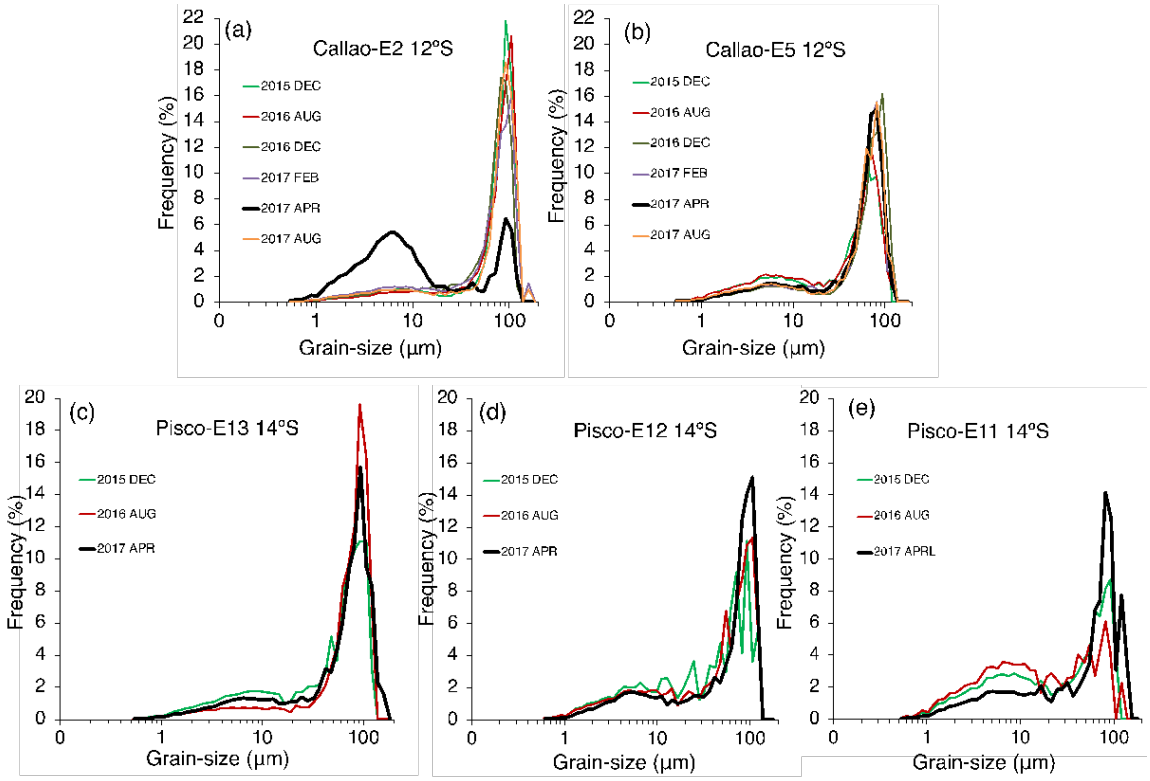

Figure 2. Grain-size distribution of surface sediments in Callao (a, b) and Pisco stations (c, d, e).

2.4.2. Grain-size distribution of the marine core

The mean grain-size distribution per climatic period analyzed is shown in figure 3a and 3b. During the Late HS1 (16-14.7 kyr BP), the abundance of fine particles (< 10

µm) is higher than during the Early HS1 (18-16 kyr BP) and B-A in Callao and Pisco (Fig. 3a and 3b). This increase is more marked in Callao (Fig. 3a). On the other hand, during the B-A (14.7-13 kyr BP), the sediments are characterized by high abundance of coarser particles (Fig 3a and 3b).

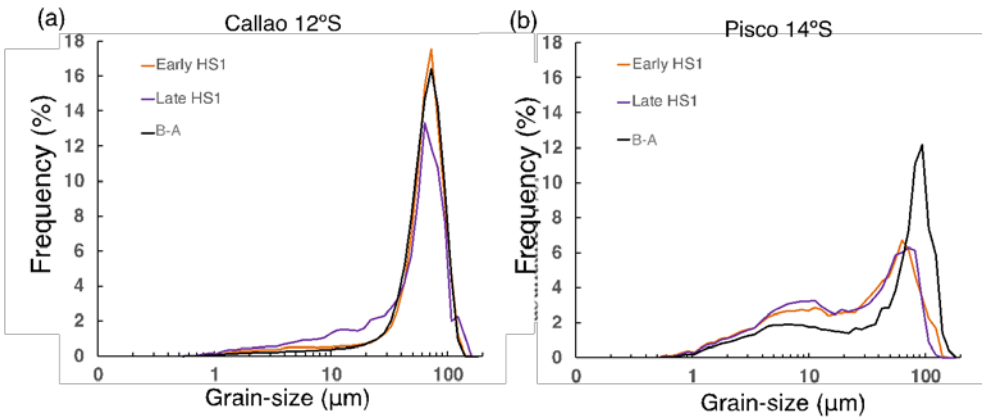

Figure 3. Mean Grain-size distribution by climatic period in Callao (a) and Pisco (b).

2.4.3. End-member analysis

Based on a multiple correlation coefficient, a model with 4 end members was chosen in Callao and Pisco, explaining 98% and 95% of the variance of the grain-size distribution data set respectively (Fig. 4a and 4b). The measured and modeled grain size distribution are highly correlated (R^2: 0.86-0.99) for each analyzed sample, attesting that the use of 4 end-members is appropriate for our interpretation. Although a model with 2 end-member model explains 95% of the variance of the data in Callao, the variability of each end-members contribution is different (Fig. 5) suggesting that each end member indicates different processes or sources (Fig. 5). Each of the 4 end members (EM) presents a unimodal distribution, its median being respectively at 11 µm (EM1), 58 µm (EM2), 77 µm (EM3) and 101 µm (EM4) in Callao (Fig. 4c). In Pisco, each EM is represented by a unimodal distribution centered at 10 µm (EM1), 52 µm (EM2), 75 µm (EM3) and 94 µm (EM4) (Fig. 4d).

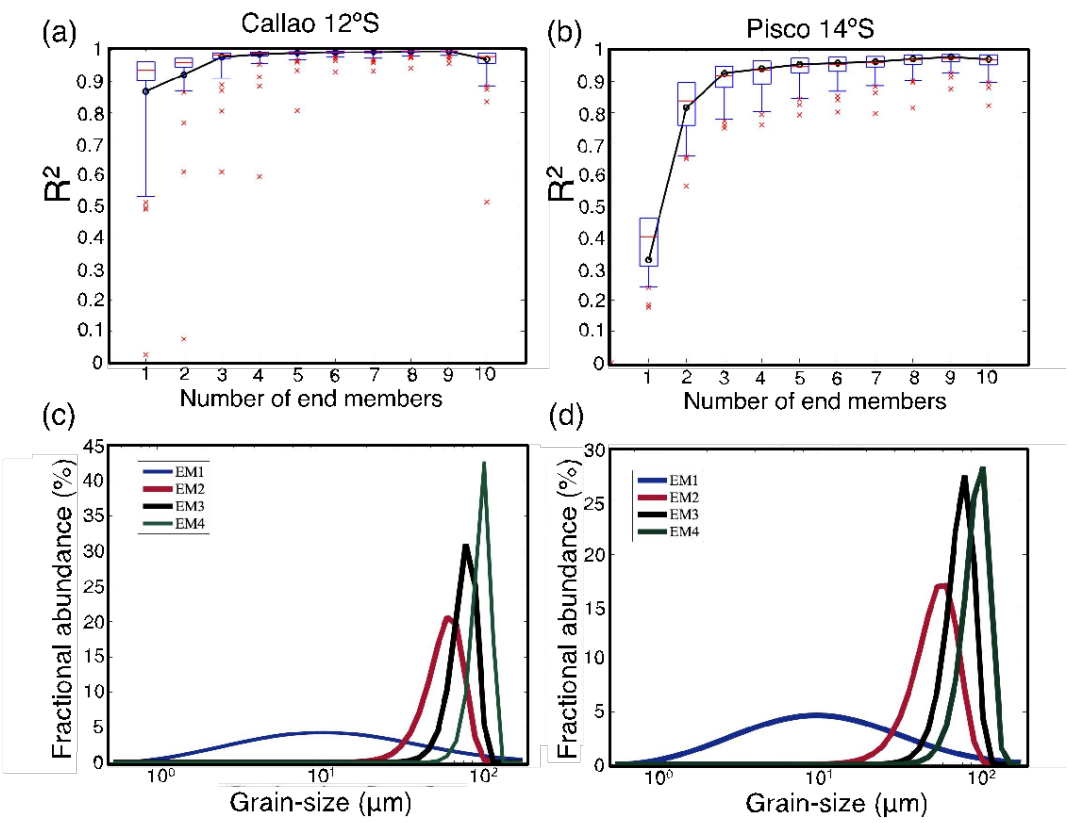

Figure 4. Coefficient of determination (r2) as a function of the number of end members chosen to model the observed grain-size distribution in Callao (a) and Pisco (b). Grain size distribution of the 4 end-members in Callao (c) and Pisco (d).

2.4.4. XRF analysis

In Callao, the Ti/Zr record from core 106KL indicate an increase of fluvial discharge during the HS1 with higher fluvial discharge between ~15.5-14.9 kyr BP and decrease of fluvial inputs afterwards, during the B-A (Fig. 6f).

2.5. Discussion

2.5.1. Assignment of end-members

The terrigenous materials deposited on the Peruvian margin are transported by rivers and by wind activity, however, there are also other diffused sources, such as the material produced by coastal erosion transported offshore by marine currents. The terrigenous sediments in Callao and Pisco are multimodal which suggest that different processes are involved in the transport and deposition of these sediments. In both cores, we observed one end-member corresponding to a fine fraction (EM1) and three end-

members to coarse fractions (EM2, EM3 and EM4). A previous study in Pisco used the variations of fine (10 μm) and coarse (50 μm and 100 μm) particles as proxies of river discharge and aeolian inputs respectively for the last few centuries (Briceño-Zuluaga et al., 2016). However, the differences in the aeolian sources, shelf and slope morphology, currents intensity and hydrodynamics between Callao and Pisco, may modify the interpretation of the proxies described by Briceño-Zuluaga et al. (2016).

EM1 shows a mode at 11 μm and 10 μm in Callao and Pisco respectively that we interpret as a proxy for fluvial source, based on our interpretations and the literature (e.g., Stuut and Lamy, 2004; Stuut et al., 2007; Briceño-Zuluaga et al., 2016; Beuscher et al., 2017). Previous studies in the Pisco area for the last few centuries suggest that abundance of fine particles (~ 10 μm) can be used as a proxy for fluvial inputs and precipitation patterns (Briceño-Zuluaga et al., 2016). The increase of fine particles (<10 μm) and EM1 contribution in surface marine sediments (Fig. 2a and Fig. 5a) associated with local high fluvial discharges in Callao during the 2017 Coastal El Niño (Guzman et al., 2020) corroborates the use of variations in the abundance of fine particles as an indicator of fluvial inputs. These results are consistent with the grain size of fine particles (~ 6-14 μm) in marine cores associated with river inputs reported in different areas of the world (e.g., Stuut and Lamy, 2004; Stuut et al., 2007; Beuscher et al., 2017).

Previous studies in South Eastern Pacific used the abundance and fluxes of coarse particles (~ 36-100 μm) in marine sediments as a proxy for wind intensity linked to the expansion/contraction of the SPSH (e.g., Flores-Aqueveque et al., 2015; Briceño-Zuluaga et al., 2016). Based on HYSPLIT (Hybrid Single-Particle Lagrangian Integrated Trajectory) simulations, Briceño-Zuluaga et al. (2017) showed that coarse particles (50-90 μm) can directly reach the continental shelf in Pisco during Paracas storms (characterized by wind velocities surpassing 10-15 m/s).

The end members associated with the coarse fraction present similar modes in Callao and Pisco sediments (EM2, ~ 55 μm, EM3, ~ 75 μm and EM4, ~ 90-100 μm). Pisco is characterized by a large coastal desert and frequent dust storms. Also, since the shelf at Pisco is narrow, the distance from terrestrial sources that can be transported by winds did not vary significantly during the deglaciation compared to modern conditions. Based on this, particles between 50-90 μm (EM2, EM3 and EM4) are interpreted as indicators of aeolian input, as proposed by Briceño-Zuluaga et al. (2016). An increment of the coarse particle abundance in Pisco's surface sediments was recorded in the stations

most distant from the coast E12 and E11 during April 2017 (Fig. 2d and 2e), when alongshore wind stress was anomalously enhanced at the mature phase of the Coastal El Niño, particularly off central and southern Peru (Echevin et al., 2018). This observation supports the hypothesis that these particles have an aeolian origin and the increase of their contribution suggests that during events with stronger alongshore winds, these particles can be transported to a greater distance than during normal conditions, modifying their amplitude in the sediments. It is important to note that the number of surface sediment samples in Pisco was small, however a change in the abundance of the coarse fraction was recorded during April 2017 (Fig. 2d and 2e). Finally, although EM2, EM3 and EM4 reflect an aeolian source, their contributions variations during the last deglaciation were different (Fig. 5b). This is possibly explained by changes in wind intensity. Periods with stronger (weaker) winds result in an increase (decrease) in the amplitude of coarser particles.

In Callao, the context is different, since there are no large deserts near the coast and dust storms are rare, it is unlikely for ~ 100 μm particles (EM4) to be transported directly to the sampling site. The presence of ~100 μm particles is possibly linked to bottom hydrodynamic processes. Indeed, during events of higher hydrodynamic energy, resuspension of fine particles and increase in the relative frequency of coarser particles are expected. EM4 (101 μm) does not show drastic changes during the last deglaciation, suggesting that it does not influence the relative contribution of the other modes at millennial-scale (Fig. 5a).

EM2 (58 μm) is the dominant mode in Callao ranging from 40 to 80% (Fig. 5a). Although these coarse sediments can be transported by winds (Briceño-Zuluaga et al., 2016, 2017), it is unlikely that this high percentage of coarse particles could be solely transported by the wind directly to the sampling site off Callao. It is more likely that ~ 58 μm particles derive from different sources (winds, coastal erosion) and are distributed on the continental shelf by the Peru-Chile Undercurrent (Reinhardt et al., 2002).

During the Coastal Niño April 2017 event, we observed that at the E5 station (55 km offshore from the coast line), only the contribution of ~ 77 μm particles (EM3) increased (Fig. 5a), probably as a result of more intense alongshore winds. On the other hand, the relative stability of the EM2 (58 μm) and EM4 (101 μm) contributions show that these modes are not sensitive to wind intensity and probably respond to other processes (Fig. 5a). On the opposite, EM3 appears as the best proxy of a wind source. In

summary, in Callao, we propose that changes in the contribution of EM3 suggest changes in aeolian inputs and wind intensity, while changes in the contribution of EM2 and EM4 are associated with other processes associated with diffuse sources and hydrodynamic energy.

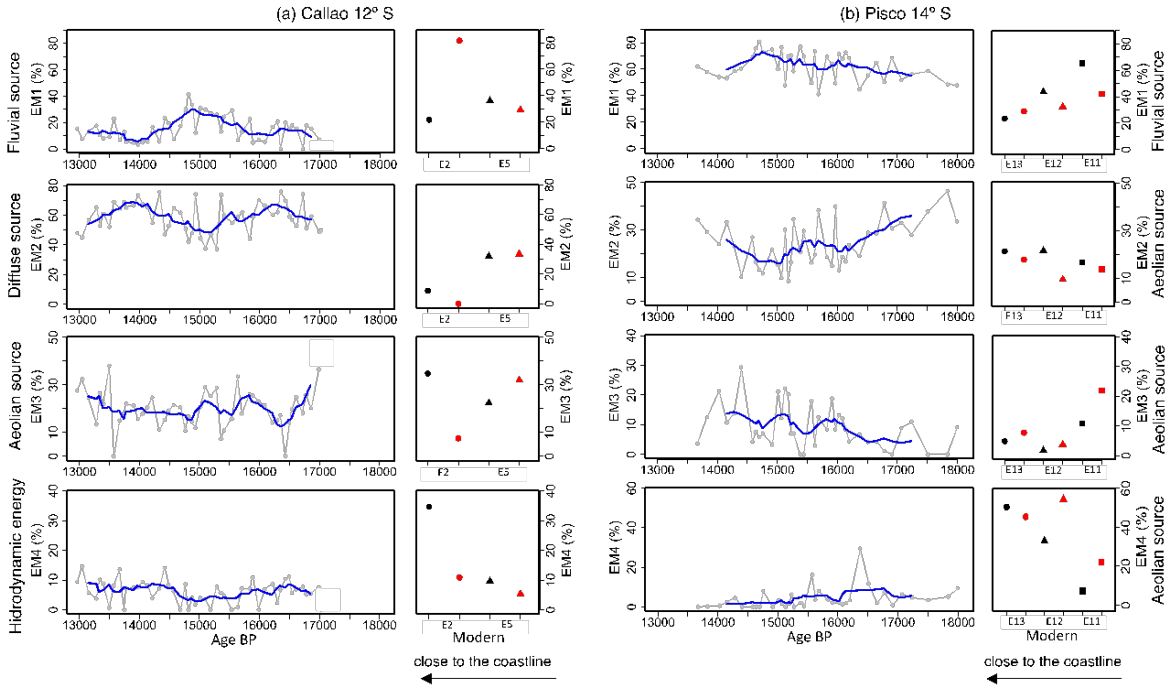

Figure 5. Variation in contribution of the grain size end-members from marine cores and surface sediments in Callao (a) and Pisco (b). The Modern period is represented by the mean end-member contribution of surface sediments collected during normal conditions (black symbols) and Coastal El Niño April 2017 event (red symbols).

2.5.2. Millennial variability of fluvial and aeolian inputs during the last deglaciation

The analysis of end-members allows a quantification of the main granulometric modes, however, as the sum of the contribution of the modes corresponds to 100%, it is difficult to consider the modes individually since the increase of one may reduce the others and influence their contribution variability. Thus, for a better visualization, a ratio between end-members indicative of a fluvial (EM1 in Callao and Pisco) and aeolian (EM3 in Callao and the sum of EM2, EM3 and EM4 in Pisco) source will be used as a proxy of the variations in the fluvial and aeolian inputs.

An increase in fluvial inputs based on the grain-size and end-member analysis was observed during the Late HS1 (~16-14.7 kyr BP) with maximum values between ~15.5-14.7 kyr BP in Callao (M77/2-005-3) and Pisco (G14) (Fig. 6g and 6h). Likewise, the Ti

/Zr record in Callao (106KL) indicates an increase in fluvial input during HS1, with maximum discharges between ~15.5-14.9 kyr BP. These observations support the idea that Ti, linked to the fine fraction of marine sediments, is mainly transported by rivers to the Peruvian margin and can be used as a proxy of river discharge and precipitation (e.g., Mollier-Vogel et al., 2013; Salvatteci et al., 2014; Fleury et al., 2015).

The contrasting differences between our record of fluvial input (based on grain size and Ti/Zr) and the record of lithic content based on reflectance (Rein et al., 2005) in Callao can be explained by the difference in methodology and interpretation of the proxies. Rein et al. (2005) interpret the lithic content as a proxy for river discharges, however, as observed in our data (Fig. 5) and the literature (Briceño-Zuluaga et al., 2016), the terrigenous material can be transported to the central-southern Peruvian margin by different sources (e.g., fluvial and aeolian) and the variability of fluvial and aeolian transport follow different patterns and therefore respond to different forcing.

Since heavy precipitation associated with the El Niño events in Callao and Pisco coastal regions are occasional, a larger average fluvial discharge in Callao and Pisco is likely related to precipitation fluctuations at higher elevations in the watersheds, in the Andes. Previous studies suggest a correlation between North Atlantic cooling and massive meltwater discharges with increased precipitation in the Central Andes (Baker et al., 2001a, 2001b; Blard et al., 2011, Martin et al., 2018; González-Pinilla et al., 2021). During the last deglaciation, cooling in the North Atlantic and higher meltwater discharges generated a weakening of the AMOC (MacManus et al., 2004; Mulitza et al., 2017; Ng et al., 2018). The latter generated an interhemispheric temperature contrast and an impact on precipitation in the central Andes associated with a southward shift of the ITCZ and an intensification of the South American Monsoon in different regions: Central Andes (Baker et al., 2001a, 2001b, Blard et al., 2011; Gonzalez-Pinilla et al. 2021), southeast (Cruz et al. 2005; Stríkis et al., 2015) and southwest Brazil (Novello et al., 2017) and in western Amazonia (Sublette Mosblech et al., 2012; Cheng et al., 2013). Indeed, the higher river discharges we evidenced in Callao and Pisco during Late HS1 (~16-14.7 kyr BP) occurred simultaneously with the well-dated highstand of the giant paleolake Tauca (~16.6-14.5 kyr BP) (Martin et al., 2018). Therefore, the increase and decrease of river discharges in central Peru during HS1 and B-A, respectively, would be explained by changes in precipitation in the Andes in response to changes in the intensity of the AMOC and meltwater pulses in the North Atlantic.

During the last decades, the seasonal ITCZ have shifted poleward in South Pacific and generally narrowed and strengthened (Zhou et al., 2020). A recent study suggests a narrowing and southward shift of ITCZ in Eastern Pacific in response to the SSP3-7.0 scenario by 2100 (Mamalakis et al., 2021). Although there are uncertainties about the effects of current global warming on AMOC intensity, there is evidence of AMOC slowing over the last century (Rahmstorf et al., 2015; Caesar et al., 2018) and in climate model simulations of future climate change, AMOC is projected to decline generating a southward displacement of the ITCZ (Bellomo et al., 2021). In the context of global warming, a large-scale precipitation and fluvial discharge increases in Peru related to AMOC decline and southward displacement of the ITCZ should be considered.

Concerning the variations of the aeolian inputs and surface wind intensity in the Peruvian margin, changes in the intensity of Walker Circulation and meridional displacements of the ITCZ-SPSH system have been proposed as mechanisms to regulate surface alongshore winds and upwelling dynamics in the Humboldt Current System at multiple timescales (e.g., Gutiérrez et al., 2009; Briceño-Zuluaga et al., 2016; Salvatteci et al., 2014, 2019). On centennial timescales, a northern displacement of the SPSH-ITCZ, in response to stronger Walker circulation produce an increase of alongshore winds and upwelling in Central-South Peruvian margin (Salvatteci et al., 2014; Briceño-Zuluaga et al., 2016). SST proxies indicate an increase of the zonal SST gradient in the equatorial Pacific suggesting a more intense Walker circulation in B-A than during HS1 (Fig. 7a) (Koutavas and Joanides, 2012). Moreover, a northern displacement of the ITCZ was also recorded during B-A. (Peterson et al., 2000; Deplazes et al., 2013). These conditions should have provoked the increase of alongshore winds and aeolian supply in central Peru during B-A. Indeed, in Callao and Pisco, the aeolian inputs was the main transport from 14.7 to 13 kyr BP suggesting, at regional-scale, an increase of alongshore wind and upwelling in Central-South Peru and an expansion of the SPSH (Fig. 7d and 7e). Our record of surface wind intensity variations and an alkenone-derived SST reconstruction based on alkenones (Salvatteci et al., 2019) in the same core collected in Callao show similar trends (Fig. 7c). During HS1, a short cooling between 16 and 15.5 kyr BP, coincided with stronger alongshore winds (Fig. 7c and d). In addition, during the B-A, a cooling at 14.7-13 kyr BP, stronger aeolian transport associated with more intense alongshore winds occurred (Fig. 7c and 7d). These observations suggest that local processes such as upwelling variations in response to changes in alongshore wind intensity may control SST variations during the last deglaciation, in addition to other

process like the advection of the Southern Ocean and Antarctic climate signals by the Humboldt Current.

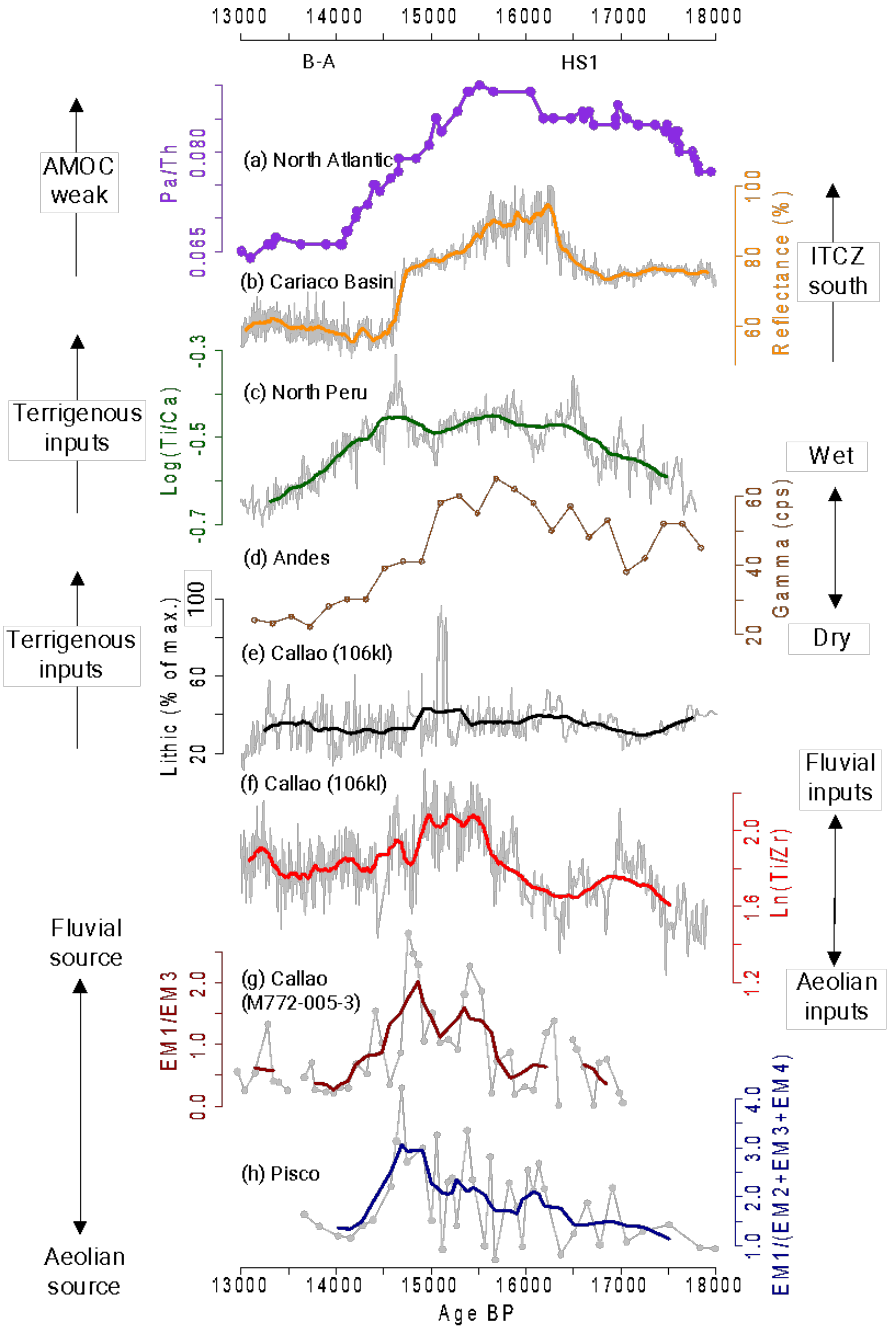

Figure 6. (a) Composite $^{231}Pa/^{230}Th$ record that reflect past changes in AMOC (Ng et al., 2018). (b) Reflectance (%) from Cariaco Basin as a proxy for the latitudinal displacement of the ITCZ (Deplazes et al., 2013). (c) Log (Ti/Ca) for core M77/2-059 from northern Peru (4º S) (Mollier-Vogel et al., 2003). (d) Natural γ-radiation as a proxy for effective moisture in Tropical Andes (Baker et al., 2021b). (e) Relative concentration of lithics for core 106Kl from Callao (Rein et al, 2005). (f) Ln (Ti/Zr) as a proxy for fluvial vs aeolian inputs in core 106KL from Callao (this study). (g) EM1/EM2 ratio as a proxy for fluvial and aeolian source in Callao (this study). (h) EM1/(EM2+EM3+EM4) ratio as a proxy for fluvial and aeolian source in Callao (this study).

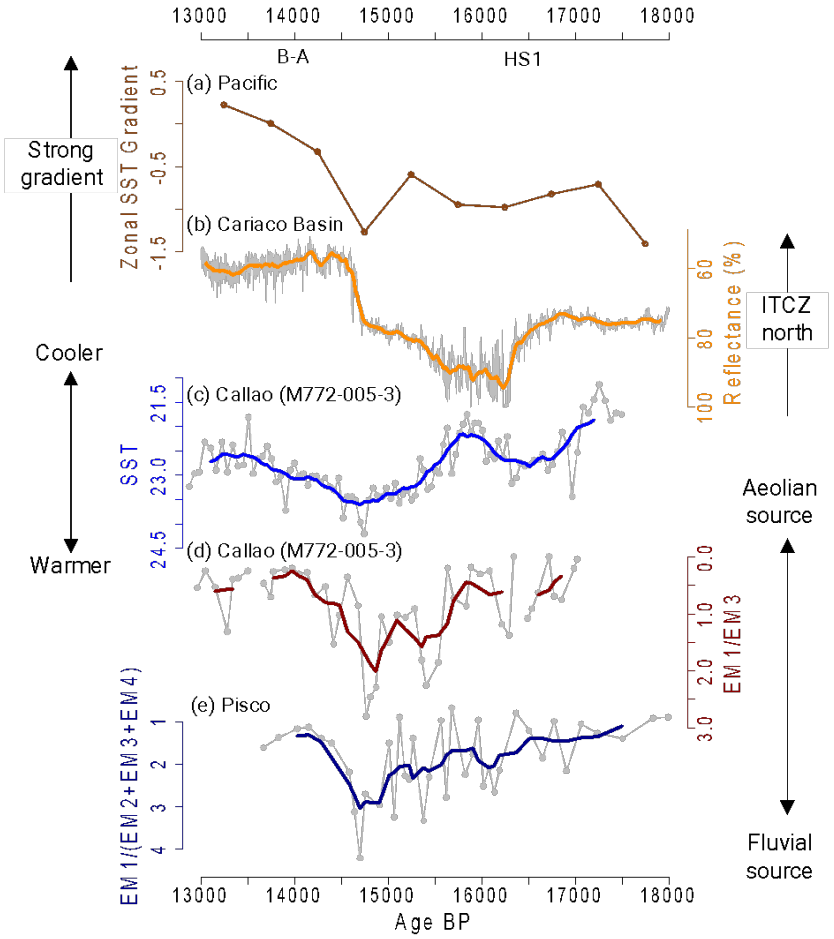

Figure 7. (a) Zonal SST gradient anomaly during the last deglaciation calculated as the difference between western and eastern Pacific averages (Koutavas and Joanides, 2012). (b) Reflectance (%) from Cariaco Basin as a proxy for the latitudinal displacement of the ITCZ (Deplazes et al., 2013). (c) Alkenone-derived near surface temperature from M77/2-005-3 core, Callao (Salvatteci et al., 2019). (d) EM1/EM2 ratio (Reversal scale) as a proxy for fluvial and aeolian source in Callao (this study). (e) EM1/(EM2+EM3+EM4) ratio (Reversal scale) as a proxy for fluvial and aeolian source in Pisco (this study).

2.6. Conclusion

The variability of the grain size distribution of marine sediments from the central-southern Peruvian margin (12ºS and 14ºS) reveals millennial-scale changes in the transport and sedimentation processes of the terrigenous material during the last deglaciation (18-13 kyr BP). We identified four granulometric end-members for both Callao and Pisco sediments, each of them reflecting different processes and sources and whose interpretation must consider regional contexts. In the case of the Pisco core, located within the range of the aeolian inputs, as it has been shown earlier, the modes (EM2 to EM4) correspond to aeolian origin. In the case of Callao core, located further from the

coast and where sources of eolian particles are scarce, the EM2 and EM4 modes are interpreted as reflecting local hydrodynamics, while EM3 represents the eolian supply. Our results support a tight relationship between high latitude forcing and precipitation in the western flank of the Andes during the last deglaciation. During late HS1 (16-15 kyr BP), enhanced fluvial inputs in Callao and Pisco occurred associated with higher precipitation in Central Andes in response to the slowdown of AMOC and meltwater discharge in North Atlantic. Finally, the increase in aeolian input during the B-A, could be a result of stronger alongshore winds linked to a northern displacement of the ITCZ-SPSH system in response to a strong gradient of the Walker circulation. There is still uncertainty about the effects of current Climate Change, there is evidence of a slowing of the AMOC over the past century and in future climate model simulations. In the latter, the decline in AMOC is accompanied by a southward shift in the ITCZ. Thus, we can probably expect an increase in precipitation and river flow in the future in Peru.

2.7. References

Bahr, A., Hoffmann, J., Schönfeld, J., Schmidt, M., Nürnberg, D., Batenburg, S. and Voigt, S.: Low-latitude expressions of high-latitude forcing during Heinrich Stadial 1 and the Younger Dryas in northern South America, Global and Planetary Change, 160, 1-9, doi:10.1016/j.gloplacha.2017.11.008, 2018.

Baker, P. A., Seltzer, G. O., Fritz, S. C., Dunbar, R. B., Grove, M. J., Tapia, P. M., Cross, S. L., Rowe, H. D. and Broda, J. P: The History of South American Tropical Precipitation for the Past 25,000 Years. Science, 291(5504), 640–643, doi:10.1126/science.291.5504.640, 2001a.

Baker, P., Rigsby, C., Seltzer, G., Fritz, S., Lowenstein, T., Bacher, N. and Veliz, C.: Tropical climate changes at millennial and orbital timescales on the Bolivian Altiplano, Nature, 409(6821), 698-701, doi:10.1038/35055524, 2001b.

Blard, P., Sylvestre, F., Tripati, A., Claude, C., Causse, C., Coudrain, A., Condom, T., Seidel, J., Vimeux, F., Moreau, C., Dumoulin, J. and Lavé, J.: Lake highstands on the Altiplano (Tropical Andes) contemporaneous with Heinrich 1 and the Younger Dryas: new insights from 14C, U–Th dating and δ18O of carbonates, Quaternary Science Reviews, 30(27-28), 3973-3989, doi:10.1016/j.quascirev.2011.11.001, 2011.

Beuscher, S., Krüger, S., Ehrmann, W., Schmiedl, G., Milker, Y., Arz, H. and Schulz, H.: End-member modelling as a tool for climate reconstruction—An Eastern Mediterranean case study, PLoS ONE, 12(9), e0185136, doi:10.1371/journal.pone.0185136, 2017.

Bellomo, K., Angeloni, M., Corti, S. and von Hardenberg, J.: Future climate change shaped by inter-model differences in Atlantic meridional overturning circulation response, Nature Communications, 12(1), doi:10.1038/s41467-021-24015-w, 2021.

Bourrel, L., Rau, P., Dewitte, B., Labat, D., Lavado, W., Coutaud, A., Vera, A., Alvarado, A. and Ordoñez, J.: Low-frequency modulation and trend of the relationship between ENSO and precipitation along the northern to centre Peruvian Pacific coast, Hydrological Processes, 29(6), 1252-1266, doi:10.1002/hyp.10247, 2014.

Briceño-Zuluaga, F. J., Sifeddine, A., Caquineau, S., Cardich, J., Salvatteci, R., Gutierrez, D., Ortlieb, L., Velazco, F., Boucher, H. and Machado, C.: Terrigenous material supply to the Peruvian central continental shelf (Pisco, 14° S) during the last 1000 years: paleoclimatic implications, Clim. Past, 12(3), 787–798, doi:10.5194/cp-12-787-2016, 2016.

Briceño-Zuluaga, F., Castagna, A., Rutllant, J. A., Flores-Aqueveque, V., Caquineau, S., Sifeddine, A., Velazco, F., Gutierrez, D. and Cardich, J.: Paracas dust storms: Sources, trajectories and associated meteorological conditions, Atmospheric Environment, 165, 99–110, doi:10.1016/j.atmosenv.2017.06.019, 2017.

Caesar, L., Rahmstorf, S., Robinson, A., Feulner, G. and Saba, V.: Observed fingerprint of a weakening Atlantic Ocean overturning circulation, Nature, 556(7700), 191-196, doi:10.1038/s41586-018-0006-5, 2018.

Chamorro, A., Echevin, V., Colas, F., Oerder, V., Tam, J. and Quispe-Ccalluari, C.: Mechanisms of the intensification of the upwelling-favorable winds during El Niño 1997–1998 in the Peruvian upwelling system, Climate Dynamics, 51(9-10), 3717-3733, doi:10.1007/s00382-018-4106-6, 2018.

Cheng, H., Sinha, A., Cruz, F., Wang, X., Edwards, R., d'Horta, F., Ribas, C., Vuille, M., Stott, L. and Auler, A.: Climate change patterns in Amazonia and biodiversity, Nature Communications, 4(1), doi:10.1038/ncomms2415, 2013.

Cheng, H., Sinha, A., Wang, X., Cruz, F. W. and Edwards, R. L.: The Global Paleomonsoon as seen through speleothem records from Asia and the Americas, Clim Dyn, 39(5), 1045–1062, doi:10.1007/s00382-012-1363-7, 2012.

Clark, P. U., Shakun, J. D., Baker, P. A., Bartlein, P. J., Brewer, S., Brook, E., Carlson, A. E., Cheng, H., Kaufman, D. S. and Liu, Z.: Global climate evolution during the last deglaciation, Proceedings of the National Academy of Sciences, 109(19), E1134–E1142, doi:10.1073/pnas.1116619109, 2012.

Cruz, F. W., Burns, S. J., Karmann, I., Sharp, W. D., Vuille, M., Cardoso, A. O., Ferrari, J. A., Silva Dias, P. L. and Viana, O.: Insolation-driven changes in atmospheric circulation over the past 116,000 years in subtropical Brazil, Nature, 434(7029), 63–66, doi:10.1038/nature03365, 2005.

Deplazes, G., Lückge, A., Peterson, L. C., Timmermann, A., Hamann, Y., Hughen, K. A., Röhl, U., Laj, C., Cane, M. A. and Sigman, D. M.: Links between tropical rainfall and North Atlantic climate during the last glacial period, Nature Geosci, 6(3), 213–217, doi:10.1038/ngeo1712, 2013.

Dewitte, B., Illig, S., Renault, L., Goubanova, K., Takahashi, K., Gushchina, D., Mosquera, K. and Purca, S.: Modes of covariability between sea surface temperature and wind stress intraseasonal anomalies along the coast of Peru from satellite observations (2000–2008), Journal of Geophysical Research, 116(C4), doi:10.1029/2010jc006495, 2011.

Dypvik, H. and Harris, N.: Geochemical facies analysis of fine-grained siliciclastics using Th/U, Zr/Rb and (Zr+Rb)/Sr ratios, Chemical Geology, 181(1-4), 131-146, doi:10.1016/s0009-2541(01)00278-9, 2001.

Echevin, V., Colas, F., Espinoza-Morriberon, D., Vasquez, L., Anculle, T. and Gutierrez, D.: Forcings and Evolution of the 2017 Coastal El Niño Off Northern Peru and Ecuador, Frontiers in Marine Science, 5, doi:10.3389/fmars.2018.00367, 2018.

Fleury, S., Martinez, P., Crosta, X., Charlier, K., Billy, I., Hanquiez, V., Blanz, T. and Schneider, R. R.: Pervasive multidecadal variations in productivity within the Peruvian Upwelling System over the last millennium, Quat. Sci. Rev., 125, 78–90, doi:10.1016/j.quascirev.2015.08.006, 2015.

Flores-Aqueveque, V., Alfaro, S., Vargas, G., Rutllant, J. A. and Caquineau, S.: Aeolian particles in marine cores as a tool for quantitative high-resolution reconstruction of upwelling favorable winds along coastal Atacama Desert, Northern Chile, Prog. Oceanogr., 134, 244–255, doi:10.1016/j.pocean.2015.02.003, 2015.

Flores-Aqueveque, V., Caquineau, S., Alfaro, S., Valdes, J. and Vargas, G.: Using Image-Based Size Analysis For Determining the Size Distribution and Flux of Eolian Particles Sampled In Coastal Northern Chile (23 S), Journal of Sedimentary Research, 84(4), 238-244, doi:10.2110/jsr.2014.23, 2014.

Garreaud, R., Vuille, M., Compagnucci, R. and Marengo, J.: Present-day South American climate, Palaeogeography, Palaeoclimatology, Palaeoecology, 281(3-4), 180-195, doi:10.1016/j.palaeo.2007.10.032, 2009.

González-Pinilla, F., Latorre, C., Rojas, M., Houston, J., Rocuant, M., Maldonado, A., Santoro, C., Quade, J. and Betancourt, J.: High- and low-latitude forcings drive Atacama Desert rainfall variations over the past 16,000 years, Science Advances, 7(38), doi:10.1126/sciadv.abg1333, 2021.

Gutiérrez, D., Bouloubassi, I., Sifeddine, A., Purca, S., Goubanova, K., Graco, M., Field, D., Méjanelle, L., Velazco, F., Lorre, A., Salvatteci, R., Quispe, D., Vargas, G., Dewitte, B. and Ortlieb, L.: Coastal cooling and increased productivity in the main upwelling zone off Peru since the mid-twentieth century, Geophys. Res. Lett., 38(7), doi:10.1029/2010GL046324, 2011.

Gutiérrez, D., Sifeddine, A., Field, D., Ortlieb, L., Vargas, G., Chávez, F., Velazco, F., Ferreira, V., Tapia, P., Salvatteci, R., Boucher, H., Morales, M., Valdés, J., Reyss, J., Campusano, A., Boussafir, M., Mandeng-Yogo, M., García, M. and Baumgartner, T.: Rapid reorganization in ocean biogeochemistry off Peru towards the end of the Little Ice Age, Biogeosciences, 6(5), 835-848, doi:10.5194/bg-6-835-2009, 2009.

Gutiérrez, D., Sifeddine, A., Reyss, J. L., Vargas, G., Velazco, F., Salvatteci, R., Ferreira, V., Ortlieb, L., Field, D., Baumgartner, T., Boussafir, M., Boucher, H., Valdés, J., Marinovic, L., Soler, P. and Tapia, P.: Anoxic sediments off Central Peru record interannual to multidecadal changes of climate and upwelling ecosystem during the last two centuries, Adv. Geosci., 6, 119–125, doi:10.5194/adgeo-6-119-2006, 2006.

Guzman, E., Ramos, C. and Dastgheib, A.: Influence of the El Niño Phenomenon on Shoreline Evolution. Case Study: Callao Bay, Perú, Journal of Marine Science and Engineering, 8(2), 90, doi:10.3390/jmse8020090, 2020.

Haug, G., Hughen, K., Sigman, D., Peterson, L. and Röhl, U.: Southward Migration of the Intertropical Convergence Zone Through the Holocene, Science, 293(5533), 1304-1308, doi:10.1126/science.1059725, 2001.

Holz, C., Stuut, J. B. W., Henrich, R. and Meggers, H.: Variability in terrigenous sedimentation processes off northwest Africa and its relation to climate changes: Inferences from grain-size distributions of a Holocene marine sediment record, Sediment. Geol., 202(3), 499–508, doi:10.1016/j.sedgeo.2007.03.015, 2007.

Humphries, M. S., Benitez-Nelson, C. R., Bizimis, M. and Finch, J. M.: An aeolian sediment reconstruction of regional wind intensity and links to larger scale climate variability since the last deglaciation from the east coast of southern Africa, Global and Planetary Change, 156, 59–67, doi:10.1016/j.gloplacha.2017.08.002, 2017.

Jansen, J., Van der Gaast, S., Koster, B. and Vaars, A.: CORTEX, a shipboard XRF-scanner for element analyses in split sediment cores, Marine Geology, 151(1-4), 143-153, doi:10.1016/s0025-3227(98)00074-7, 1998.

Jiang, H., Zhong, N., Li, Y., Ma, X., Xu, H., Shi, W., Zhang, S. and Nie, G.: A continuous 13.3-ka record of seismogenic dust events in lacustrine sediments in the eastern Tibetan Plateau, Sci Rep, 7(1), doi:10.1038/s41598-017-16027-8, 2017.

Just, J., Heslop, D., von Dobeneck, T., Bickert, T., Dekkers, M. J., Frederichs, T., Meyer, I. and Zabel, M.: Multiproxy characterization and budgeting of terrigenous end-members at the NW African continental margin, Geochem. Geophys. Geosyst., 13(9), doi:10.1029/2012GC004148, 2012.

Koutavas, A. and Joanides, S.: El Niño-Southern Oscillation extrema in the Holocene and Last Glacial Maximum, Paleoceanography, 27(4), doi:10.1029/2012pa002378, 2012.

Lagos, P., Silva, Y., Nickl, E. and Mosquera, K.: El Niño – related precipitation variability in Perú, Advances in Geosciences, 14, 231-237, doi:10.5194/adgeo-14-231-2008, 2008.

Mamalakis, A., Randerson, J., Yu, J., Pritchard, M., Magnusdottir, G., Smyth, P., Levine, P., Yu, S. and Foufoula-Georgiou, E.: Zonally contrasting shifts of the tropical rain belt in response to climate change, Nature Climate Change, 11(2), 143-151, doi:10.1038/s41558-020-00963-x, 2021.

Martin, L. C. P., Blard, P. H., Lavé, J., Condom, T., Prémaillon, M., Jomelli, V., Brunstein, D., Lupker, M., Charreau, J., Mariotti, V., Tibari, B., Team, A. and Davy, E.: Lake Tauca highstand (Heinrich Stadial 1a) driven by a southward shift of the Bolivian High, Sci. Adv., 4(8), doi:10.1126/sciadv.aar2514, 2018.

McGee, D., Donohoe, A., Marshall, J. and Ferreira, D.: Changes in ITCZ location and cross-equatorial heat transport at the Last Glacial Maximum, Heinrich Stadial 1, and the mid-Holocene, Earth Planet. Sci. Lett., 390, 69–79, doi:10.1016/j.epsl.2013.12.043, 2014.

McManus, J. F., Francois, R., Gherardl, J. M., Kelgwin, L. and Drown-Leger, S.: Collapse and rapid resumption of Atlantic meridional circulation linked to deglacial climate changes, Nature, 428(6985), 834–837, doi:10.1038/nature02494, 2004.

Mollier-Vogel, E., Leduc, G., Böschen, T., Martinez, P. and Schneider, R. R.: Rainfall response to orbital and millennial forcing in northern Peru over the last 18ka, Quat. Sci. Rev., 76, 29–38, doi:10.1016/j.quascirev.2013.06.021, 2013.

Montade, V., Kageyama, M., Combourieu-Nebout, N., Ledru, M. P., Michel, E., Siani, G. and Kissel, C.: Teleconnection between the intertropical convergence zone and southern westerly winds throughout the last deglaciation, Geology, 43(8), 735–738, doi:10.1130/G36745.1, 2015.

Morera, S., Condom, T., Crave, A., Steer, P. and Guyot, J.: The impact of extreme El Niño events on modern sediment transport along the western Peruvian Andes (1968–2012), Scientific Reports, 7(1), doi:10.1038/s41598-017-12220-x, 2017.

Mulitza, S., Chiessi, C. M., Schefuß, E., Lippold, J., Wichmann, D., Antz, B., Mackensen, A., Paul, A., Prange, M., Rehfeld, K., Werner, M., Bickert, T., Frank, N., Kuhnert, H., Lynch-Stieglitz, J., Portilho-Ramos, R. C., Sawakuchi, A. O., Schulz, M., Schwenk, T., Tiedemann, R., Vahlenkamp, M. and Zhang, Y.: Synchronous and proportional deglacial changes in Atlantic meridional overturning and northeast Brazilian precipitation, Paleoceanography, 32(6), 622–633, doi:10.1002/2017PA003084, 2017.

Ng, H. C., Robinson, L. F., McManus, J. F., Mohamed, K. J., Jacobel, A. W., Ivanovic, R. F., Gregoire, L. J. and Chen, T.: Coherent deglacial changes in western Atlantic Ocean circulation, Nat Commun, 9(1), doi:10.1038/s41467-018-05312-3, 2018.

Novello, V. F., Cruz, F. W., Vuille, M., Stríkis, N. M., Edwards, R. L., Cheng, H., Emerick, S., de Paula, M. S., Li, X., Barreto, E. de S., Karmann, I. and Santos, R. V.: A

high-resolution history of the South American Monsoon from Last Glacial Maximum to the Holocene, Sci. Rep., 7(March), 44267, doi:10.1038/srep44267, 2017.

Ortlieb, L., Vargas, G. and Sali??ge, J. F.: Marine radiocarbon reservoir effect along the northern Chile-southern Peru coast (14-24??S) throughout the Holocene, Quat. Res., 75(1), 91–103, doi:10.1016/j.yqres.2010.07.018, 2011.

Paterson, G. A. and Heslop, D.: New methods for unmixing sediment grain size data, Geochem. Geophys. Geosyst., 16(12), 4494–4506, doi:10.1002/2015GC006070, 2015.

Peterson, L., Haug, G., Hughen, K. and Röhl, U.: Rapid Changes in the Hydrologic Cycle of the Tropical Atlantic During the Last Glacial, Science, 290(5498), 1947-1951, doi:10.1126/science.290.5498.1947, 2000.

Pettijohn, F.: Persistence of Heavy Minerals and Geologic Age, The Journal of Geology, 49(6), 610-625, doi:10.1086/624992, 1941.

Pichevin, L., Cremer, M., Giraudeau, J. and Bertrand, P.: A 190 ky record of lithogenic grain-size on the Namibian slope: Forging a tight link between past wind-strength and coastal upwelling dynamics, Mar. Geol., 218(1–4), 81–96, doi:10.1016/j.margeo.2005.04.003, 2005.

Rahmstorf, S., Box, J., Feulner, G., Mann, M., Robinson, A., Rutherford, S. and Schaffernicht, E.: Exceptional twentieth-century slowdown in Atlantic Ocean overturning circulation, Nature Climate Change, 5(5), 475-480, doi:10.1038/nclimate2554, 2015.

Rahn, D. and Garreaud, R.: A synoptic climatology of the near-surface wind along the west coast of South America, International Journal of Climatology, 34(3), 780-792, doi:10.1002/joc.3724, 2013.

Rau, P., Bourrel, L., Labat, D., Melo, P., Dewitte, B., Frappart, F., Lavado, W. and Felipe, O.: Regionalization of rainfall over the Peruvian Pacific slope and coast, International Journal of Climatology, 37(1), 143-158, doi:10.1002/joc.4693, 2016.

Rein, B., Lückge, A. and Sirocko, F.: A major Holocene ENSO anomaly during the Medieval period, Geophysical Research Letters, 31(17), doi:10.1029/2004gl020161, 2004.

Rein, B., Lückge, A., Reinhardt, L., Sirocko, F., Wolf, A. and Dullo, W. C.: El Niño variability off Peru during the last 20,000 years, Paleoceanography, 20(4), 1–18, doi:10.1029/2004PA001099, 2005.

Reinhardt, L., Kudrass, H. R., Lückge, A., Wiedicke, M., Wunderlich, J., & Wendt, G.: High-resolution sediment echosounding off Peru: Late Quaternary depositional sequences and sedimentary structures of a current-dominated shelf, *Marine Geophysical Researches*, *23*(4), 335-35,2002

Salvatteci, R., Gutiérrez, D., Field, D., Sifeddine, A., Ortlieb, L., Bouloubassi, I., Boussafir, M., Boucher, H. and Cetin, F.: The response of the Peruvian Upwelling Ecosystem to centennial-scale global change during the last two millennia, Clim. Past, 10(2), 715–731, doi:10.5194/cp-10-715-2014, 2014a.

Salvatteci, R., Field, D., Sifeddine, A., Ortlieb, L., Ferreira, V., Baumgartner, T., Caquineau, S., Velazco, F., Reyss, J., Sanchez-Cabeza, J. and Gutierrez, D.: Cross-stratigraphies from a seismically active mud lens off Peru indicate horizontal extensions of laminae, missing sequences, and a need for multiple cores for high resolution records, Marine Geology, 357, 72-89, doi:10.1016/j.margeo.2014.07.008, 2014b.

Salvatteci, R., Gutierrez, D., Sifeddine, A., Ortlieb, L., Druffel, E., Boussafir, M. and Schneider, R.: Centennial to millennial-scale changes in oxygenation and productivity in the Eastern Tropical South Pacific during the last 25,000 years, Quat. Sci. Rev., 131, 102–117, doi:10.1016/j.quascirev.2015.10.044, 2016.

Salvatteci, R., Schneider, R. R., Blanz, T. and Mollier-Vogel, E.: Deglacial to Holocene Ocean Temperatures in the Humboldt Current System as Indicated by Alkenone Paleothermometry, Geophys. Res. Lett., 46(1), 281–292, doi:10.1029/2018GL080634, 2019.

Saukel, C., Lamy, F., Stuut, J. B. W., Tiedemann, R. and Vogt, C.: Distribution and provenance of wind-blown SE Pacific surface sediments, Mar. Geol., 280(1–4), 130–142, doi:10.1016/j.margeo.2010.12.006, 2011.

Scheidegger, K. F. and Krissek, L. A.: Dispersal and deposition of eolian and fluvial sediments off Peru and northern Chile., Geol. Soc. Am. Bull., 93(2), 150–162, doi:10.1130/0016-7606(1982)93<150:DADOEA>2.0.CO;2, 1982.

Shakun, J. D., Clark, P. U., He, F., Marcott, S. A., Mix, A. C., Liu, Z., Otto-Bliesner, B., Schmittner, A. and Bard, E.: Global warming preceded by increasing carbon dioxide concentrations during the last deglaciation, Nature, 484(7392), 49–54, doi:10.1038/nature10915, 2012.

Sifeddine, A., Gutierrez, D., Ortlieb, L., Boucher, H., Velazco, F., Field, D., Vargas, G., Boussafir, M., Salvatteci, R., Ferreira, V., García, M., Valdés, J., Caquineau, S., Mandeng Yogo, M., Cetin, F., Solis, J., Soler, P. and Baumgartner, T.: Laminated sediments from the central Peruvian continental slope: A 500 year record of upwelling system productivity, terrestrial runoff and redox conditions, Prog. Oceanogr., 79(2–4), 190–197, doi:10.1016/j.pocean.2008.10.024, 2008.

Stríkis, N. M., Chiessi, C. M., Cruz, F. W., Vuille, M., Cheng, H., De Souza Barreto, E. A., Mollenhauer, G., Kasten, S., Karmann, I., Edwards, R. L., Bernal, J. P. and Sales, H. D. R.: Timing and structure of Mega-SACZ events during Heinrich Stadial 1, Geophys. Res. Lett., 42(13), 5477–5484, doi:10.1002/2015GL064048, 2015.

Stríkis, N., Cruz, F., Barreto, E., Naughton, F., Vuille, M., Cheng, H., Voelker, A., Zhang, H., Karmann, I., Edwards, R., Auler, A., Santos, R. and Sales, H.: South American monsoon response to iceberg discharge in the North Atlantic, Proceedings of the National Academy of Sciences, 115(15), 3788-3793, doi:10.1073/pnas.1717784115, 2018.

Strub, P. T., Mesias, J. M., Montecino, V., Rutllant, J., and Salinas, S.: Coastal ocean circulation off western South America, in: The Sea, Vol. 11, edited by: Robinson, A. and Brink, K., John Wi- ley & Sons, New York, USA, 273–313, 1998.

Stuut, J. B. W., Kasten, S., Lamy, F. and Hebbeln, D.: Sources and modes of terrigenous sediment input to the Chilean continental slope, Quat. Int., 161(1), 67–76, doi:10.1016/j.quaint.2006.10.041, 2007.

Stuut, J. B. W., Prins, M. A., Schneider, R. R., Weltje, G. J., Fred Jansen, J. H. and Postma, G.: A 300-kyr record of aridity and wind strength in southwestern Africa: Inferences from grain-size distributions of sediments on Walvis Ridge, SE Atlantic, Mar. Geol., 180(1–4), 221–233, doi:10.1016/S0025-3227(01)00215-8, 2002.

Stuut, J. B. W., Temmesfeld, F. and De Deckker, P.: A 550ka record of aeolian activity near north west cape, australia: Inferences from grain-size distributions and bulk chemistry of SE indian ocean deep-sea sediments, Quat. Sci. Rev., 83, 83–94, doi:10.1016/j.quascirev.2013.11.003, 2014.

Stuut, J.-B. W. and Lamy, F.: Climate variability at the southern boundaries of the Namib (southwestern Africa) and Atacama (northern Chile) coastal deserts during the last 120,000 yr, Quat. res., 62(3), 301–309, doi:10.1016/j.yqres.2004.08.001, 2004.

Suess, E., Kulm, L. D. and Killingley, J. S.: Coastal upwelling and a history of organic-rich mudstone deposition off Peru, Geological Society, London, Special Publications, 26(1), 181–197, doi:10.1144/GSL.SP.1987.026.01.11, 1987.

Sublette Mosblech, N., Chepstow-Lusty, A., Valencia, B. and Bush, M.: Anthropogenic control of late-Holocene landscapes in the Cuzco region, Peru, The Holocene, 22(12), 1361-1372, doi:10.1177/0959683612449760, 2012.

Vuille, M., Burns, S., Taylor, B., Cruz, F., Bird, B., Abbott, M., Kanner, L., Cheng, H. and Novello, V.: A review of the South American monsoon history as recorded in stable isotopic proxies over the past two millennia, Climate of the Past, 8(4), 1309-1321, doi:10.5194/cp-8-1309-2012, 2012.

Weltje, G. J. and Prins, M. A.: Genetically meaningful decomposition of grain-size distributions, Sedimentary Geology, 202(3), 409–424, doi:10.1016/j.sedgeo.2007.03.007, 2007.

Weltje, G. J. and Prins, M. A.: Muddled or mixed? Inferring palaeoclimate from size distributions of deep-sea clastics, Sedimentary Geology, 162(1–2), 39–62, doi:10.1016/s0037-0738(03)00235-5, 2003.

Wu, L., Wilson, D., Wang, R., Yin, X., Chen, Z., Xiao, W. and Huang, M.: Evaluating Zr/Rb Ratio From XRF Scanning as an Indicator of Grain-Size Variations of Glaciomarine Sediments in the Southern Ocean, Geochemistry, Geophysics, Geosystems, 21(11), doi:10.1029/2020gc009350, 2020.

Yarincik, K., Murray, R. and Peterson, L.: Climatically sensitive eolian and hemipelagic deposition in the Cariaco Basin, Venezuela, over the past 578,000 years: Results from Al/Ti and K/Al, Paleoceanography, 15(2), 210-228, doi:10.1029/1999pa900048, 2000.

Zhang, Y., Chiessi, C. M., Mulitza, S., Zabel, M., Trindade, R. I. F., Helena, M., Hollanda, B. M., Dantas, E. L., Govin, A., Tiedemann, R. and Wefer, G.: Origin of increased terrigenous supply to the NE South American continental margin during Heinrich Stadial 1 and the Younger Dryas, Earth Planet. Sci. Lett., 432, 493–500, doi:10.1016/j.epsl.2015.09.054, 2015.

Zhou, W., Leung, L., Lu, J., Yang, D. and Song, F.: Contrasting Recent and Future ITCZ Changes From Distinct Tropical Warming Patterns, Geophysical Research Letters, 47(22), doi:10.1029/2020gl089846, 2020. Bahr, A., Hoffmann, J., Schönfeld, J., Schmidt, M., Nürnberg, D., Batenburg, S. and Voigt, S.: Low-latitude expressions of high-latitude forcing during Heinrich Stadial 1 and the Younger Dryas in northern South America, Global and Planetary Change, 160, 1-9, doi:10.1016/j.gloplacha.2017.11.008, 2018.

2.8. Supplementary information

Supplementary Table 1

Location of surface sediment sampling stations

Site	Station	LONG	LAT	Depth (m)	Distance coastline (km)
Callao	E2	-77.3	-12.0	92	14.8
Callao	E5	-77.6	-12.0	178	55.5
Pisco	E13	-76.4	-14.0	120	9.2
Pisco	E12	-76.4	-14.1	182	20.3
Pisco	E11	-76.5	-14.1	311	25.9

Supplementary Table 2

Uncalibrated and calibrated ^{14}C ages in core M772-005-3 used to elaborate the chronological model. * Indicate the ^{14}C ages reported in Salvatteci et al., 2019.

Depth (cm)	Uncalibrated Age BP (years)	Delta-R (years)	Age cal. BP (maximum probability)
13	1902±20	367±40	1092
52	2605±30	367±40	1841
84	3160±30	226±98	2692
*113	11646±44	511±278	12650
134	12320±60	511±278	13277
153	12690±60	511±278	13678
169	12730±70	511±278	13728
210	13150±70	511±278	14125
244	13180±70	511±278	14150
*303	13792±53	511±278	15325
319	13810±80	511±278	15346
349	13840±70	511±278	15399
378	13790±70	511±278	15316
385	13870±70	511±278	15447
*403	14449±68	511±278	16300
418	13990±70	511±278	15725
452	14100±70	511±278	15775
469	14410±70	511±278	16265
503	14510±80	511±278	16313
522	14660±80	511±278	16600
542	14780±80	511±278	16825
590	14850±80	511±278	16913
*623	15930±66	511±278	18288
647	16530±90	511±278	18838
672	17680±110	511±278	20230
700	21390±170	511±278	24663

Supplementary Figure 1

Location of the sampling of the sediment cores M772-005-3 and G14 core and surface sampling station (black stars) in the Peruvian margin.

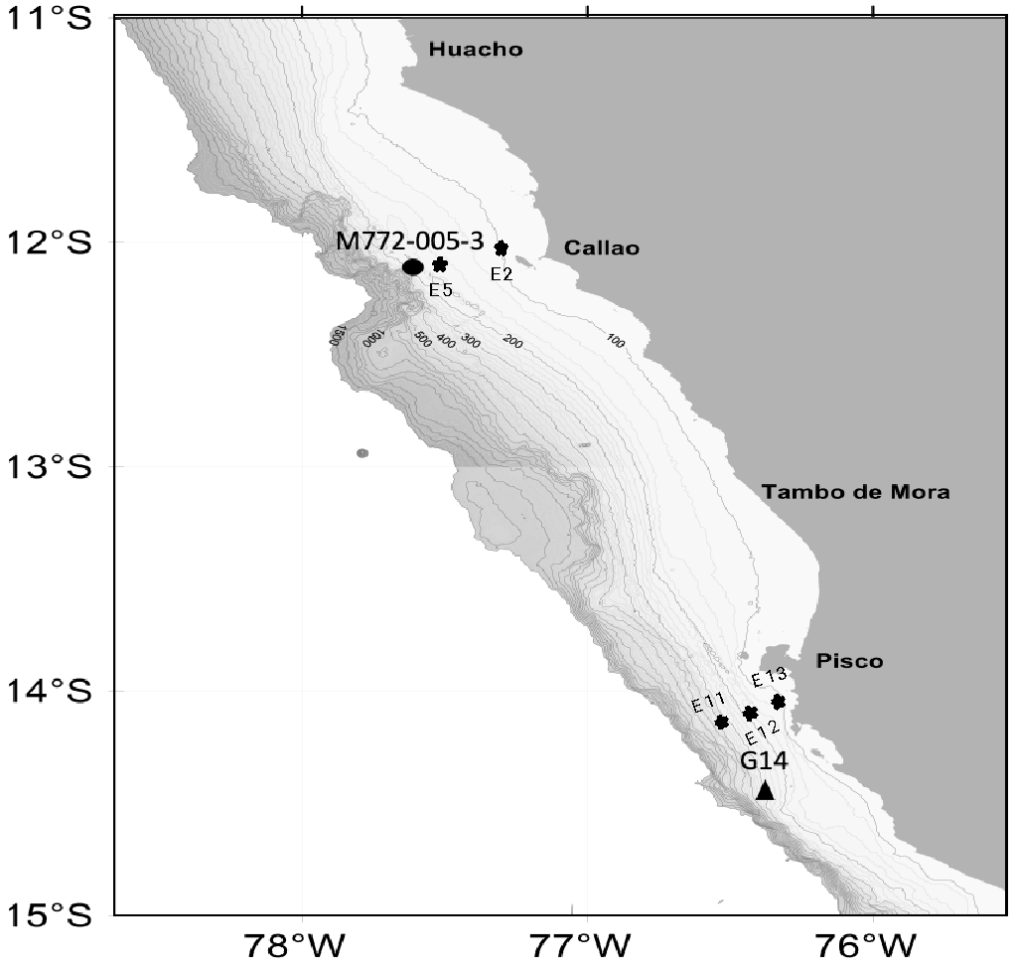

Supplementary Figure 2

Chronological model for Callao (M772-005-3 and 106KL) and Pisco (G-14) cores.

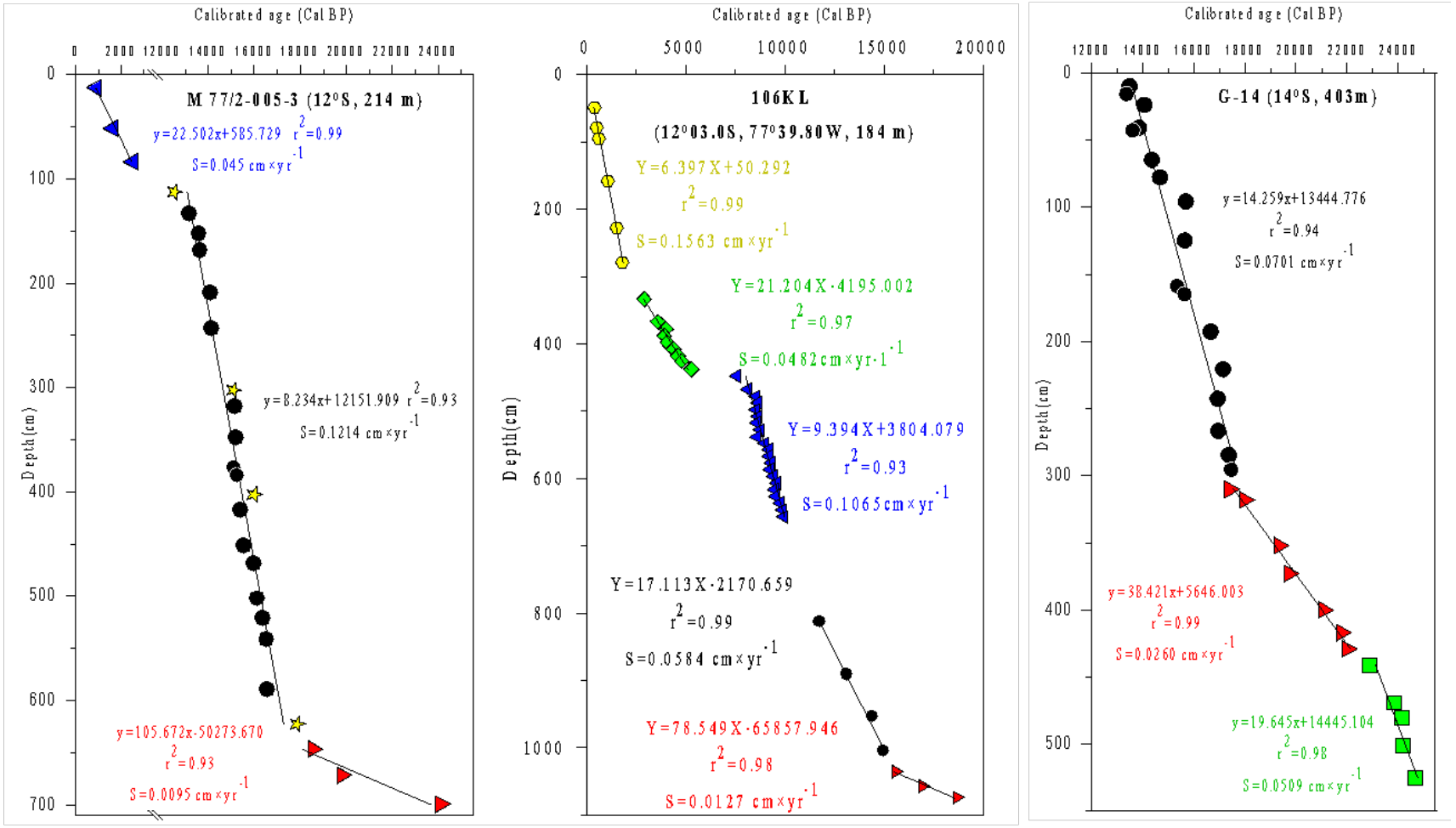

3. Increased El Niño amplitude during the last deglacial warming

Marco Yseki[1*], Bruno Turcq[1], Dimitri Gutiérrez[2,3], Renato Salvatteci[4], Dante Espinoza-Morriberón[5,6], Hugues Boucher[1], Philippe Martinez[7] & Matthieu Carré[1,8]

[1]LOCEAN-IPSL, Laboratoire d'Océanographie et du Climat: Expérimentation et Approches Numériques, Sorbonne Université/CNRS/IRD/MNHN, Paris, France.
[2]Dirección General de Investigaciones Oceanográficas y de Cambio Climático, Instituto del Mar del Peru, Callao, Peru.
[3]Laboratorio de Ciencias del Mar, Facultad de Ciencias y Filosofía, Universidad Peruana Cayetano Heredia, Lima, Peru.
[4]Center for Ocean and Society, Kiel University, Kiel, Germany
5Instituto del Mar del Peru, Laboratorio de Modelado Oceanográfico y de Cambio Climático, Callao, Peru.
[6]Universidad Tecnológica del Peru (UTP), Facultad de Ingenieria, Lima, Peru.
[7]UMR 5805 EPOC, Université de Bordeaux-CNRS-EPHE. Pessac Cedex, France.
[8]Universidad Peruana Cayetano Heredia, Facultad de Ciencias y Filosofia, Centro de Investigación para el Desarrollo Integral y Sostenible, Laboratorios de Investigación y Desarrollo, Lima, Peru.

Chapter II focuses on objective 2 of the thesis, which is to reconstruct interannual variability of fluvial discharge in the central-southern Peruvian margin during the last deglaciation and to infer ENSO variability. We present here a record of fluvial discharge interannual variability derived from high-resolution X-ray fluorescence Titanium (Ti-XRF) counts in two marine sediment cores collected on the Peruvian margin (M77/2-005-3, Callao and G14, Pisco). Since Ti-XRF is related to river discharge and ENSO is the primary driver of interannual variability of rainfall in Peru, on the coast as well as in the Andes, the 2.5-8 year frequency band of Ti-XRF in sediment cores provide us with an unprecedented 4000-year long record of ENSO-related rainfall interannual variability during the last deglaciation. This chapter was submitted to *Nature communications* on January 27 2022 and is now under review.

3.1. Abstract

It is still unclear how El Niño Southern Oscillation (ENSO), the leading mode of global-scale interannual climate variability, will respond to global warming. The last deglaciation offers natural experimental conditions to observe the behavior of ENSO in a period of abrupt warming and sea level rise. Here we present a record of ENSO-related interannual variability of river discharge in Peru during the last deglaciation (17.5-13 kyr BP) and the Late Holocene (2.7-1.4 kyr BP), based on high resolution records of Titanium in marine sediments from the Peruvian margin (Callao, 12ºS and Pisco 14ºS). We find that the amplitude of ENSO events was 50 to 190 % larger during the deglaciation compared to the Late Holocene, which supports the hypothesis that ENSO in the Eastern Pacific is strengthened by ice sheet meltwater discharge. A possible strengthening of ENSO in response to future ice sheet melting should be considered.

3.2. Introduction

The El Niño-Southern Oscillation (ENSO) is the main mode of interannual climate variability in the world[1,2] and especially affects South American precipitation through atmospheric teleconnections[3,4,5,6]. Large uncertainties in projections of ENSO reflect important gaps in our understanding of ENSO natural variability and its relationship with the mean climate state[7,8,9]. Reconstructions of ENSO centennial to millennial scale response to past natural climate change provide insights into the sensitivity of ENSO to changes in the background state and observational constraints to climate models[10,11].

The last deglaciation (~19-11 kyr BP) was a period of rapid global warming associated with a ~80 ppm increases in atmospheric CO_2[12]. The deglacial climate was also characterized by the melting of polar ice sheets[13] causing a rapid sea level rise[14] and a series of abrupt millennial-scale events[15]. The behavior of ENSO during the last deglaciation is still unclear. In the Eastern Equatorial Pacific (EEP), the spread of individual foraminifera Mg/Ca and $\delta^{18}O$ values estimated in three deglacial snapshots suggest a 16 to 60% increase in ENSO variability at 12.5, 15.1 and 17.9 kyr BP compared to the Late Holocene (1.6 kyr BP)[16], while no increase was found at 16.8 kyr BP using a different foraminifera species[17]. The lithic flux measured in the 106KL marine core from Callao, one of the few high-resolution records in the Eastern Tropical Pacific (ETP), was

interpreted as a proxy for El Niño intensity[18]. However, the lithic flux has a fluvial and aeolian mixed origin in Callao[19], and the record's resolution for the last deglaciation did not allow to resolve the ENSO frequency band in this core.

In paleoclimate model experiments, deglacial meltwater pulses in the North Atlantic induce a weakening of the Atlantic Meridional Overturing Circulation (AMOC) intensity, a southern shift of the Intertropical Convergence Zone (ITCZ) and an increase in ENSO variability[20,21,22,23]. Meltwater forcing has been invoked to explain that ENSO in the early Holocene was not as reduced as predicted by insolation forcing alone[24,25], but still requires to be tested with records from the deglaciation, when the meltwater flux was at its highest level. The last deglaciation is not equivalent to the current anthropogenic global warming, but offers us the opportunity to assess how ENSO characteristics were affected by this abrupt climate change.

3.3. Results and discussion

3.3.1. A high-resolution sediment record of ENSO variability

We present here a record of fluvial discharge interannual variability derived from high-resolution X-ray fluorescence Titanium (Ti-XRF) counts in two marine sediment cores collected on the Peruvian margin (Fig. 1). The core M77/2-005-3 (12º05 S, 77º40,07 W) was collected off Callao at 214 m depth, and core G14 (14.38ºS, 76.42ºW) was collected off Pisco at 390 m depth. Despite sedimentation hiatus due to erosion, both cores record the last deglaciation (17.5-13 kyr BP) and a Late Holocene section (2.7-1.3 kyr BP) is recorded in Callao[19] (see depth-age models in supplementary Fig. 1). The sedimentation rate in the deglacial period, determined by 19 radiocarbon dates in Callao and 17 in Pisco is stable and high over the period (supplementary Fig. 1). The sections analyzed show irregularly spaced but well-preserved laminae indicating minimized sediment mixing (supplementary Fig. 2 and 3). The fast sedimentation (Late Holocene: 0.5 mm/yr in Callao; deglaciation: 1.2 mm/yr in Callao and 0.7 mm/yr in Pisco)[19] combined to the high resolution of the XRF measurements (1 mm) yields an unprecedented record of interannual climate variability in the ETP over thousands of years.

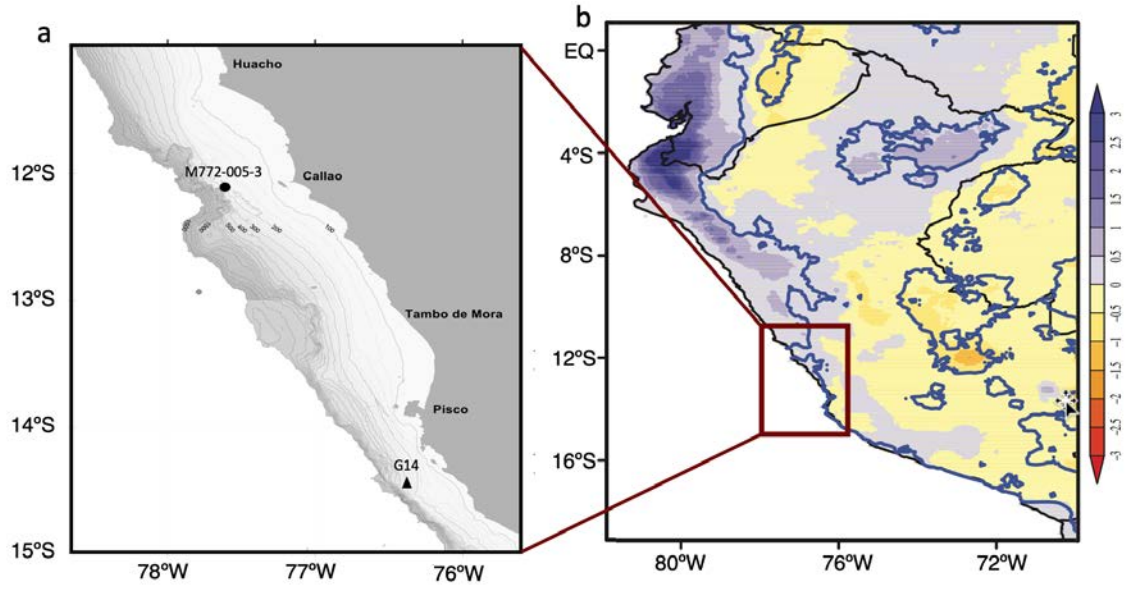

Figure 1. A) Location of the sampling of the sediment cores M77/2-005-3 (black circle) and G14 (black triangle) in the Peruvian margin. B) Linear regression coefficients between ENSO Eastern Pacific indices and precipitation (Figure adapted from Sulca *et al.*[5]).

Since Ti is relatively immobile during chemical weathering, Ti has been widely used as an indicator of terrigenous detrital input to sediments[26]. Ti-XRF variations in the central-southern Peruvian margin has been shown to be related to the fluvial fraction of terrestrial input[19] and is therefore used here as a proxy for river discharge (see Methods). The core M77/2-005-3 off Callao receives a Ti flux primarily from the discharge of the rivers Chancay, Chillón, Rimac, and Lurín, while the G14 core off Pisco is influenced by the Pisco and Ica rivers. Under the current climate, the flow of coastal rivers is usually low and increases during austral summer because of the monsoon rainfall in the High Andes[3,27,28]. During El Niño events, especially those with high sea surface temperature (SST) anomalies in the Eastern Pacific (EP), strong thunderstorms and precipitation occur on the coast[5,29,30,31,32]. These events produce catastrophic flash floods and large discharge of sediments during a few days[33,34,35].

Since Ti is related to river discharge and ENSO is the primary driver of interannual variability of rainfall in Peru, on the coast as well as in the Andes[5], the 2.5-8 year frequency band of Ti-XRF in Pisco and Callao sediment cores provide us with an unprecedented 4000-year long record of ENSO-related rainfall interannual variability during the last deglaciation. Ti-XRF counts records were normalized so that both cores could be compared (supplementary Fig. 4). Changes in the amplitude of interannual

variability were estimated by the standard deviation of the 2.5-8 years band-pass filtered Ti-XRF series calculated over a 300-years long sliding window (see Methods).

3.3.2. Precipitation and ENSO in Peru during the last deglaciation

Strong similarity is observed in the variations of Ti-XRF in Callao and Pisco during the last deglaciation, considering the chronological uncertainty (Fig. 2a). More importantly, the amplitude of Ti-XRF interannual variability varies coherently on millennial timescales in both sites (Fig. 2c). The regional scale reproducibility of the records demonstrates that the dataset is not affected by analytic or local biases and that Ti-XRF variations faithfully reflect regional scale climate variability.

Compared to the 1400-year long Late Holocene section, which can be considered as representative of modern conditions based on multiple studies[16,17,24,25,36,37,38], higher Ti-XRF is found during the deglacial period (Fig. 2a). Lower sea level during the deglaciation might be partly responsible for the higher Ti-XRF off Callao and Pisco because of the reduced distance to the river mouths. However, the sediment source was only 20 km closer to the Callao core 18 kyr BP compared to today and at about the same distance for the Pisco core. In addition, the sea level rose strongly from 18 to 13 kyr BP, a trend that is not reflected in the Ti-XRF record, neither in Callao nor in Pisco. Hence, the larger deglacial Ti-XRF is likely the result of increased river discharge in central-southern Peru. A deglacial increase in sediment discharge with a marked maximum during the Heinrich Stadial 1 cold spell was also recorded in a marine core from northern[38] and central-southern Peru[19]. Since coastal precipitation only occasionally occurs during strong El Niño events, the larger average river flow was likely primarily caused by increased precipitation in the Andes in agreement with records of strengthened south American monsoon in the central Andes[39,40,41,42] and evidence of a southern shift of the ITCZ mean position at that time[43,44,45].

We find a 50 to 190% increase in the amplitude of ENSO frequency band variability during the deglacial climate (17.5-13 kyr BP) compared to the Late Holocene (2.7-1.4 kyr BP) (Fig. 2c and 3g), when ENSO had similar to modern characteristics[11,17,24,25,46]. The record shows centennial to millennial scale modulation of ENSO amplitude is consistent with evidence obtained from individual foraminifera in the EEP[16] (Fig. 3f). ENSO amplitude is known to be subject to large decadal to centennial internal unforced variability[8,37,25,47] but is, during the deglaciation, consistently higher

during more than 4000 years, compared to its modern level. The length of these interannual records (both of the Late Holocene and of the last deglaciation) yield an exceptional statistical robustness to this reconstruction of ENSO (for comparison, Holocene fossil corals and mollusks of the whole Pacific altogether record ~2500 years[25]). A robust increase of ENSO amplitude over such a long period could not be caused by stochastic internal variability. Therefore, the larger deglacial amplitude of ENSO must have been the result of a dynamical response to different boundary conditions.

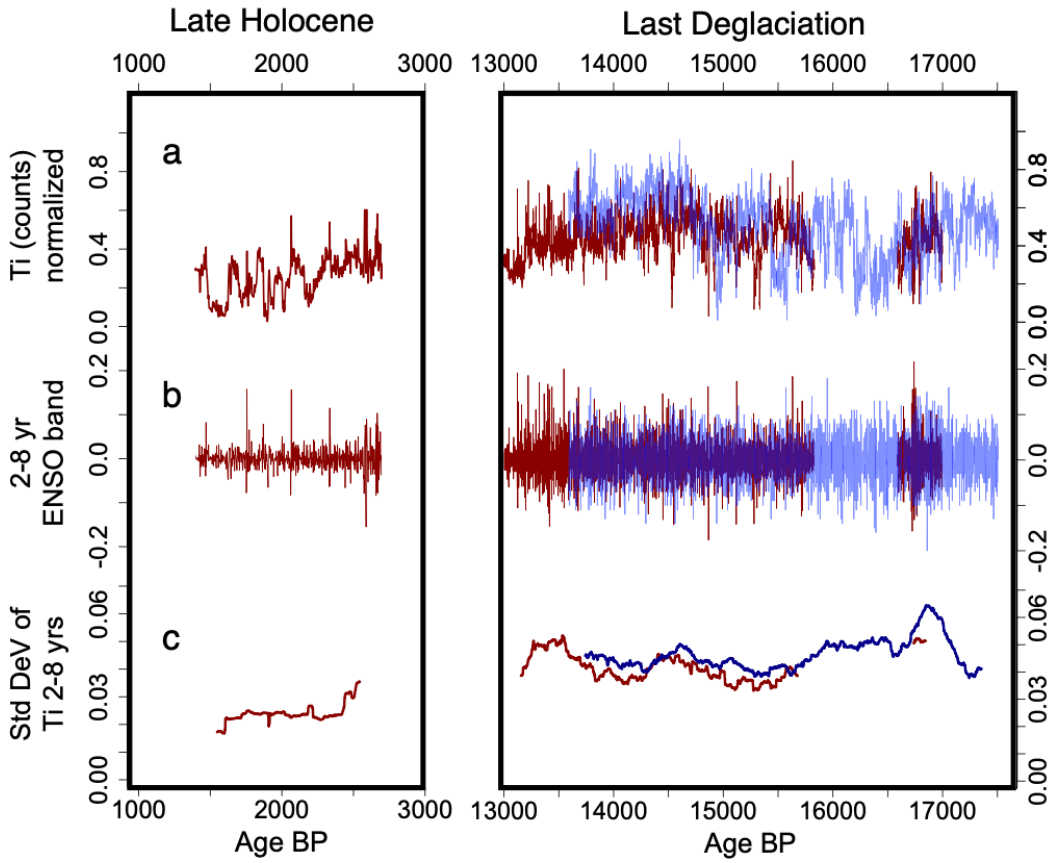

Figure 2. A) Ti-XRF counts normalized record in Callao (red) and Pisco (blue). B) 2.5-8 years frequency band of the Ti-XRF record in Callao (red) and Pisco (blue). C) Standard deviation (over 300 years moving windows) of the 2.5-8 years frequency band of the Ti-XRF record in Callao (red) and Pisco (blue) as a proxy of ENSO variability.

3.3.3. ENSO and forcing mechanism during the last deglaciation

During the deglacial time, ENSO could have been affected by a number of forcing factors, including insolation, greenhouse gases, the presence of large polar ice sheets and meltwater discharge. The change in the seasonal flux of solar energy related to the Earth's orbital parameters has been shown to be a driver of ENSO in models [48,49,50] and to account

for Holocene ENSO minimum (6-3 kyr BP) in paleoclimate records[25]. The damping effect of this external forcing was, however, stronger during the deglaciation and could therefore not explain the high variability recorded here (Fig 3a).

How increasing greenhouse gases influence ENSO is still unclear. While CMIP5 and CMIP6 models together tend to suggest an increased ENSO variability with increasing atmospheric CO_2 concentrations[51,52,53], two recent studies found that ENSO is weakening with increasing CO_2 when simulations last several millennia[8] or when model biases are minimized with an ultra-high-resolution model[9]. The 80 ppm increase of CO_2 during the deglaciation is slightly lower than the current 100 ppm anthropogenic CO_2 increase that has not produced a clearly detectable impact on ENSO, and is much lower than the x2 or x4 scenarios tested for the future that yields contradictory effects. Thus, CO_2 changes could arguably be considered as a minor forcing of ENSO during the deglaciation.

In contrast to the Late Holocene, the deglaciation is mainly characterized by large remnant continental ice sheets and massive meltwater discharge[15,54,55,56,57]. The presence of a large ice sheet in the northern hemisphere strengthens the mid-latitude jet stream and remotely affects the tropical Pacific through atmospheric bridges and had a slight strengthening effect on ENSO in the EP in the IPSL-CM4 climate model[23]. Conversely, in the NCAR-CCSM3 transient simulation of the past 21,000 years forced uniquely by continental ice sheet variations, an abrupt ENSO increase (25%) is found at 14 kyr BP in response to a marked retreat of the Laurentide ice sheet[58]. This effect disappeared when all forcing were combined[58]. On the other hand, a meltwater discharge into the northern Atlantic consistently causes an increase of ENSO amplitude in multiple modeling experiments[20,21,22] and an eastward shift of anomalies[22,23,59], which would also result in increased variability in Peru. The 120 m sea level rise during the deglaciation[60] gives a measure of the magnitude of the corresponding meltwater flux into the North Atlantic and the Southern Ocean. Despite variations and some abrupt discharge events[61], the sea level never stopped rising from 20 to 7 kyr BP. The sustained meltwater flux during the whole deglaciation period seems thus the most likely forcing of the multi-millennial increase in ENSO strength recorded in Peru.

The AMOC is weakened by meltwater discharge in the North Atlantic and in the Southern Ocean[62,63,64]. The resulting change in the meridional-oceanic temperature gradient induces a southward displacement of the mean annual position of ITCZ, a weaker

zonal SST gradient across the equatorial Pacific and more symmetric annual mean climate in the EEP resulting in an amplified ENSO[20,21,22]. Although the underlying mechanisms responsible for the change in ENSO amplitude is still not clearly understood, the chain of response from the North Atlantic to the tropical Pacific is robust in model experiments.

Geochemical proxies of ocean circulation in marine sediments indicate a slowdown of the AMOC during the deglaciation due to large meltwater flux[65,66,67] (Fig. 3b). Records of tropical rainfall also point to a southern position of the mean annual position of the ITCZ in the deglaciation compared to the Late Holocene[43,44,45]. In addition, reduced zonal and meridional SST gradients were reconstructed in the Tropical Pacific (Fig. 3c) by Sadekov *et al*.[16] who also showed a strong link with ENSO amplitude. The deglacial climate, although rapidly changing, maintained an El Niño-like mean state in the tropical Pacific under the sustained influence of the meltwater flux weakening the AMOC. Our 4000-year long record shows that this mean state was associated with a long-term increase in El Niño amplitude in the EP, and provides observational support for the positive influence of meltwater flux on ENSO amplitude suggested by climate model experiments. Very few model experiments have, however, explored the combined influence of multiple external forcing on ENSO during the deglaciation. The behavior of ENSO has been examined in the CCSM3 model TraCE-21ka transient simulation of the past 21 thousand years forced by orbital parameters, greenhouse gases, continental ice sheets and meltwater discharge, combined and separately[58]. Although meltwater discharge alone produces an increase in ENSO amplitude in the model, a compensation by the dampening effects of atmospheric CO_2 and insolation in TraCE-21ka results in a reduced ENSO during the last deglaciation[58] (Fig. 3e). Although TraCE-21ka reproduces correctly large-scale features of the evolution of the global climate (e.g., AMOC intensity, cross-Equator SST contrast, tropical Pacific SST)[58], the simulated deglacial reduction of ENSO is at odd with the increased amplitude recorded in Peruvian sediments. This disagreement indicates an overestimation of the dampening effect of CO_2 and insolation and/or an underestimation of the response to meltwater discharge in this model, an issue that is possibly shared by other climate models.

An underestimation of the impact of meltwater discharge on the tropical climate variability in climate models raises serious issues in the context of current global warming. There is multiple evidence for a slowdown of AMOC in the 20th century, possibly as a result of Greenland ice sheet melting[68,69,70,71] which is accelerating with

global warming[72]. The future weakening of AMOC was considered as very likely in IPCC AR5[73,74,75]. The impact of AMOC slowdown on ENSO has been so far overlooked in climate change projections, possibly because of uncertainties in icesheet melting rate, or undetected for an underestimated response in projections. However, our record of ENSO in the EP during the last great ice sheet melting period suggests that ENSO is more sensitive to freshwater flux than previously thought, pointing to a potential strengthening with future ice sheet melting in a greenhouse climate. Additional transient simulations of the last deglaciation are urgently needed to better assess the ability of models to predict ENSO response.

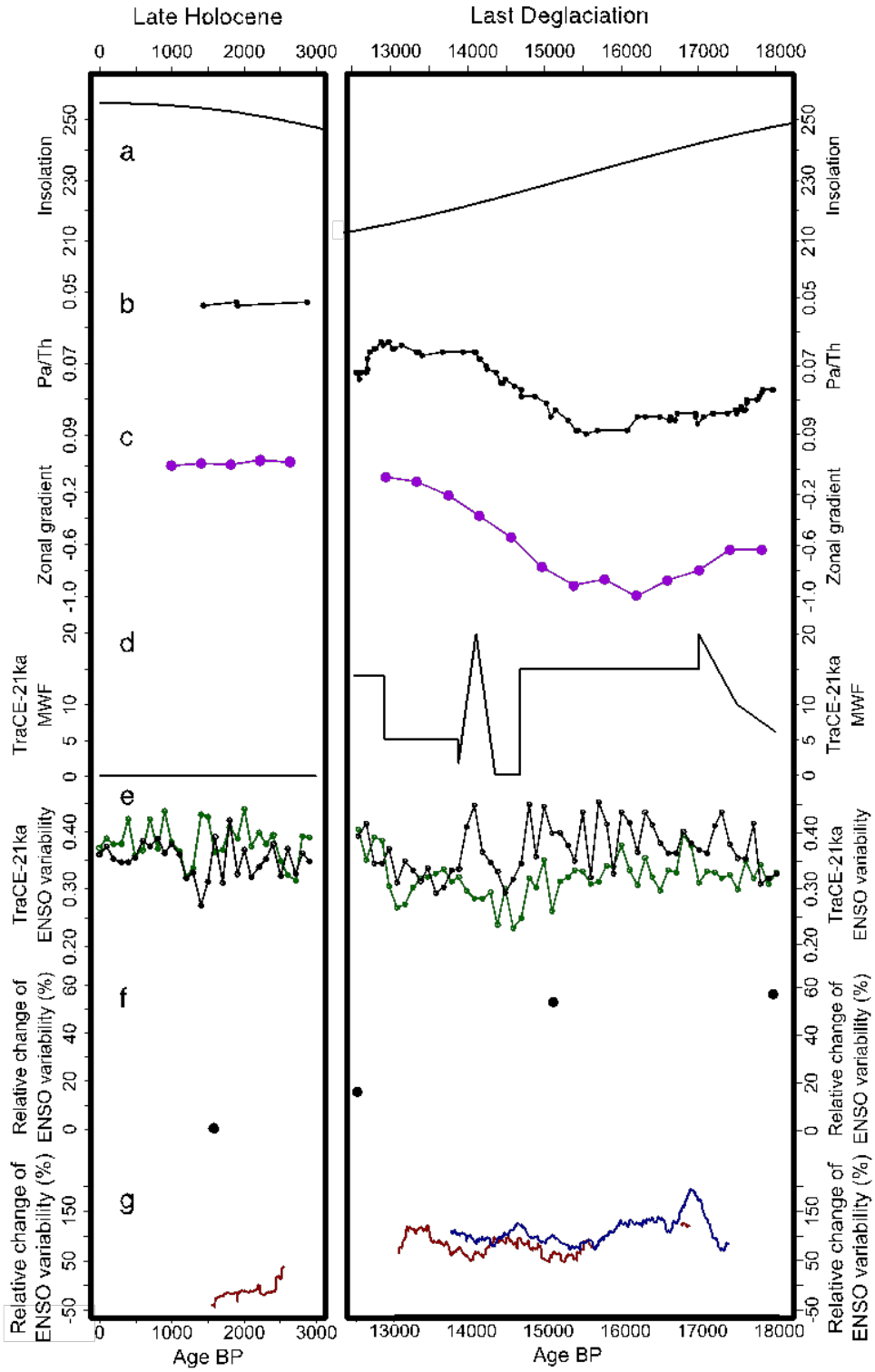

Figure 3. A) December, January and February minus June, July and August (DJF–JJA) insolation at 30ºS[76]. B) Composite $^{231}Pa/^{230}Th$ record that reflect past changes in AMOC[67]. C) Changes in zonal gradient across the equatorial Pacific[16]. D) Meltwater flux forcing (m/kyr) in TraCE-21ka[58]. E) ENSO variability in only meltwater flux experiment (black) and ENSO variability in all forcing experiment in TraCE-21ka (green)[58]. F) Individual foraminifera Mg/Ca variability[16]. G) ENSO-related interannual variability of river discharge in Callao (red) and Pisco (blue).

3.4. Methods

3.4.1. Marine sediments core

The cores M77/2-005-3 and G14 were retrieved from the Southeast Pacific continental slope during the M77-2 and Galathea-3 expedition respectively[77,78]. The lithology of both cores, previously described by Salvatteci *et al*.[77,78] is here complemented by X-Ray images and presented in supplementary Fig. 2 and 3. The Late Holocene and deglacial sediments are mainly composed of “irregularly spaced laminae” and “isolated laminae”, as defined by Brodie and Kemp[79]. The “irregularly spaced laminae” are packets of laminae (several centimeters to decimeters thick) separated by intervals of homogeneous sediments (several centimeters to decimeters thick). These laminae packages include alternations between diatom oozes and diatomaceous mud, the latter with a higher content of clay minerals. The "isolated laminae" are packets of millimetric and sub-millimetric laminae (solitary diatom ooze) enclosed in homogeneous mud. The G14 core is more finely laminated than the M77/2-005-3 core. Depth-age models based on 26 ^{14}C ages for the core M77/2-005-3 and 29 ^{14}C datings for G14 was built by Yseki *et al*.[19] and is presented for both cores in supplementary Fig. 1. The analyzed section (36-588 cm) of core M77/2-005-3 included the last deglaciation (17-13 kyr BP; 102-588 cm), and, above a sedimentation hiatus at 94 cm, part of the Late Holocene (2.7-1.4 kyr BP; 36-93 cm). Probably because of erosion, Holocene sediments were not recovered in G14. The analyzed section (10-285 cm) of core G14 included the last deglaciation (17.5-13.5 kyr BP).

3.4.2. XRF Analysis

Ti was measured at high resolution (1 mm) in both cores using a XRF scanner only in the laminated or banded sections of the sediment cores in order to guarantee that the analyzed sections are a result of deposition from the water column and not from reworking of upslope deposits[77]. XRF analysis were performed on core M77/2-005-3 and G14 at ALYSES facility (IRD-Sorbonne University, Bondy, France) and the University of Bordeaux 1 respectively. Measurements were done every 1 mm at 25kV and 500 uA during 10 s in core M772-005-3, and every 1 mm at 10kV and 400uA during 10 s in core G14.

Ti is present in marine sediments as titanium oxide resulting from soil pedogenesis and transported by rivers to the ocean along with clay minerals[80]. Ti-XRF has therefore been used as an indicator of river discharge, precipitation and ENSO variability[81,82]. XRF counts of Ti as well as other elements do not only depend on the mass concentration of Ti. It is also influenced by sediment heterogeneity that creates irregularities of the scanned core surface and mostly sediment inhomogeneity along the core such as variations in grain size or water content[83]. It is also influenced by the presence of elements that cannot be measured by this method, such as organic matter, causing a dilution effect, and more generally by matrix effects which includes the interactions of other elements present in the sediment on the XRF measurement of a given element[83]. For these reasons, the ratio or log ratio of XRF counts is frequently used in XRF core studies to correct for trends in sediment properties[38,84,85]. However, in the context of this study, which focuses on the high frequency variability of a sedimentary signal related to river inputs, considering the XRF counts of Ti in relation to another element would introduce an unnecessary noise that would disturb our analysis of the proxy fluctuation. Centennial to millennial scale variations of fluvial and aeolian input during the last deglaciation were inferred from the grain size distribution in sediments from cores M77/2-005 and G14[19]. Downcore Ti-XRF variations in cores M77/2-005-3 and G14 covary with changes in fine particles of fluvial origin[19]. Maximum (minimum) Ti-XRF values occur when fluvial inputs increase (decrease) (supplementary Fig. 6), suggesting that Ti-XRF is associated with particles of fluvial origin and not of aeolian and can be considered a potential proxy for fluvial discharges. To allow for the comparison of XRF data from different laboratories and different cores, a normalization to the maximum value of titanium counts was performed (supplementary Fig. 4).

3.4.3. Extracting ENSO amplitude

The XRF analyses with 1 mm steps yield a temporal resolution of 0.8 years in the deglacial sections of core M77/2-005-3, and 2.2 years in the Late Holocene section (2.7-1.3 kyr). The temporal resolution of the XRF record in the deglacial section of core G14 is 1.3 years.

The records were resampled by linear interpolation at 0.5-year resolution in the deglacial and Late Holocene sections (supplementary Fig. 5). A 2.5-8 years band pass filter was then applied to all records to extract the ENSO frequency band. The ENSO

band was calculated based on the difference of moving averages. The amplitude of ENSO-related variability was estimated by the standard deviation of the filtered signal over 300-years moving windows. The relative change of ENSO variability in Callao and Pisco was calculated in reference to the Late Holocene record from Callao. The reproducibility of the normalized Ti-XRF records and of the filtered Ti-XRF standard deviation in Callao and Pisco allows us to use the Callao Late Holocene section as a common modern reference.

3.5. References

1. Deser, C., Alexander, M., Xie, S. & Phillips, A. Sea Surface Temperature Variability: Patterns and Mechanisms. *Annual Review of Marine Science*2, 115-143 (2010).
2. McPhaden, M. J., Zebiak, S. E. & Glantz, M. H. ENSO as an Integrating Concept in Earth Science. *Science* **314,** 1740–1745 (2006).
3. Garreaud, R. D., Vuille, M., Compagnucci, R. & Marengo, J. Present-day South American climate. *Palaeogeography, Palaeoclimatology, Palaeoecology* **281,** 180–195 (2009).
4. Grimm, A. & Tedeschi, R. ENSO and Extreme Rainfall Events in South America. *Journal of Climate* 22, 1589-1609 (2009).
5. Sulca, J., Takahashi, K., Espinoza, J., Vuille, M. & Lavado-Casimiro, W. Impacts of different ENSO flavors and tropical Pacific convection variability (ITCZ, SPCZ) on austral summer rainfall in South America, with a focus on Peru. *International Journal of Climatology* 38, 420-435 (2017).
6. Cai, W. et al. Climate impacts of the El Niño–Southern Oscillation on South America. *Nature Reviews Earth & Environment* 1, 215-231 (2020).
7. Cai, W. et al. Changing El Niño–Southern Oscillation in a warming climate. *Nature Reviews Earth & Environment* 2, 628-644 (2021).
8. Callahan, C. et al. Robust decrease in El Niño/Southern Oscillation amplitude under long-term warming. *Nature Climate Change* 11, 752-757 (2021).
9. Wengel, C. et al. Future high-resolution El Niño/Southern Oscillation dynamics. *Nature Climate Change* 11, 758-765 (2021).
10. Braconnot, P. et al. Evaluation of climate models using palaeoclimatic data. *Nature Climate Change* 2, 417-424 (2012).
11. Emile-Geay, J. et al. Links between tropical Pacific seasonal, interannual and orbital variability during the Holocene. *Nature Geoscience* 9, 168-173 (2016).
12. Marcott, S. et al. Centennial-scale changes in the global carbon cycle during the last deglaciation. *Nature* 514, 616-619 (2014).
13. Peltier, W., Argus, D. & Drummond, R. Space geodesy constrains ice age terminal deglaciation: The global ICE-6G_C (VM5a) model. *Journal of Geophysical Research: Solid Earth* 120, 450-487 (2015).
14. Lambeck, K., Rouby, H., Purcell, A., Sun, Y. & Sambridge, M. Sea level and global ice volumes from the Last Glacial Maximum to the Holocene. *Proceedings of the National Academy of Sciences* 111, 15296-15303 (2014).

15. Clark, P. et al. Global climate evolution during the last deglaciation. *Proceedings of the National Academy of Sciences* 109, E1134-E1142 (2012).
16. Sadekov, A. et al. Palaeoclimate reconstructions reveal a strong link between El Niño-Southern Oscillation and Tropical Pacific mean state. *Nature Communications* 4, (2013).
17. Koutavas, A. & Joanides, S. El Niño-Southern Oscillation extrema in the Holocene and Last Glacial Maximum. *Paleoceanography* 27, (2012).
18. Rein, B. et al. El Niño variability off Peru during the last 20,000 years. *Paleoceanography* 20, n/a-n/a (2005).
19. Yseki, M. et al. Millennial variability of terrigenous transport to the central-southern Peruvian margin during the last deglaciation (18–13 kyr BP). Preprint at https://cp.copernicus.org/preprints/cp-2021-183/ (2022).
20. Timmermann, A. et al. The Influence of a Weakening of the Atlantic Meridional Overturning Circulation on ENSO. *Journal of Climate* 20, 4899-4919 (2007).
21. Merkel, U., Prange, M. & Schulz, M. ENSO variability and teleconnections during glacial climates. *Quaternary Science Reviews* 29, 86-100 (2010).
22. Braconnot, P., Luan, Y., Brewer, S. & Zheng, W. Impact of Earth's orbit and freshwater fluxes on Holocene climate mean seasonal cycle and ENSO characteristics. *Climate Dynamics* 38, 1081-1092 (2011).
23. Luan, Y., Braconnot, P., Yu, Y. & Zheng, W. Tropical Pacific mean state and ENSO changes: sensitivity to freshwater flux and remnant ice sheets at 9.5 ka BP. *Climate Dynamics* 44, 661-678 (2015).
24. Carré, M. et al. Holocene history of ENSO variance and asymmetry in the eastern tropical Pacific. *Science* 345, 1045-1048 (2014).
25. Carré, M. et al. High-resolution marine data and transient simulations support orbital forcing of ENSO amplitude since the mid-Holocene. *Quaternary Science Reviews* 268, 107125 (2021).
26. Haug, G., Hughen, K., Sigman, D., Peterson, L. & Röhl, U. Southward Migration of the Intertropical Convergence Zone Through the Holocene. *Science* 293, 1304-1308 (2001).
27. Vega-Jácome, F., Lavado-Casimiro, W. & Felipe-Obando, O. Assessing hydrological changes in a regulated river system over the last 90 years in Rimac Basin (Peru). *Theoretical and Applied Climatology* 132, 347-362 (2017).
28. Lavado Casimiro, W., Ronchail, J., Labat, D., Espinoza, J. & Guyot, J. Basin-scale analysis of rainfall and runoff in Peru (1969–2004): Pacific, Titicaca and Amazonas drainages. *Hydrological Sciences Journal* 57, 625-642 (2012).
29. Lagos, P., Silva, Y., Nickl, E. & Mosquera, K. El Niño – related precipitation variability in Perú. *Advances in Geosciences* 14, 231-237 (2008).
30. Lavado-Casimiro, W. & Espinoza, J. Impactos de El Niño y La Niña en las lluvias del Perú (1965-2007). *Revista Brasileira de Meteorologia* 29, 171-182 (2014).
31. Sanabria, J. et al. Rainfall along the coast of Peru during strong El Niño events. *International Journal of Climatology* 38, 1737-1747 (2017).
32. Bourrel, L. et al. Low-frequency modulation and trend of the relationship between ENSO and precipitation along the northern to centre Peruvian Pacific coast. *Hydrological Processes* 29, 1252-1266 (2014).
33. Morera, S., Condom, T., Crave, A., Steer, P. & Guyot, J. The impact of extreme El Niño events on modern sediment transport along the western Peruvian Andes (1968–2012). *Scientific Reports* 7, (2017).
34. Takahashi, K. & Martínez, A. The very strong coastal El Niño in 1925 in the far-eastern Pacific. *Climate Dynamics* 52, 7389-7415 (2017).

35. Guzman, E., Ramos, C. & Dastgheib, A. Influence of the El Niño Phenomenon on Shoreline Evolution. Case Study: Callao Bay, Perú. *Journal of Marine Science and Engineering* 8, 90 (2020).
36. Moy, C., Seltzer, G., Rodbell, D. & Anderson, D. Variability of El Niño/Southern Oscillation activity at millennial timescales during the Holocene epoch. *Nature* 420, 162-165 (2002).
37. Wittenberg, A. Are historical records sufficient to constrain ENSO simulations?. *Geophysical Research Letters* 36, (2009).
38. Mollier-Vogel, E., Leduc, G., Böschen, T., Martinez, P. & Schneider, R. Rainfall response to orbital and millennial forcing in northern Peru over the last 18 ka. *Quaternary Science Reviews* 76, 29-38 (2013).
39. Baker, P. et al. The History of South American Tropical Precipitation for the Past 25,000 Years. *Science* 291, 640-643 (2001).
40. Baker, P. et al. Tropical climate changes at millennial and orbital timescales on the Bolivian Altiplano. *Nature* 409, 698-701 (2001).
41. Martin, L. et al. Lake Tauca highstand (Heinrich Stadial 1a) driven by a southward shift of the Bolivian High. *Science Advances* 4, (2018).
42. González-Pinilla, F. et al. High- and low-latitude forcings drive Atacama Desert rainfall variations over the past 16,000 years. *Science Advances* 7, (2021).
43. Cheng, H., Sinha, A., Wang, X., Cruz, F. & Edwards, R. The Global Paleomonsoon as seen through speleothem records from Asia and the Americas. *Climate Dynamics* 39, 1045-1062 (2012).
44. Deplazes, G. et al. Links between tropical rainfall and North Atlantic climate during the last glacial period. *Nature Geoscience* 6, 213-217 (2013).
45. McGee, D., Donohoe, A., Marshall, J. & Ferreira, D. Changes in ITCZ location and cross-equatorial heat transport at the Last Glacial Maximum, Heinrich Stadial 1, and the mid-Holocene. *Earth and Planetary Science Letters* 390, 69-79 (2014).
46. Rodbell, D. et al. An ~15,000-Year Record of El Niño-Driven Alluviation in Southwestern Ecuador. *Science* 283, 516-520 (1999).
47. Cobb, K. M., Charles, C. D., Cheng, H. & Edwards, R. L. El Niño/Southern Oscillation and tropical Pacific climate during the last millennium. *Nature* **424,** 271–276 (2003).
48. Clement, A., Seager, R. & Cane, M. Orbital controls on the El Niño/Southern Oscillation and the tropical climate. *Paleoceanography* 14, 441-456 (1999).
49. Otto-Bliesner, B. El Niño/La Niña and Sahel precipitation during the Middle Holocene. *Geophysical Research Letters* 26, 87-90 (1999).
50. Brown, J. et al. Comparison of past and future simulations of ENSO in CMIP5/PMIP3 and CMIP6/PMIP4 models. *Climate of the Past* 16, 1777-1805 (2020).
51. Cai, W. et al. Increasing frequency of extreme El Niño events due to greenhouse warming. *Nature Climate Change* 4, 111-116 (2014).
52. Cai, W. et al. ENSO and greenhouse warming. *Nature Climate Change* 5, 849-859 (2015).
53. Cai, W. et al. Increased variability of eastern Pacific El Niño under greenhouse warming. *Nature* 564, 201-206 (2018).
54. Licciardi, J. M., Teller, J. T. & Clark, P. U. Freshwater routing by the Laurentide Ice Sheet during the last deglaciation. *Mechanisms of Global Climate Change at Millennial Time Scales* 177–201 (1999).
55. Carlson, A. & Clark, P. Ice sheet sources of sea level rise and freshwater discharge during the last deglaciation. *Reviews of Geophysics* 50, (2012).

56. Dynamics of meltwater discharge from Northern Hemisphere ice sheets during the last deglaciation. *Nature* 310, 674-677 (1984).
57. Brendryen, J., Haflidason, H., Yokoyama, Y., Haaga, K. & Hannisdal, B. Eurasian Ice Sheet collapse was a major source of Meltwater Pulse 1A 14,600 years ago. *Nature Geoscience* 13, 363-368 (2020).
58. Liu, Z. *et al.* Evolution and forcing mechanisms of El Niño over the past 21,000 years. *Nature* **515,** 550–553 (2014).
59. Williamson, M. et al. Effect of AMOC collapse on ENSO in a high resolution general circulation model. *Climate Dynamics* 50, 2537-2552 (2018).
60. Fairbanks, R. A 17,000-year glacio-eustatic sea level record: influence of glacial melting rates on the Younger Dryas event and deep-ocean circulation. *Nature* 342, 637-642 (1989).
61. Bard, E. et al. Deglacial sea-level record from Tahiti corals and the timing of global meltwater discharge. *Nature* 382, 241-244 (1996).
62. Seidov, D. Meltwater and the global ocean conveyor: northern versus southern connections. *Global and Planetary Change* 30, 257-270 (2001).
63. Stouffer, R., Seidov, D. & Haupt, B. Climate Response to External Sources of Freshwater: North Atlantic versus the Southern Ocean. *Journal of Climate* 20, 436-448 (2007).
64. Swingedouw, D., Fichefet, T., Goosse, H. & Loutre, M. Impact of transient freshwater releases in the Southern Ocean on the AMOC and climate. *Climate Dynamics* 33, 365-381 (2008).
65. McManus, J., Francois, R., Gherardi, J., Keigwin, L. & Brown-Leger, S. Collapse and rapid resumption of Atlantic meridional circulation linked to deglacial climate changes. *Nature* 428, 834-837 (2004).
66. Mulitza, S. et al. Synchronous and proportional deglacial changes in Atlantic meridional overturning and northeast Brazilian precipitation. *Paleoceanography* 32, 622-633 (2017).
67. Ng, H. et al. Coherent deglacial changes in western Atlantic Ocean circulation. *Nature Communications* 9, (2018).
68. Rahmstorf, S. et al. Exceptional twentieth-century slowdown in Atlantic Ocean overturning circulation. *Nature Climate Change* 5, 475-480 (2015).
69. Caesar, L., Rahmstorf, S., Robinson, A., Feulner, G. & Saba, V. Observed fingerprint of a weakening Atlantic Ocean overturning circulation. *Nature*556, 191-196 (2018).
70. Caesar, L., McCarthy, G., Thornalley, D., Cahill, N. & Rahmstorf, S. Current Atlantic Meridional Overturning Circulation weakest in last millennium. *Nature Geoscience* 14, 118-120 (2021).
71. Yang, Q. et al. Recent increases in Arctic freshwater flux affects Labrador Sea convection and Atlantic overturning circulation. *Nature Communications* 7, (2016).
72. Bevis, M. et al. Accelerating changes in ice mass within Greenland, and the ice sheet's sensitivity to atmospheric forcing. *Proceedings of the National Academy of Sciences* 116, 1934-1939 (2019).
73. Collins, M. et al. "Long-term climate change: projections, commitments and irreversibility." Climate Change 2013-The Physical Science Basis: Contribution of Working Group I to the Fifth Assessment Report of the Intergovernmental Panel on Climate Change. *Cambridge University Press*, 1029-1136 (2013).

74. Swingedouw, D. et al. On the reduced sensitivity of the Atlantic overturning to Greenland ice sheet melting in projections: a multi-model assessment. *Climate Dynamics* 44, 3261-3279 (2014).
75. Bakker, P. et al. Fate of the Atlantic Meridional Overturning Circulation: Strong decline under continued warming and Greenland melting. *Geophysical Research Letters* 43, 12,252-12,260 (2016).
76. Berger, A. Long-Term Variations of Daily Insolation and Quaternary Climatic Changes. *Journal of the Atmospheric Sciences* 35, 2362-2367 (1978).
77. Salvatteci, R. et al. Centennial to millennial-scale changes in oxygenation and productivity in the Eastern Tropical South Pacific during the last 25,000 years. *Quaternary Science Reviews* 131, 102-117 (2016).
78. Salvatteci, R., Schneider, R., Blanz, T. & Mollier-Vogel, E. Deglacial to Holocene Ocean Temperatures in the Humboldt Current System as Indicated by Alkenone Paleothermometry. *Geophysical Research Letters* 46, 281-292 (2019).
79. Brodie, I. & Kemp, A. Variation in biogenic and detrital fluxes and formation of laminae in late Quaternary sediments from the Peruvian coastal upwelling zone. *Marine Geology* 116, 385-398 (1994).
80. Yarincik, K., Murray, R. & Peterson, L. Climatically sensitive eolian and hemipelagic deposition in the Cariaco Basin, Venezuela, over the past 578,000 years: Results from Al/Ti and K/Al. *Paleoceanography* 15, 210-228 (2000).
81. Du, X. et al. Interannual Southern California Precipitation Variability During the Common Era and the ENSO Teleconnection. *Geophysical Research Letters* 47, (2020).
82. Du, X. et al. High-resolution interannual precipitation reconstruction of Southern California: Implications for Holocene ENSO evolution. *Earth and Planetary Science Letters* 554, 116670 (2021).
83. Weltje, G. & Tjallingii, R. Calibration of XRF core scanners for quantitative geochemical logging of sediment cores: Theory and application. *Earth and Planetary Science Letters* 274, 423-438 (2008).
84. Rothwell, R. & Rack, F. New techniques in sediment core analysis: an introduction. *Geological Society, London, Special Publications* 267, 1-29 (2006).
85. Perez, L., Crisci, C., Lüning, S., de Mahiques, M. & García-Rodríguez, F. Last millennium intensification of decadal and interannual river discharge cycles into the Southwestern Atlantic Ocean increases shelf productivity. *Global and Planetary Change* 196, 103367 (2021).

3.6. Supplementary information

Supplementary Figure 1

Chronological model for Callao (M77/2-005-3 and Pisco (G-14) cores. Figure adapted from Yseki et al. (2022)

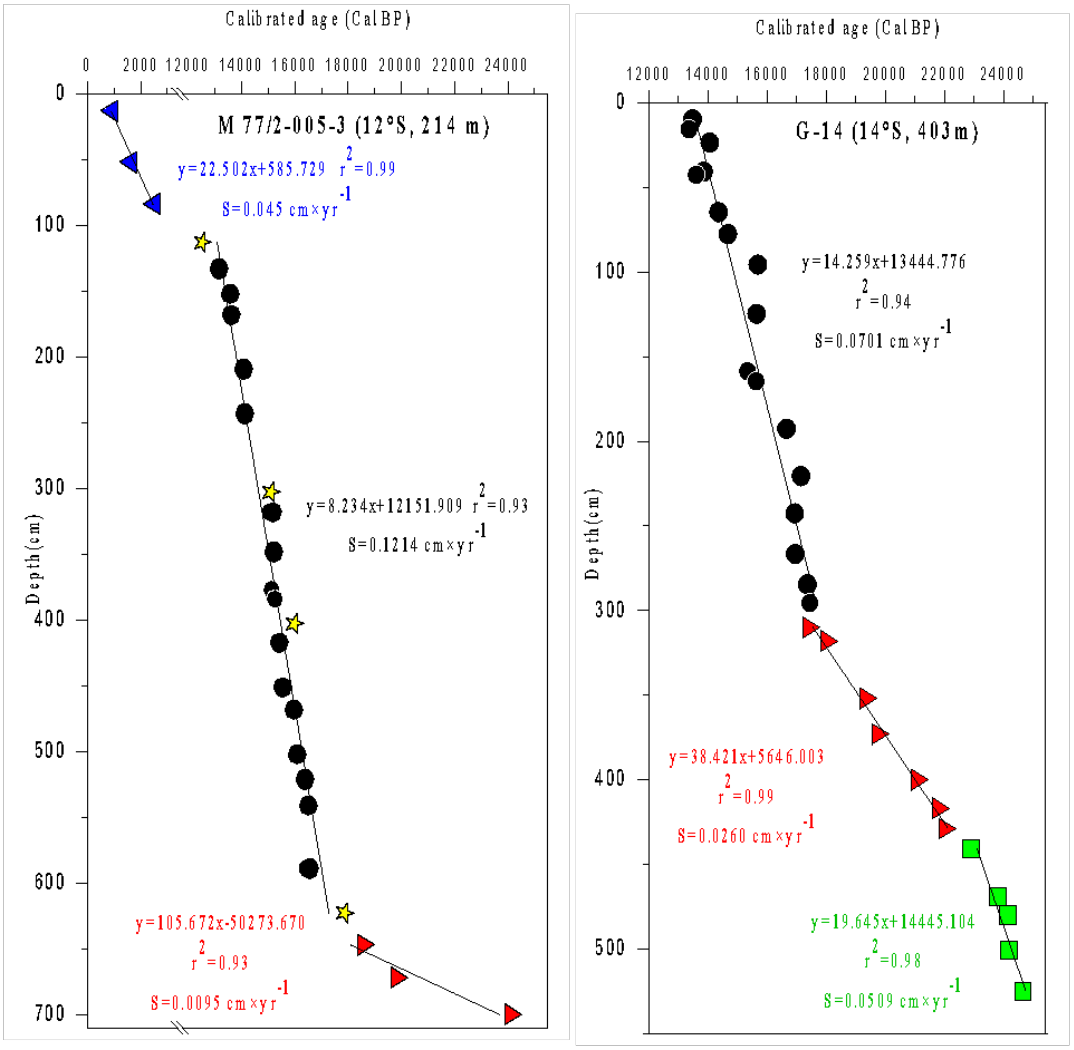

Supplementary Figure 2

X-ray images used to describe the sedimentary sequences observed in Callao (M77/2-005-3) core.

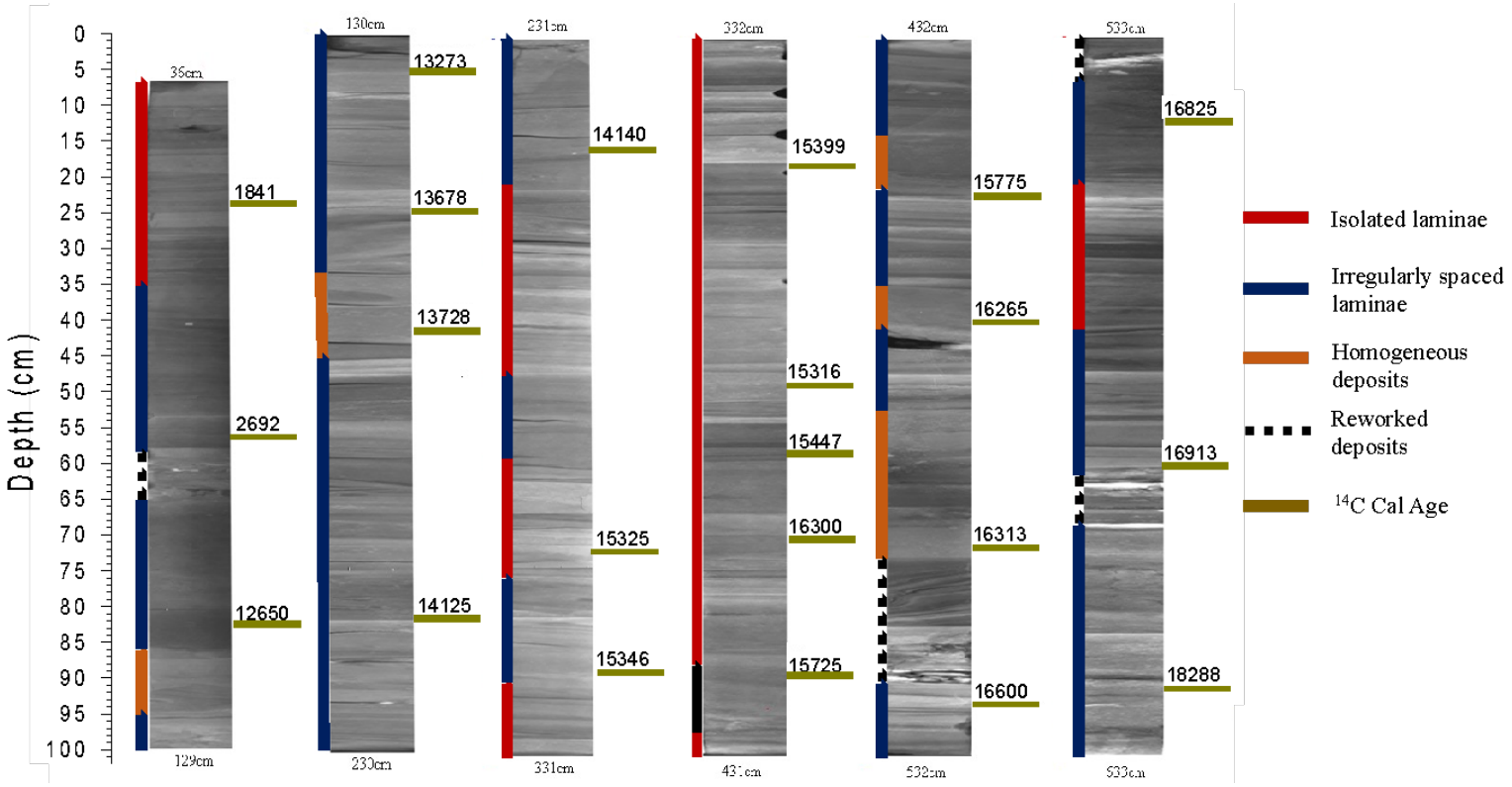

Supplementary Figure 3

X-ray images used to describe the sedimentary sequences observed in Pisco (G-14) core. Figure adapted from Salvatteci et al. (2016)

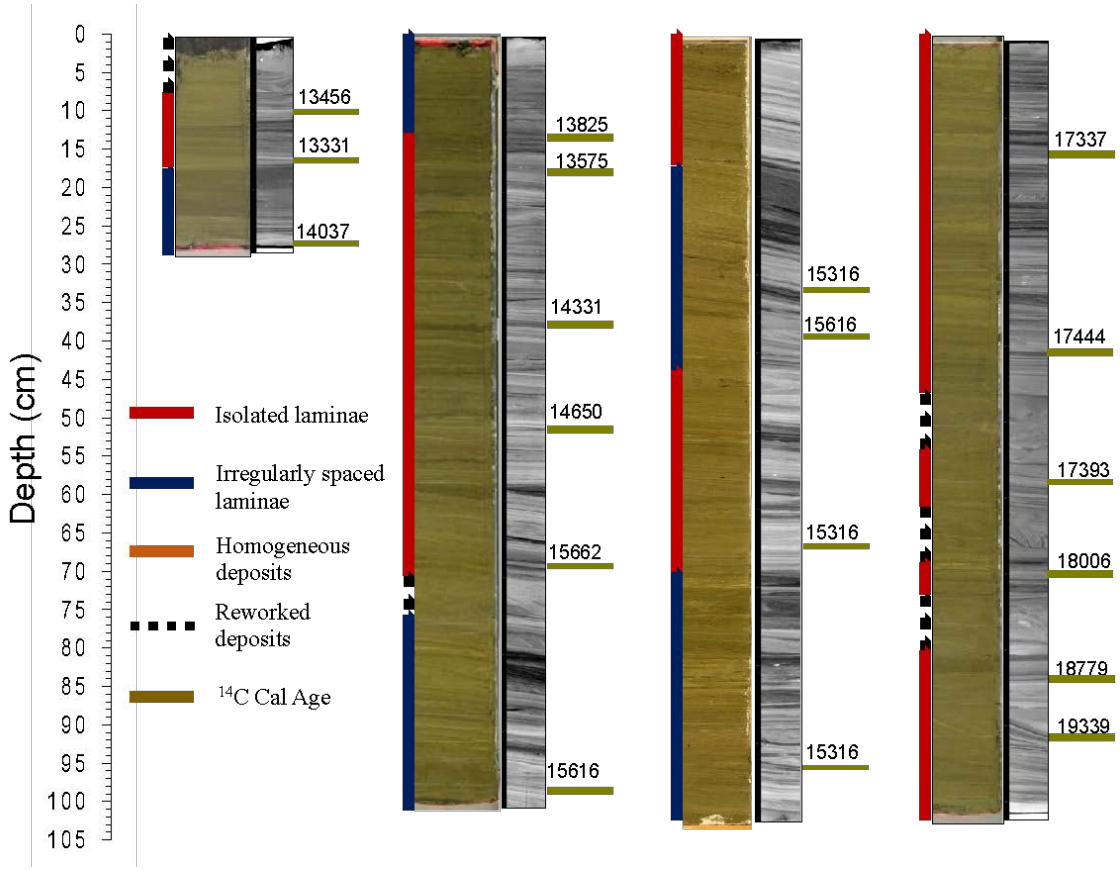

Supplementary Figure 4

Raw (black) and normalized titanium (red) from Callao (top) and Pisco (bottom) cores.

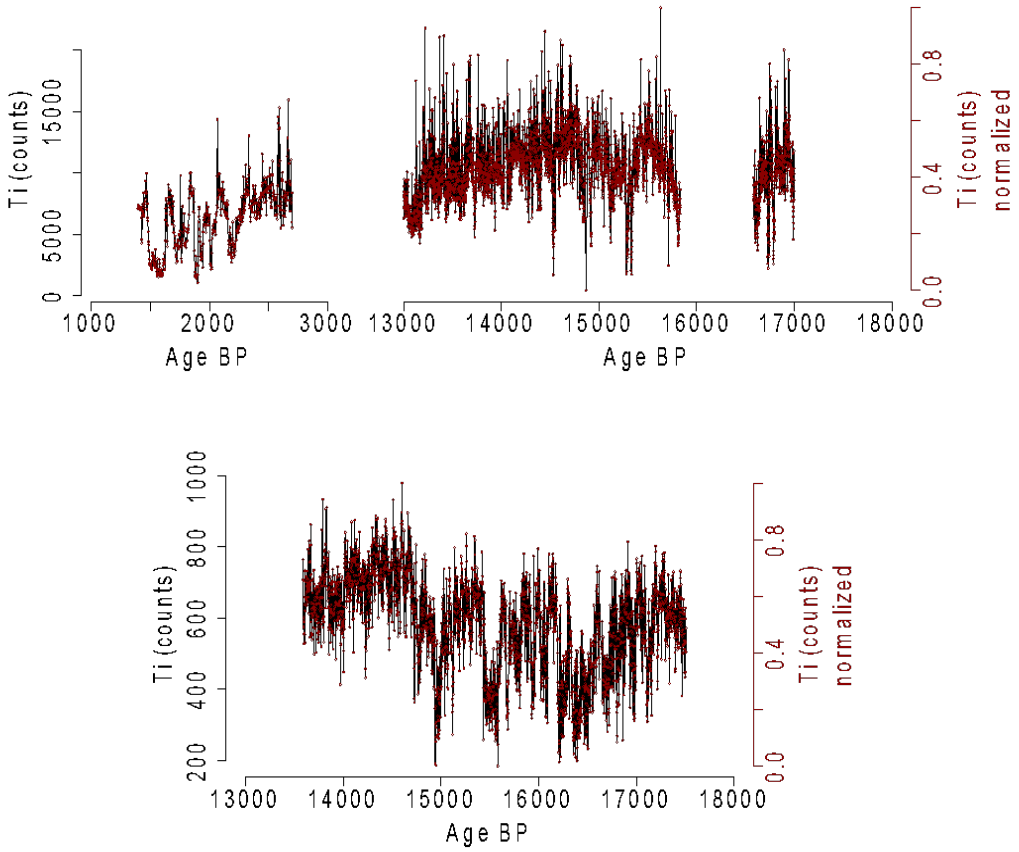

Supplementary Figure 5

Normalized (black) and resampled 0.5 yr (red) titanium from Callao (top) and Pisco (bottom) cores.

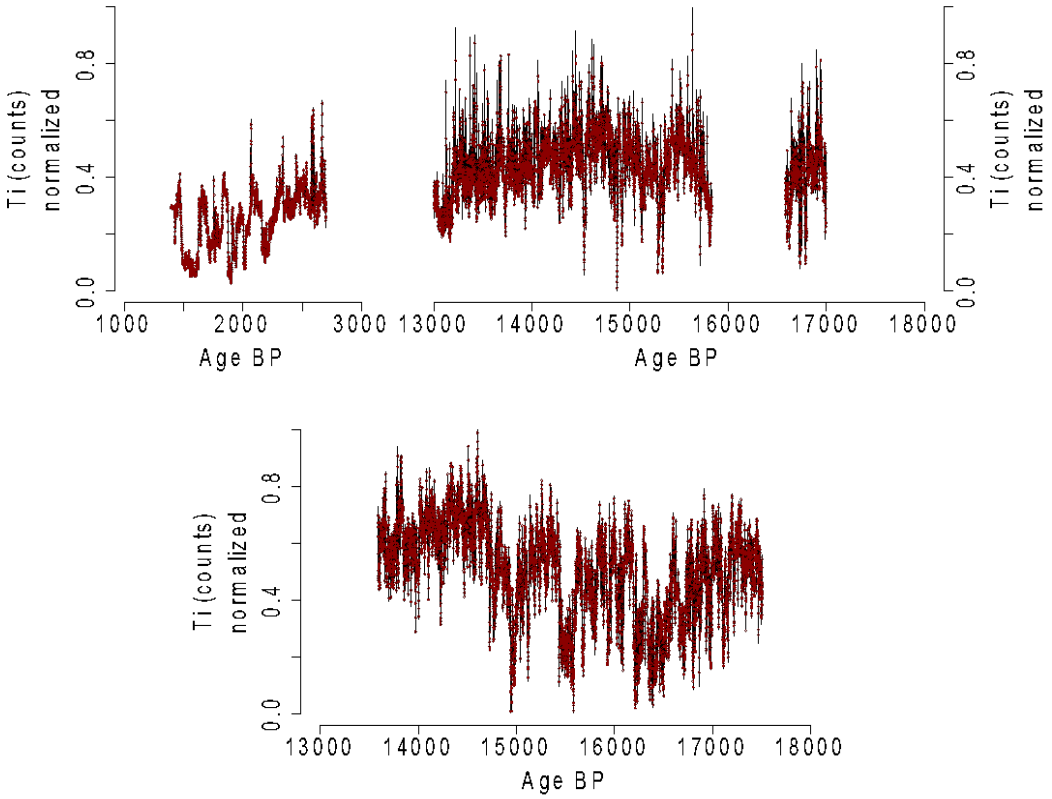

Supplementary Figure 6

Ti normalized values (150-years moving average) in Callao (red) and Pisco (blue) and fluvial vs aeolian inputs based in grain-sizes and end-member analysis in Callao (EM1/EM3) and Pisco (EM1/EM2+EM3+EM4) (Yseki et al., 2022).

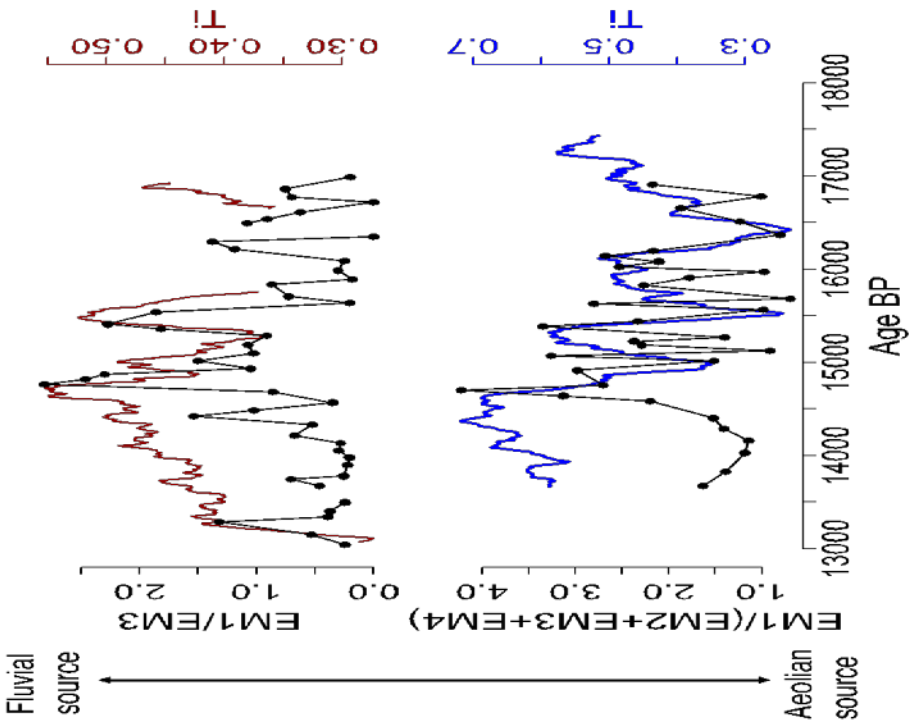

4. Enhanced upwelling-favorable wind in the Peruvian Upwelling System during the Mid-Holocene

Chapter III focuses on objective 3 of the thesis, which is to reconstruct the millennial variability of aeolian inputs and winds during the Holocene in southern Peru (17ºS). The grain-size distribution of Peruvian margin sediments is typically polymodal and for that reason provides information on sediment transport mechanisms and/or sediment sources. Grain-size distributions on sediment core M135-004-3 were measured and end-member analysis was used to deconvolved them into sub-populations. Using this methodology allows us to discriminate the different sources of terrigenous input, reconstructing the variations of aeolian inputs dependent on changes in wind intensity. Previous studies based on STT reconstruction indicate a cooling due to increased upwelling on the Peruvian margin during the Mid-Holocene. However, paleo-wind records are needed to confirm this hypothesis.

4.1. Introduction

The Peruvian Upwelling System (PUS) is one of the most productive Eastern Boundary Upwelling Systems in terms of fisheries (Chavez et al., 2008). High biological productivity is linked to the upwelling of subsurface nutrient-rich waters driven by surface wind stress (Pennington et al., 2006). The response of upwelling and wind dynamic to climate change in the PUS is uncertain. Bakun. (1990) proposed an increase in alongshore wind stress and coastal upwelling in EBUSs including the PUS due to an enhanced pressure gradient between the coast and the adjacent ocean during global warming. Gutiérrez et al. (2011) found a negative sea surface temperature (SST) trend in central-southern Peru during 1950-2010 possibly explained by an increase in coastal upwelling. A recent study using a high-resolution regional model indicates that summer winds decrease weakly (0-5%) while winter wind increase weakly (0-10%) under IPCC RCP 8.5 scenario (Chamorro et al., 2021). However, this increase is driven by the alongshore pressure gradient and intensification of the South Pacific Subtropical High (SPSH) (Chamorro et al., 2021) and not by pressure gradient between land and ocean as proposed by Bakun. (1990).

Paleoclimatic records allow us to understand the response of wind and upwelling dynamic in PUS during periods of global warming periods. The Mid-Holocene (MH, ~8-4 ka BP), was a warm period in the Northern Hemisphere due to orbital variations and insolation

changes (Kaufman et al., 2004, 2020; Renssen et al., 2009; Wanner et al., 2008; Fischer et al., 2018). Alquenones-derived temperature record (Salvatteci et al., 2019) and isotopic data from fossil mollusk (Carré et al., 2012) suggest a strong cooling in PUS during the MH due to an increase of coastal upwelling linked to an intensification of the SPSH (Carré et al., 2012; Salvatteci et al., 2019). However, paleo-wind records are needed to confirm this hypothesis. Reconstructing wind intensity during the MH and assessing, through global climate models, which forcing modulate its variability would provide information on the response of upwelling and wind dynamics in PUS to current climate change.

In the present study, we reconstruct the variability of the aeolian transport of terrigenous material dependent on wind intensity in southern Peru (17ºS). For them, grain-size distribution in laminated sediments was analyzed. In addition, the end-member analysis (EMA) was performed for deconvolved grain-size distribution into sub-populations and reconstruct the aeolian sources of terrigenous material (e.g., Beuscher et al., 2017; Humphries et al., 2017; Yseki et al., 2022). Previous studies in PUS, indicate that end-members linked to the coarse fraction (50-100 μm) can be used as indicators of aeolian transport dependent on surface wind (Briceño-Zuluaga et al., 2016; Yseki et al., 2022) Additionally, we used the output from two transient simulations (ECHAM slo43 and IPSL TR6V) to assess the effects of changes in the Intertropical Convergence Zone (ITCZ)-SPSH system on the wind dynamic during the MH.

4.1.1. Regional setting

The south of the PUS (14-18ºS), is characterized by large aeolian sources and sandstorms that reach velocities up to 10-15 m/s (Briceño-Zuluaga et al., 2017). These storms are produced by a local intensification of alongshore surface wind and by alongshore pressure gradients (Briceño-Zuluaga et al., 2017). In this area, wind transport coarse silt and sand to the continental shelf and slope (Scheidegger and Krissek, 1982, Briceño-Zuluaga et al., 2016, 2017). In the PUS, wind intensity presents a seasonal variability associated regionally with the north shift of the ITCZ and SPSH with stronger wind during winter and locally to the land-ocean and alongshore pressure gradient (Strub et al., 1998; Karstensen and Ulloa, 2009; Gutiérrez et al., 2011; Chamorro et al., 2018).

4.2. Materials and methods

4.2.1. Marine sediment core

M135-004-3 core was retrieved from the Southern Peruvian margin (17º2 S, 71º4 W, 229 m water depth) (Fig. 1) during the Meteor cruise M135 (Salvatteci et al., 2019). Chronology and lithology were described extensively in Salvatteci et al. (2019). The age model was done using a linear regression based on 10 ^{14}C ages and M135-004-3 core cover the last 9 ka with a sediment rate of 0.78 $mm.y^{-1}$ (Salvatteci et al., 2019). In contrast to the cores that contain Holocene sequences, M135-004-3 shows fewer disturbed and more laminated sequences, being the most complete record during the Holocene (0-9 ka BP) recovered in the Peruvian margin (Salvatteci et al., 2019).

4.2.2. Grain-size and end-member analysis

Grain-size analysis was performed only on the laminated sections in order to avoid the effect of particle resuspension and guarantees that the analyzed sediments are a result of deposition from the water column. To isolate the terrigenous fraction of the sediment, organic matter, calcium carbonates and biogenic silica were removed using hydrogen peroxide (H_2O_2 30% at 60ºC for 3 to 4 days), hydrochloric acid (HCl 10% for 12h) and sodium carbonate (Na_2CO_3, 1M at 90ºC for 3h) respectively following the procedure described in Briceño-Zuluaga et al. (2016).

An automated image analysis system (model FPIA3000, Malvern Instruments) with a measurement range of 0.5-200 μm was used for grain-size distribution analysis. Detailed descriptions of the FPIA3000 are described in Flores-Aqueveque et al. (2014) and Briceño-Zuluaga et al. (2016). All samples were sieved with a 200 μm mesh before the analysis because the analytical conditions applied in this work can only measure particles smaller than 200 μm. We considered that our analysis covers the entire grain-size range present in the sediment due no particles larger than 200 μm were found.

The AnalySize modeling algorithm performed by Paterson and Heslop (2015) was used to unmix the grain-size distribution. AnalySize is based on the unmixing performed in hyperspectral image analysis (Paterson and Heslop, 2015). The objective of the algorithm is to establish a physical mixing model that transforms the measured grain-size distribution to a finite number of unimodal grain-size end-members. To estimate the minimum number of end-

members, the coefficient of determination (r^2), which represents the proportion of the variance of each grain-size class, is calculated. More specific details are available from Paterson and Heslop (2015).

Principal component analysis (PCA) in end-members contribution data set was carried out using Factoextra package (Kassambara and Mundt, 2017) in R software.

4.2.3. Transient model simulation

We used ECHAM sol43 and IPSL TR6V transient simulation from climate models MPI-ESMR and IPSL-CM6 respectively (Table 1). Both experiments were forced by orbital parameters calculated according to Berger (1978), as suggested for PMIP4 transient simulations (Otto-Bliesner et al., 2017). Greenhouse gas concentration is prescribed according updated ice core data for the MPI-ESM simulation (Dallmeyer et al., 2020) and to the PMIP4 protocol (Otto-Bliesner et al., 2017) in the IPSL-CM6 simulation. The ECHAM slo43 simulation corresponds to the simulation with dynamic vegetation described in detail in Dallmeyer et al. (2020) and the IPSL TR6V simulation was run with a version of the IPSLCM5-MR model (Dufresne et al., 2013) in which land surface component was changed adding a new snow model and dynamic vegetation. More specific model details are available from Braconnot et al. (2019). In both transient simulations, the SST and near-coastal wind outputs at 17ºS (Fig. 1) were calculated.

Table 1. Main characteristic of transient simulations

	MPI-ESMR	IPSL-CM6
Atmosphere grid (lat,lon)	1.875º x 1.875º	1.25º x 2.5º
Atmosphere vertical levels	47	39
Ocean grid	1.5º	2º
Ocean vertical levels	40	31
Carbon cycle	interactive	interactive
Vegetation	dynamic	dynamic
Time period (years BP)	7950-100	6000-0

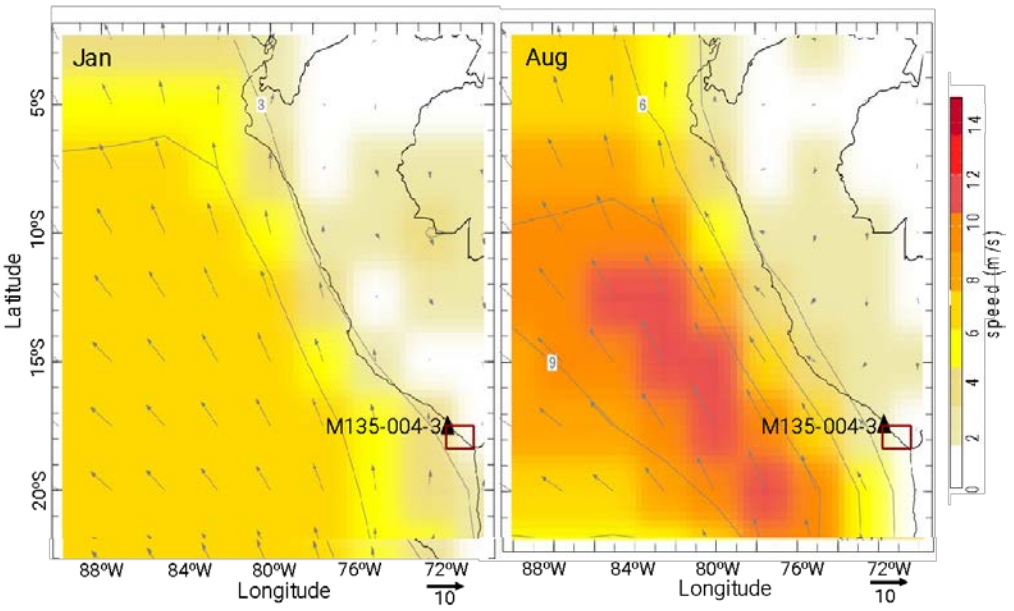

Figure 1. Location of the sampling of the sediment core M135-004-3. Average wind speed (m/s) at 1000 hPa in January and August during 1991-2020. (http://iridl.ldeo.columbia.edu). Red square indicates the area of SST and near-coastal wind in the transient simulations.

4.3. Results

4.3.1. Grain-size distribution and end-member analysis

Sediments of a core M135-005-4 display a polymodal distribution. For the EMA, a model with 4 end-members was chosen based on multiple correlation coefficient (r^2) and it explain 98% of the grain-size distribution data set variance (Fig. 2a). Each of the 4 end-members (EM) present a unimodal distribution with a median at 11 µm, 57 µm, 87 µm and 110 µm respectively (Fig. 2b).

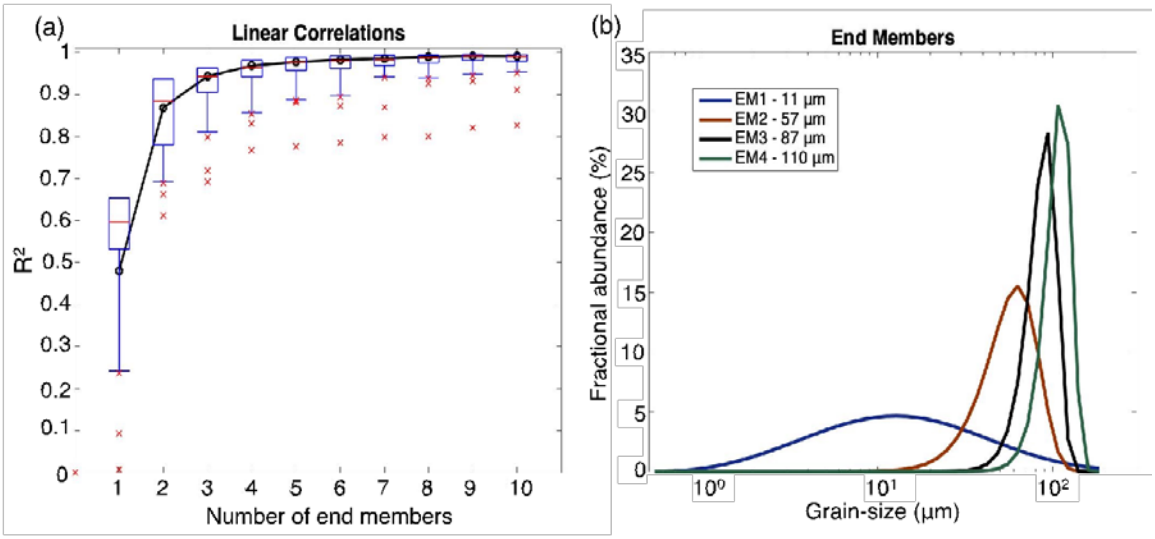

Figure 2. Coefficient of determination (r^2) as a function of the number of end-members chosen to model the observed grain-size distribution in M135-005-4 core (a) and Grain size distribution of the 4 end-members (b).

The contribution of EM3 and EM4 was higher in the MH than during the Late Holocene (Fig. 3). EM2 contribution is low during the MH and shows a peak in the recent part (0.3 ka BP) (Fig. 3). Finally, the contribution of EM1 is low during the MH except for a peak at 8.2-8 ka and 4.4-4.2 ka BP, while during the Late Holocene an increase is found (Fig. 3).

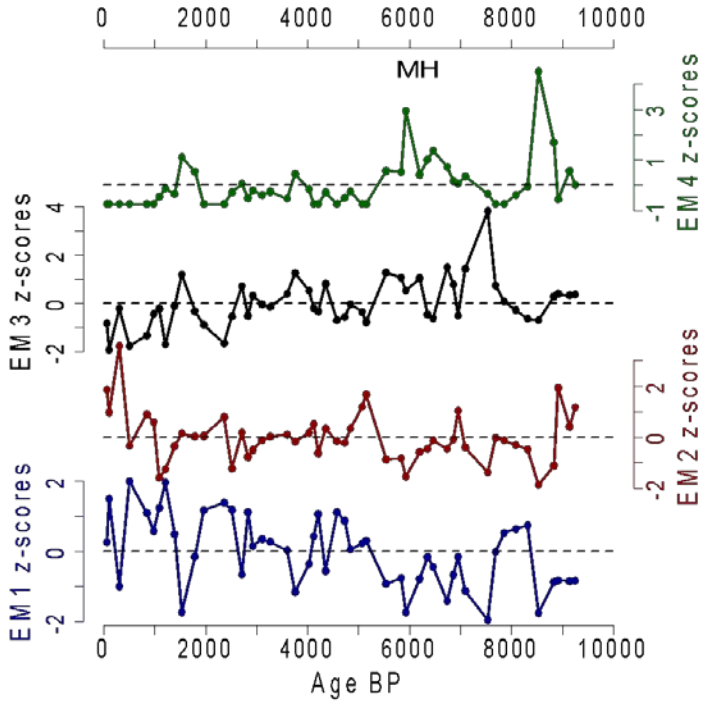

Figure 3. Variation in contribution of the grain-size end-members.

4.3.2. Transient simulation

In the southern part of the Peruvian margin, 17ºS (Fig. 1), both transient simulations indicate a slight cooling in austral summer (0-0.4ºC) and austral winter (0-0.2ºC) during the MH (Fig. 4a and 4c). However, an increase in near-coastal wind is only observed during the austral winter in both transient simulations. This increment is more marked in the transient model ECHAM slo43 (Fig. 4b and 4d).

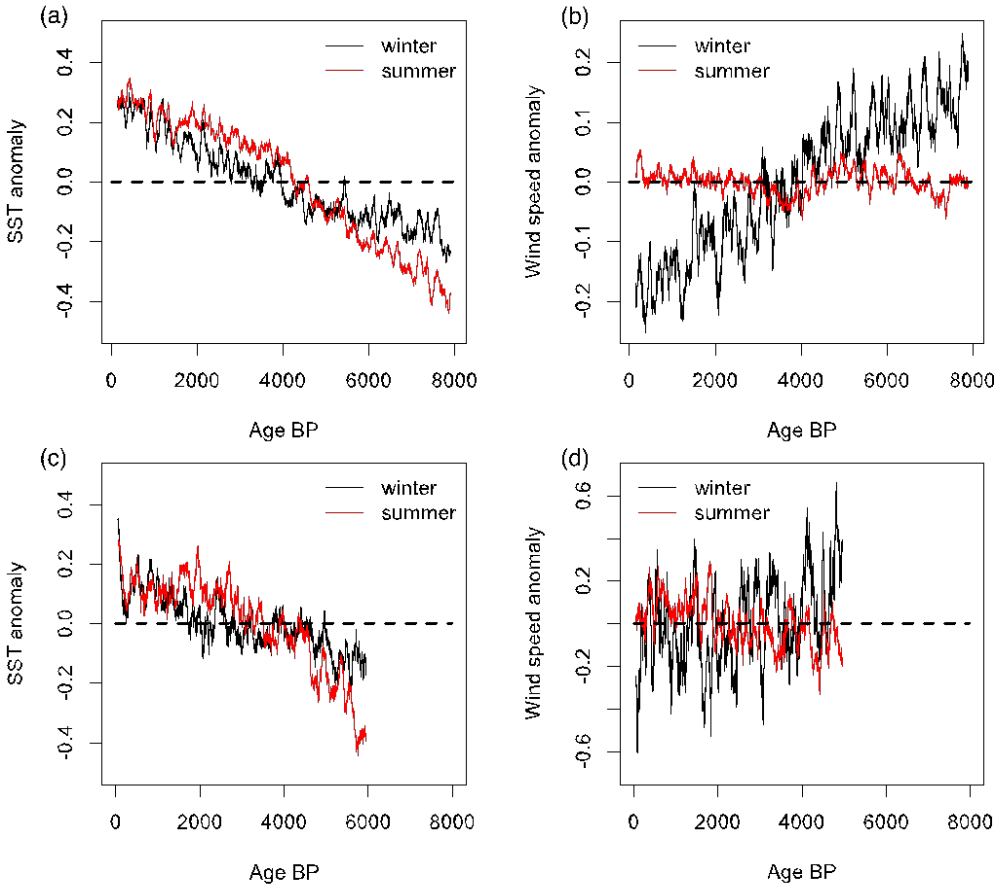

Figure 4. SST and near-coastal wind speed anomalies at southern Peruvian margin (17ºS) in ECHAM slo43 (a, b) and IPSL TR6V (c, d) transient simulation.

4.4. Discussion

4.4.1. Assignment of end-members

In order to assign a process or source to each end-member, it is necessary to contemplate the regional context (Yseki et al. 2022). The study area (17ºS) presents similar characteristics to the previous studied Pisco region (14ºS) such as a narrow continental shelf, large aeolian sources and presence of sandstorms. Briceño-Zuluaga et al. (2016) and Yseki et al. (2022) suggest that the fine particles (10 um) present in the marine cores collected in Pisco proceed from a fluvial origin. These interpretations are robust with the grain size of fine particles (□6-14 μm) in marine cores related to fluvial contributions recorded in different areas of the world (e.g., Stuut and Lamy, 2004; Stuut et al., 2007; Beuscher et al., 2017).

Regarding the coarse fraction (50-100 μm), Yseki et al. (2022) show that during events characterized by a large increase in wind speed, the frequency of particles between 70-100 μm increases in the surface sediments of Pisco and can be transported a long distance across the

continental margin. Likewise, based on Hybrid Single-Particle Lagrangian Integrated Trajectory, Briceño-Zuluaga et al. (2017) indicate that coarse particles (50-90 µm) can be transported directly from aeolian sources to the continental shelf during sandstorms events in Pisco. Therefore, end-members with a median of 50 um, 70 um, 90-100 um has been assigned an aeolian origin in marine cores collected in Pisco during the last millennium (Briceño-Zuluaga et al., 2016) and the last deglaciation (Yseki et al., 2022).

Since Pisco (14ºS) and the study area (17ºS) have similar characteristics within the regional context and the end-members reported in this study have a similar median to the end-members recorded in Pisco (Briceño-Zuluaga et al., 2016; Yseki et al., 2022), the contribution variations of the end-member related to fine particles (EM1, 11 µm) and end-member associated with the coarse fraction (EM2, 57 µm; EM3, 87 µm and EM4, 110 µm) in M135-004-3 sediments will be interpreted as indicators of fluvial and aeolian inputs respectively. Although EM2, EM3 and EM4 are all characteristic of an aeolian source, an increase in the contributions of the coarser end-members EM3 and EM4 would be related to intense wind events such as sandstorms in the study area (17ºS).

Since the sum of the contributions of all end-members is obviously 100% and thus the increase/decrease in the contribution of one end-member influences the others, it is difficult to use the variability of a single end-member's contribution as a proxy. Therefore, a PCA of end-members contribution data set was performed. The first principal component (PC1) explains 55.7% of the end-members variance. PC1 is positively correlated with particles of aeolian source (EM3 and EM4) and strongly negatively correlated with particles of fluvial origin (EM1) (Fig. 5). Therefore, The PC1 will be interpreted as an indicator of variations in aeolian source linked to intense wind events (EM3 and EM4) versus fluvial source (EM1).

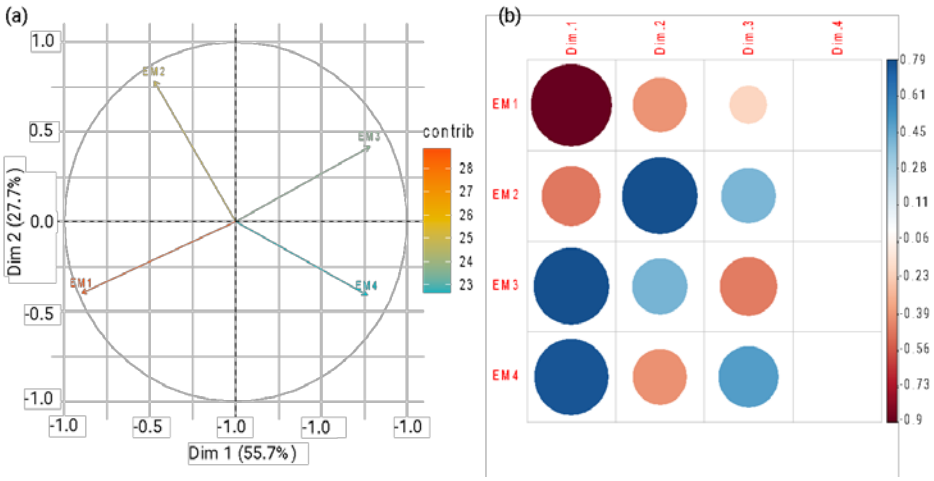

Figure 5. Principal component analysis (a) and correlation of end-members to principal components (b).

4.4.2. Increased upwelling-favorable wind during the Mid-Holocene in PUS

During the MH, paleoclimatic records indicate a cooling in the southern Peruvian margin attributed to an increase in wind stress and coastal upwelling as a result of an intensified SPSH (Carré et al., 2012; Salvatteci et al., 2019) (Fig. 6c). Our findings show an increment in aeolian input and enhanced transport of coarse particles (90-110 μm) in southern Peru (17ºS) during the MH (Fig. 6f). The transport of these coarse particles to the continental shelf in the study area requires large aeolian sources and intense wind events such as sandstorms (Briceño-Zuluaga et al., 2017). Since the occurrence of these storms is linked to an intensification of the alongshore surface wind (Briceño-Zuluaga et al., 2017), our results suggest an enhanced upwelling-favorable wind during the MH. The latter is consistent with STT diminution reported in the study area and support the idea that the cooling at the southern margin of Peru is due to an increase in the coastal upwelling.

At different times-scale, variations of the wind and upwelling dynamics in PUS have been attributed to a meridional shift of the ITCZ-SPSH system and changes in Walker circulation (Carré et al. 2012, Salvatteci et al., 2014, 2019; Briceño-Zuluaga et al., 2016; Yseki et al., 2022). Multiple evidences during the Mid-Holocene suggest a strong SST Pacific zonal gradient (Fig. 6a) and thus an intensified Walker Circulation (Koutavas and Joanides, 2012) also known as La Niña-type conditions in the tropical Pacific (Carré et al., 2012). During this key period, a northern shift of the ITCZ (Haug et al., 2001; McGee et al., 2014) is also recorded in response to NH summer insolation increase due to insolation forcing (Fig. 6b). Records of interannual variability based on $\partial^{18}O$ and Sr/Ca of corals and bivalves in tropical eastern and central Pacific evidenced a period of ENSO minimum that culminates between 5 and 4 kyr BP (Carré et al., 2021). This corresponds to a minimum of sand grain from eolian source in our record and weaks El Niño are coherent with an intensification of Walker circulation. Moreover, it confirms that it is the eolian input that control the minimum of the proxy since an increase in fluvial transport is very improbable during a period of weak El Nino.

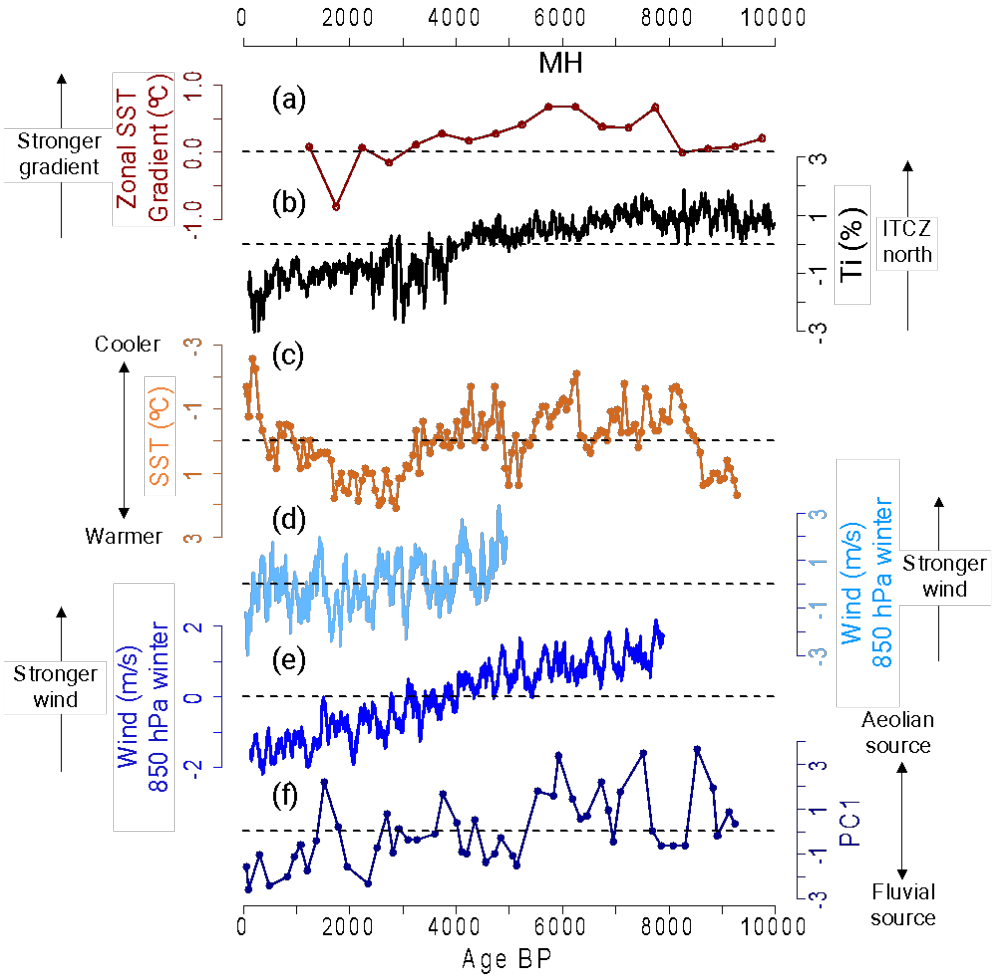

Figure 6. (a) Zonal SST gradient anomaly calculated as the difference between western and eastern Pacific averages (Koutavas and Joanides, 2012). Titanium concentration (z-scores) of Cariaco Basin as a proxy for the latitudinal displacement of the ITCZ (Haug et al., 2001). Alkenone-derived near surface temperature (z-scores) from M135-004-3 core, 17ºS (Salvatteci et al., 2019). Near-coastal wind speed anomalies during austral winter at 17ºS in IPSL TR6V € and ECHAM slo43 (f) transient simulations. PC1 as a proxy for aeolian vs fluvial source from M135-004-3 core, 17ºS (this study).

4.4.3. Transient simulations-proxy data comparison

Both models indicate an enhancement of near-coastal wind in the austral winter during the MH in the study area (Fig. 6d and 6e). These results are consistent with the increase in upwelling-favorable wind inferred from our paleo-wind record. Since regional changes in ITCZ-SPHP system impact near-coastal wind in the PUS (Strub et al., 1998; Karstensen and Ulloa, 2009), the characteristics of the SPHP and ITCZ, represented by sea level pressure and precipitation respectively were investigated in the simulations (Fig.7 and 8). Both models suggest an intensification (weakening) of the SPSH core during austral winter (austral summer)

during the MH (Fig. 7 and 8). In addition, during the austral winter, both models show an expansion and a northern shift of the SPSH with a core located ~25ºS (Fig. 7 and 8). The ITCZ seems also shifted northward with higher precipitation north of the equator in both models in austral winter (Fig. 7 and 8). In the region considered by the two climate simulations, the shift is limited to the eastern Pacific (Fig. 7 and 8), probably because it is influenced by the northward shift of the ITCZ in the Atlantic Ocean in Northern Hemisphere summer, as shown in the data (Haug et al., 2001, Wanner et al., 2008) and in the models (Braconnot et al., 2007). The PMIP2 models show that this shift is related to the stronger North Hemisphere summer insolation during MH that provoked an increase in the meridional SST gradient between the North Atlantic and the Tropical Atlantic and an intensification of the West African monsoon (Braconnot et al., 2007).This shift would be responsible for the increase in the zonal equatorial SST gradient in the Pacific (Koutavas et al., 2006; Koutavas and Joanides 2012) although this relation does not appears in the two studied simulations where the zonal temperature gradient is weaker in winter at MH (Fig. 7 and 8).

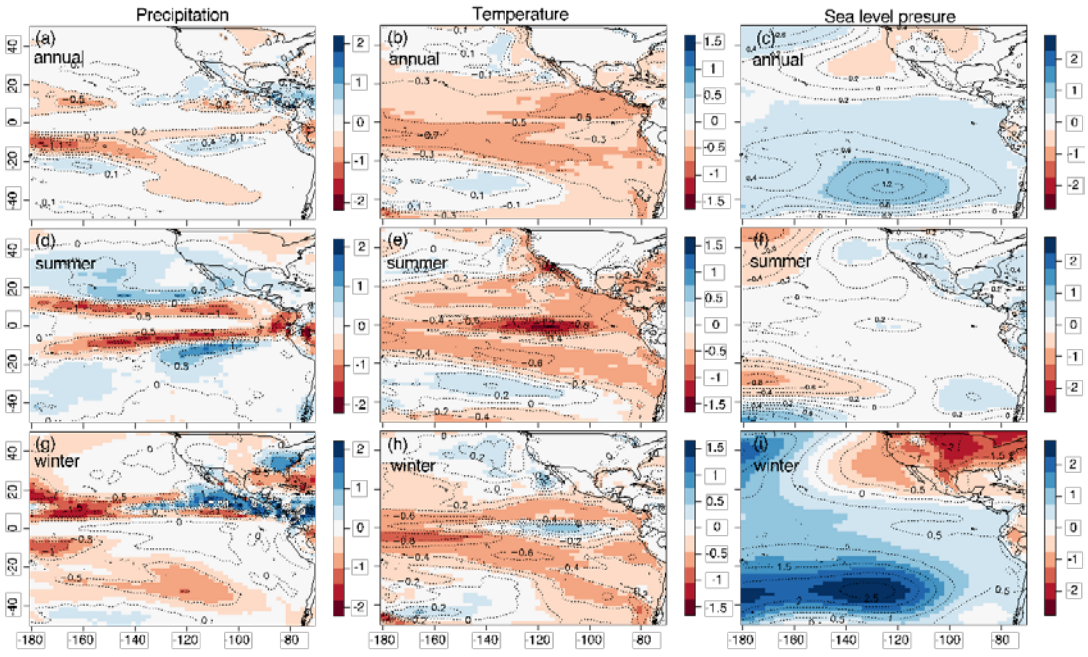

Figure 7. Mid-Holocene (6-5.5 ka BP) and Late-Holocene (1-0.5 ka BP) differences in ECHAM slo43 transient simulation. Precipitation (a), Temperature (b) and Sea level (c) pressure at annual scale. Precipitation (d), Temperature (e) and Sea level (f) pressure at summer scale. Precipitation (g), Temperature (h) and Sea level (f) pressure at winter scale.

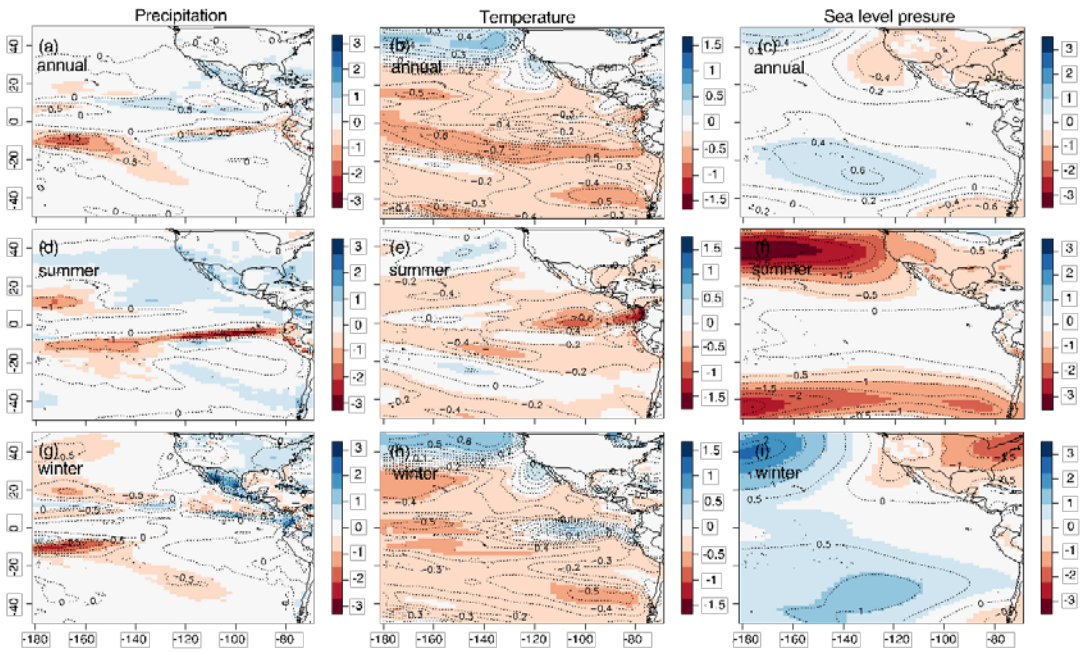

Figure 8. Mid-Holocene (6-5.5 ka BP) and Late-Holocene (1-0.5 ka BP) differences in IPSL TR6V transient simulation. Precipitation (a), Temperature (b) and Sea level (c) pressure at annual scale. Precipitation (d), Temperature (e) and Sea level (f) pressure at summer scale. Precipitation (g), Temperature (h) and Sea level (f) pressure at winter scale.

The cooling (0-0.5ºC) during austral winter and austral summer in the Peruvian margin recorded in both transient simulations (Fig. 7 and 8) is small but consistent with the mean annual cooling (1- 4ºC) recorded on fossil mollusk (Carré et al., 2012) and with the summer-spring cooling (0-2ºC) based on alkenones from marine core in the southern Peruvian margin (Salvatteci et al., 2019). The SST maps from both models (Fig. 7 and 8) show that the MH cooling is widespread in this region of the Pacific Ocean in both austral summer and austral winter except for the cold tongue of the eastern equatorial Pacific which is colder in austral summer and warmer in austral winter. The MH cooling of the southern hemisphere in austral summer is consistent with a decrease in insolation during this period due to orbital precession. On the other hand, in the austral winter, insolation was higher during the MH and the observed cooling must therefore be due to a reorganization of the large-scale circulation of the South East Pacific. The MH increase in insolation during the austral winter is less pronounced at high latitudes because there the daily insolation duration is shorter in this season. The fact that the Equatorial Pacific cold tongue is warmer while the South East Pacific temperatures are colder (Fig. 7 and 8) increases the meridional temperature gradient which reinforces the SPSH.

The difference in the magnitude of the cooling between the proxies and the transient simulations suggests that the models do not adequately reproduce the coastal upwelling at the Peruvian margin. This may be due to the large-scale simulation of atmospheric or/and oceanic

circulation or to regional problems (simulation of near-coastal wind and/or of water circulation in the upwelling). At a local-scale, changes in the land-ocean (Bakun, 1990) and alongshore pressure gradient (Chamorro et al., 2021) have been proposed as a mechanism that may impacts near-coastal wind in the PUS. The use of high-resolution regional model forced by GCM simulations probably may compensate this bias.

4.4.4. Proxy-derived perspective for future climate

In the context of global warming, the findings of this work together with previous studies (Carré et al., 2012; Briceño-Zuluaga et al., 2016; Salvatteci et al., 2019; Yseki et al., 2022) suggest that during warm (cold) periods in the northern hemisphere occurred an intensification (weakening) of winds and coastal upwelling in PUS in response to a northern (southern) shift of the ITCZ-SPSH system and an intensification (weakening) of the Walker circulation at centennial to millennial scale. Although there are uncertainties about the effects of current global warming on ITCZ, a future narrowing seems a robust projection with climate change (Byrne and Schneider, 2016). Conversely, changes in the position of the ITCZ in the models is unclear due to model biases. Indeed, multimodel mean indicate a zero zonal-mean shift of the ITCZ (McFlarne and Frierson, 2017). A recent study, based on projections from 27 state-of-the-art climate models that explores the changes in the location of the ITCZ in different longitudinal sectors, shows a robust southward shift in the eastern Pacific in response to the SSP3-7.0 scenario by 2100 (Mamalakis et al., 2021). In a possible future scenario where a southern shift of the ITCZ in the eastern Pacific occurs, paleo-records suggest a possible weakening of wind and upwelling. The latter may negatively affect biological productivity.

4.5. Conclusion

Similar to previous work in the PUS, we identify four granulometric end-members (EM) at 17ºS during the Holocene. We propose that variations in the contribution of fine (EM1) and coarse (EM2, EM3 and EM4) particles mainly reflect changes in fluvial and aeolian inputs, respectively. Our results suggest an increase in aeolian inputs linked to stronger wind during the MH and support the hypothesis that the cooling in the study area occurred due to an increase in upwelling during the MH. The enhanced upwelling-favorable wind at 17ºS could be explained by a northern displacement of the ITCZ-SPSH system. Although there remains uncertainty about the effects of current climate change on wind and upwelling dynamics in

PUS, our results and previous studies suggest a northern (southern) shift of the ITCZ-SPSH system may generate an intensification (weakening) of wind and upwelling in PUS at different times-scale.

4.6. References

Bakun, A., 1990. Global climate change and intensification of coastal ocean upwelling. Science, 247(4939), pp.198-201.

Berger, A., 1978. Long-term variations of daily insolation and Quaternary climatic changes. Journal of Atmospheric Sciences, 35(12), pp.2362-2367.

Beuscher, S., Krüger, S., Ehrmann, W., Schmiedl, G., Milker, Y., Arz, H. and Schulz, H., 2017. End-member modelling as a tool for climate reconstruction—an Eastern Mediterranean case study. Plos one, 12(9), p.e0185136.

Braconnot, P., Otto-Bliesner, B., Harrison, S., Joussaume, S., Peterchmitt, J.Y., Abe-Ouchi, A., Crucifix, M., Driesschaert, E., Fichefet, T., Hewitt, C.D. and Kageyama, M., 2007. Results of PMIP2 coupled simulations of the Mid-Holocene and Last Glacial Maximum–Part 2: feedbacks with emphasis on the location of the ITCZ and mid-and high latitudes heat budget. Climate of the Past, 3(2), pp.279-296.

Braconnot, P., Zhu, D., Marti, O. and Servonnat, J., 2019. Strengths and challenges for transient Mid-to Late Holocene simulations with dynamical vegetation. Climate of the Past, 15(3), pp.997-1024.

Briceño-Zuluaga, F.J., Sifeddine, A., Caquineau, S., Cardich, J., Salvatteci, R., Gutierrez, D., Ortlieb, L., Velazco, F., Boucher, H. and Machado, C., 2016. Terrigenous material supply to the Peruvian central continental shelf (Pisco, 14° S) during the last 1000 years: paleoclimatic implications. Climate of the Past, 12(3), pp.787-798.

Briceño-Zuluaga, F., Castagna, A., Rutllant, J.A., Flores-Aqueveque, V., Caquineau, S., Sifeddine, A., Velazco, F., Gutierrez, D. and Cardich, J., 2017. Paracas dust storms: sources, trajectories and associated meteorological conditions. Atmospheric Environment, 165, pp.99-110.

Carré, M., Azzoug, M., Bentaleb, I., Chase, B.M., Fontugne, M., Jackson, D., Ledru, M.P., Maldonado, A., Sachs, J.P. and Schauer, A.J., 2012. Mid-Holocene mean climate in the south eastern Pacific and its influence on South America. Quaternary International, 253, pp.55-66.

Chamorro, A., Echevin, V., Colas, F., Oerder, V., Tam, J. and Quispe-Ccalluari, C., 2018. Mechanisms of the intensification of the upwelling-favorable winds during El Niño 1997–1998 in the Peruvian upwelling system. Climate Dynamics, 51(9), pp.3717-3733.

Chamorro, A., Echevin, V., Dutheil, C., Tam, J., Gutiérrez, D. and Colas, F., 2021. Projection of upwelling-favorable winds in the Peruvian upwelling system under the RCP8. 5 scenario using a high-resolution regional model. Climate Dynamics, 57(1), pp.1-16.

Chavez, F.P., Bertrand, A., Guevara-Carrasco, R., Soler, P. and Csirke, J., 2008. The northern Humboldt Current System: Brief history, present status and a view towards the future. Progress in Oceanography, 79(2-4), pp.95-105.

Dallmeyer, A., Claussen, M., Lorenz, S.J. and Shanahan, T., 2020. The end of the African humid period as seen by a transient comprehensive Earth system model simulation of the last 8000 years. Climate of the Past, 16(1), pp.117-140.

Dufresne, J.L., Foujols, M.A., Denvil, S., Caubel, A., Marti, O., Aumont, O., Balkanski, Y., Bekki, S., Bellenger, H., Benshila, R. and Bony, S., 2013. Climate change projections using

the IPSL-CM5 Earth System Model: from CMIP3 to CMIP5. Climate dynamics, 40(9), pp.2123-2165.

Fischer, H., Meissner, K.J., Mix, A.C., Abram, N.J., Austermann, J., Brovkin, V., Capron, E., Colombaroli, D., Daniau, A.L., Dyez, K.A. and Felis, T., 2018. Palaeoclimate constraints on the impact of 2◦ C anthropogenic warming and beyond, Nat. Geosci., 11, 474–485.

Gutiérrez, D., Bouloubassi, I., Sifeddine, A., Purca, S., Goubanova, K., Graco, M., Field, D., Méjanelle, L., Velazco, F., Lorre, A. and Salvatteci, R., 2011. Coastal cooling and increased productivity in the main upwelling zone off Peru since the mid-twentieth century. Geophysical Research Letters, 38(7).

Haug, G.H., Hughen, K.A., Sigman, D.M., Peterson, L.C. and Rohl, U., 2001. Southward migration of the intertropical convergence zone through the Holocene. Science, 293(5533), pp.1304-1308.

Humphries, M.S., Benitez-Nelson, C.R., Bizimis, M. and Finch, J.M., 2017. An aeolian sediment reconstruction of regional wind intensity and links to larger scale climate variability since the last deglaciation from the east coast of southern Africa. Global and Planetary Change, 156, pp.59-67.

Karstensen, J., & Ulloa, O., 2009. Peru-Chile current system. In J. H. Steele, S. A. Thorpe, & K. K. Turekian (Eds.), Ocean currents (2nd ed., pp. 385–392). London: Academic Press.

Kassambara, A. and Mundt, F., 2017. . Extract and visualize the results of multivariate data analyses, 76.

Kaufman, D.S., Ager, T.A., Anderson, N.J., Anderson, P.M., Andrews, J.T., Bartlein, P.J., Brubaker, L.B., Coats, L.L., Cwynar, L.C., Duvall, M.L. and Dyke, A.S., 2004. Holocene thermal maximum in the western Arctic (0–180 W). Quaternary Science Reviews, 23(5-6), pp.529-560.

Kaufman, D., McKay, N., Routson, C., Erb, M., Dätwyler, C., Sommer, P.S., Heiri, O. and Davis, B., 2020. Holocene global mean surface temperature, a multi-method reconstruction approach. Scientific data, 7(1), pp.1-13.

Koutavas, A. and Joanides, S., 2012. El Niño–Southern oscillation extrema in the holocene and last glacial maximum. Paleoceanography, 27(4).

Koutavas, A., Demenocal, P.B., Olive, G.C. and Lynch-Stieglitz, J., 2006. Mid-Holocene El Niño–Southern Oscillation (ENSO) attenuation revealed by individual foraminifera in eastern tropical Pacific sediments. Geology, 34(12), pp.993-996.

Mamalakis, A., Randerson, J.T., Yu, J.Y., Pritchard, M.S., Magnusdottir, G., Smyth, P., Levine, P.A., Yu, S. and Foufoula-Georgiou, E., 2021. Zonally contrasting shifts of the tropical rain belt in response to climate change. Nature climate change, 11(2), pp.143-151.

McFarlane, A.A. and Frierson, D.M., 2017. The role of ocean fluxes and radiative forcings in determining tropical rainfall shifts in RCP8. 5 simulations. Geophysical Research Letters, 44(16), pp.8656-8664.

McGee, D., Donohoe, A., Marshall, J. and Ferreira, D., 2014. Changes in ITCZ location and cross-equatorial heat transport at the Last Glacial Maximum, Heinrich Stadial 1, and the mid-Holocene. Earth and Planetary Science Letters, 390, pp.69-79.

Otto-Bliesner, B.L., Braconnot, P., Harrison, S.P., Lunt, D.J., Abe-Ouchi, A., Albani, S., Bartlein, P.J., Capron, E., Carlson, A.E., Dutton, A. and Fischer, H., 2017. The PMIP4 contribution to CMIP6–Part 2: Two interglacials, scientific objective and experimental design for Holocene and Last Interglacial simulations. Geoscientific Model Development, 10(11), pp.3979-4003.

Paterson, G.A. and Heslop, D., 2015. New methods for unmixing sediment grain size data. Geochemistry, Geophysics, Geosystems, 16(12), pp.4494-4506.

Pennington, J.T., Mahoney, K.L., Kuwahara, V.S., Kolber, D.D., Calienes, R. and Chavez, F.P., 2006. Primary production in the eastern tropical Pacific: A review. Progress in oceanography, 69(2-4), pp.285-317.

Renssen, H., Seppä, H., Crosta, X., Goosse, H. and Roche, D.M., 2012. Global characterization of the Holocene thermal maximum. Quaternary Science Reviews, 48, pp.7-19.

Salvatteci, R., Gutiérrez, D., Field, D., Sifeddine, A., Ortlieb, L., Bouloubassi, I., Boussafir, M., Boucher, H. and Cetin, F., 2014. The response of the Peruvian Upwelling Ecosystem to centennial-scale global change during the last two millennia. Climate of the Past, 10(2), pp.715-731.

Salvatteci, R., Schneider, R.R., Blanz, T. and Mollier-Vogel, E., 2019. Deglacial to Holocene ocean temperatures in the Humboldt Current System as indicated by alkenone paleothermometry. Geophysical Research Letters, 46(1), pp.281-292.

Scheidegger, K.F. and Krissek, L.A., 1982. Dispersal and deposition of eolian and fluvial sediments off Peru and northern Chile. Geological Society of America Bulletin, 93(2), pp.150-162.

Strub, P. T., Mesias, J. M., Montecino, V., Rutllant, J., & Salinas, S., 1998. Coastal ocean circulation off Western South America. Coastal segment (6,E). In A. Robinson & K. Brink (Eds.), The sea (Vol. 11, pp. 273–313). New York: John Wiley & Sons, Inc.

Wanner, H., Beer, J., Bütikofer, J., Crowley, T.J., Cubasch, U., Flückiger, J., Goosse, H., Grosjean, M., Joos, F., Kaplan, J.O. and Küttel, M., 2008. Mid-to Late Holocene climate change: an overview. Quaternary Science Reviews, 27(19-20), pp.1791-1828.

Yseki, M., Turcq, B., Caquineau, S., Salvatteci, R., Solis, J., Skilbeck, C.G. and Gutiérrez, D., 2022. Millennial variability of terrigenous transport to the central-southern Peruvian margin during the last deglaciation (18–13 kyr BP). Climate of the Past Discussions, pp.1-24.

5. Conclusions and Perspectives

5.1. Conclusions

How the precipitation, wind and upwelling dynamics in Peruvian Upwelling Systems would respond to climate change is uncertain. Paleoceanographic studies allow to estimate the influence of past climate variations and provide a better understanding of the mechanisms involved, favoring a better assessment of future changes. The Peruvian margin is a region with favorable conditions for the preservation of paleoceanographic records and the last deglaciation (18-11 kyr BP) and Mid-Holocene (8-4 kyr BP) offer natural experimental conditions to observe the behavior of precipitation and wind dynamic in Peruvian Upwelling System in a context of global warming.

The grain-size distribution of Peruvian margin sediments is typically polymodal and for that reason provides information on sediment transport mechanisms and/or sediment sources. In this work, the variability of fluvial and aeolian inputs during the last deglaciation and the Holocene was reconstructed in order to infer changes in precipitation and wind dynamics respectively. Grain-size distribution analysis was performed on marine cores extracted in Callao, 12ºS; Pisco, 14ºS and Ilo, 17ºS. In addition, the end-member analysis (EMA) was performed to deconvolve grain-size distribution into sub-populations corresponding to different sources and transport of terrigenous material. Using this methodology allows us to discriminate the different sources of terrigenous input, reconstructing the variations of fluvial and aeolian inputs dependent on changes in precipitation and wind intensity.

Our results indicate that the variability of the grain-size distribution and grain-size end-member of marine sediments from the central-southern Peruvian margin (12ºS, 14ºS and 17ºS) reveals millennial-scale changes in the transport and sedimentation processes of the terrigenous material during the last deglaciation and the Holocene. However, in order to assign a process or source to each end-member (EM), it is necessary to contemplate the regional context.

In the case of the Pisco and Ilo core, located within the range of the aeolian inputs, as it has been shown earlier, that variations in the contribution of fine (EM1, 11 μm) and coarse (EM2, 57 μm; EM3, 87 μm and EM4, 110 μm) particles mainly reflect changes in fluvial and aeolian inputs, respectively. In the case of Callao core, located further from the coast and where sources of aeolian particles are scarce, we propose that changes in EM4 (101 μm) and EM2 (58

μm) contribution mainly reflect hydrodynamic energy and diffuse sources, respectively, while EM3 (77 um) and EM1 (11 μm) variations reflect changes in aeolian and fluvial inputs, respectively. These results show that particle size analysis and the End Member method cannot be used as a ready-made rule, but requires an interpretation that takes into account the local conditions of the sedimentary deposit.

In this sense, it is useful to be able to use different proxies. In Callao and Pisco we show that the X-ray fluorescence (XRF) of Titanium shows a very good correlation between the two sites. Titanium is relatively immobile during chemical weathering and is present in soils in the form of Titanium oxides often associated with clays. Titanium XRF marks fluvial inputs because the fluvial deposit layers are finer, richer in Titanium and also probably less porous and less rich in organic matter than the rest of the sedimentation. At Callao, we found a good relationship between grain size and XRF Ti/Zr ratio. Using a ratio of XRF values can compensate for the effect of variations in density, porosity, organic matter content. We did not use it in Callao and Pisco because the calculation of this index introduces noise while our objective was to calculate the high-resolution variability.

During the last deglaciation, our results support a tight relationship between high latitude forcing and precipitation in the western flank of the Andes. During late Heinrich Stadial 1 (16-15 kyr BP), enhanced fluvial inputs in Callao and Pisco occurred associated with higher precipitation in Central Andes, Titicaca Lake reached its highest level at that time. This increase in precipitation has been attributed in the literature to a southerly position of the ITCZ in tropical Atlantic, to the slowdown of Atlantic Meridional Overturning Circulation associated with meltwater discharge in North Atlantic and/or to the warming of East Equatorial Pacific. These paleoclimatic situations are indeed observed in these three regions during HS1 but the mechanism of teleconnection with Central Andes precipitation is not yet well understood.

An increase of aeolian input has been observed during Bølling-Allerød. It could be the result of stronger alongshore winds linked to a northern displacement of the Intertropical Convergence Zone-South Pacific Subtropical High system in response to a stronger intensity of Walker circulation.

During the Holocene, our results suggest an increase in aeolian inputs linked to stronger wind during the Mid-Holocene until 5,5 kyr BP and support the hypothesis that the cooling observed at this time in the study area occurred due to an increase in upwelling. Comparison

with two Holocene transient simulations from IPSL and MPI models show that both models reproduce a decrease in winter wind since 5 kyr BP. The cooling (0-0.5ºC) during austral winter and austral summer in the Peruvian margin recorded in both transient is consistent with the mean annual cooling (1-4ºC) recorded on fossil mollusk and with the summer-spring cooling (0-2ºC) based on alkenones from marine core in the southern Peruvian margin. However, the difference in the magnitude of the cooling between the proxies and the transient simulations suggests that the models do not adequately reproduce the coastal upwelling at the Peruvian margin. At a local-scale, changes in the land-ocean and alongshore pressure gradient have been proposed as a mechanism that may impacts near-coastal wind in the PUS, and the use of high-resolution regional model forced by GCM simulations can probably better reproduce the PUS.

Given the limitations of the models, in particular their difficulty in reproducing the complex atmospheric circulation in the Eastern Equatorial Pacific region, with in this case a very marked double ITCZ, we can however estimate from our data and the simulations of the two transient models IPSL and MPI that the increase in winds in the study area (17ºS) during the winters can be linked to a northern displacement of the Intertropical Convergence Zone-South Pacific Subtropical High system.

The Holocene study also show a strong millennial variability of the proxies of aeolian vs fluvial sources. Records of interannual variability based on ∂^{18}O and Sr/Ca of corals and bivalves in tropical eastern and central Pacific also evidenced a strong millennial variability and, notably, a period of ENSO minimum that culminates between 5 and 4 kyr BP. This corresponds, in our record, to a minimum of sand grain from eolian source. This high millennial wind variability observed in our data is not so well marked in the simulations which rather show a gradual increase in winds since 5 kyr BP. Therefore, we have, at the moment, no clue to explain the relationship between the low inter-annual variability of the equatorial Pacific and the low intensity of coastal winds in Peru during the interval 5-4 kyr BP.

Although there remains uncertainty about the effects of current climate change on wind and upwelling dynamics in Peruvian Upwelling System, our results and previous studies suggest that a northern (southern) shift of the Intertropical Convergence Zone-South Pacific Subtropical High system may generate an intensification (weakening) of upwelling-favorable wind and upwelling in Peruvian Upwelling System at different times-scale. Concerning to precipitation, there is evidence of a slowing of the Atlantic Meridional Overturning Circulation

over the past century and in future climate model simulations. In the latter, the decline in Atlantic Meridional Overturning Circulation is accompanied by a southward shift in the Intertropical Convergence Zone. Thus, we can probably expect an increase in precipitation and river flow in the future in Peru. In a possible future scenario where a southern shift of the ITCZ in the eastern Pacific occurs, paleo-records also suggest a possible weakening of winds and upwelling. The latter may negatively affect biological productivity.

Since the El Niño-Southern Oscillation is the main mode of interannual climate variability in the world and that during El Niño events occur strong thunderstorms and precipitation on the coast of Peru, how the El Niño-Southern Oscillation variability would respond to climate change is of great interest to a wide range of scientists and stakeholders.

In this work, interannual variability of fluvial discharge derived from high-resolution X-ray fluorescence Titanium (Ti-XRF) counts in two marine sediment cores collected on the Peruvian margin (Callao and Pisco) was reconstruct during the last deglaciation and part of the Late Holocene. Since Titanium is related to river discharge and El Niño-Southern Oscillation is the primary driver of interannual variability of rainfall in Peru, on the coast as well as in the Andes, the 2.5-8 year frequency band of Ti-XRF in Pisco and Callao sediment cores provide us with an unprecedented 4000-year long record of El Niño-Southern Oscillation -related rainfall interannual variability during the last deglaciation.

Our results suggest a strong similarity in the variations of Ti-XRF in Callao and Pisco during the last deglaciation and more importantly, the amplitude of Ti-XRF interannual variability varies coherently on millennial timescales in both sites. The regional scale reproducibility of the records demonstrates that the dataset is not affected by analytic or local biases and that Ti-XRF variations faithfully reflect regional scale climate variability. Our paleo-El Niño-Southern Oscillation record shows a large and significant increase in the amplitude of El Niño-Southern Oscillation during the last deglaciation than Late Holocene that supports the hypothesis that ice-sheet melting strengthens El Niño-Southern Oscillation activity. Our analysis of TraCE-21ka meltwater flux experiment SST also indicate an increase in ENSO variability during periods of meltwater flux, but this increase is represented by peaks of very limited amplitude and there is relatively little difference between the deglaciation period and the Holocene in contrast to what the data show. This result is of particular importance because our record suggests that the sensitivity of El Niño-Southern Oscillation to meltwater discharge

is stronger than indicated by climate models, pointing to an underestimated strengthening with future ice sheet melting in a greenhouse climate.

5.2. Perspectives

In this work, the variability of fluvial and aeolian inputs dependent of precipitation and upwelling-favorable wind was reconstructed using grain-size distribution and end-member analysis in marine sediments cores. In addition, each grain-size end-member was used as a proxy for the source of terrigenous material. The results obtained in this work should be complemented with the use of other proxies of source/process of terrigenous material (e.g., neodymium and strontium isotopic analysis, mineralogical analysis and microscopic methods). In addition, to better understand how upwelling-favorable wind and upwelling dynamics in the Peruvian Upwelling System would respond to climate change, more paleo-wind records during key periods of global warming (e.g., MIS5e) are needed.

Our results show that the use of high-resolution XRF in laminated sediments allows reconstructing the interannual variability of fluvial discharges dependent on precipitation in the Peruvian margin and to infer El Niño-Southern Oscillation. Future works should focus on reconstructing centennial-millennial changes in El Niño-Southern Oscillation activity during periods of global warming such as MIS5e or the Mid-Holocene.

The use of global climate models and transient simulations provides insight into the mechanisms and forcings associated with upwelling dynamic variability during the past in the Peruvian Upwelling System. However, global climate models do not seem to be able to truly reproduce the winds and upwelling near the coast. In order to evaluate the impact of climate change on the upwelling-favorable winds during the past, it is probably necessary to use high resolution regional models to downscale the global climate models.

The main still open questions are:

Our study shows that, in the past, the western slope of central Andes can be an important source of sediment for the central-southern Peruvian margin. To confirm this hypothesis, it is necessary to better identify the sources of sediment to understand which regions of Peru have been (and will be) affected by these intense rainfall events and how this have change with time.

The dynamics of transport on the Peruvian continental margin is also poorly known. The Peru-Chile Under Current (PCUC), very active on the external shelf and high slope, is generally

considered to be the primary factor in the distribution of sediments, but little is known about the effect of storms, eddies and internal waves.

Another very important factor, difficult to appreciate in palaeoclimatological studies, is the seasonality of processes. For example, in this study, the strengthening of the wind observed in the Holocene, would be, according to the models, a strengthening of the winter wind. We can thus imagine the simultaneous existence of windy winters and rainy summers. This applies to all processes controlling sedimentation: transport, productivity etc. New approaches, which would involve more joint analysis of data and models, are probably needed for a better interpretation of this temporality.

This study highlights the existence of a natural millennial variability of climate in the eastern Pacific. This variability has also been observed in the amplitude of the ENSO. It also exists in the Atlantic Ocean (Bond cycles) where it is attributed to a variability of the AMOC. But in the Pacific Ocean its causes are not well known. This variability is not well described by current climate models and may change the trajectories of future climate forecasts. This is an important research topic that must combine climate reconstruction and modeling

Résumé:
La reconstruction des précipitations et des vents à partir des archives géologiques pourrait aider à comprendre les changements potentiels de la dynamique des précipitations et des vents en réponse au changement climatique au Pérou. Les objectifs de cette thèse étaient : 1) Reconstruire la variabilité millénaire des apports fluviaux et éoliens et déduire les changements des précipitations et des vents de surface au Pérou pendant la dernière déglaciation. 2) Reconstituer la variabilité interannuelle des débits fluviaux dépendant des précipitations et déduire la variabilité d'ENSO pendant la dernière déglaciation et 3) Reconstituer la variabilité millénaire des apports éoliens dépendant du vent de surface pendant l'Holocène. Dans ce but, la distribution granulométrique et l'analyse des membres finaux ont été utilisées pour déduire les sources de matériaux terrigènes. En outre, la concentration en titane obtenue par XRF à haute résolution a été utilisée pour déduire la variabilité ENSO. Pendant la dernière déglaciation, nos résultats suggèrent que les variations du débit fluvial dans la marge occidentale de la déglaciation de l'Amérique du Sud étaient sensibles à la circulation méridienne de retournement de l'Atlantique sur des échelles de temps millénaires. En outre, nous constatons que l'amplitude des événements ENSO était de 50 à 190 % plus importante pendant la déglaciation par rapport à l'Holocène tardif, ce qui soutient l'hypothèse selon laquelle l'ENSO dans le Pacifique oriental est renforcé par l'écoulement des eaux de fonte des calottes glaciaires. En ce qui concerne le vent de surface, au cours de l'Holocène, nos résultats suggèrent une augmentation des apports éoliens liée à un vent de surface plus fort au cours de l'Holocène moyen. Bien que les effets du changement climatique actuel sur la dynamique des vents et des remontées d'eau dans le système péruvien d'upwelling restent incertains, nos résultats et les études précédentes suggèrent qu'un déplacement vers le nord (sud) du système de la zone de convergence intertropicale et de l'anticyclone subtropical du Pacifique Sud peut générer une intensification (affaiblissement) des vents favorables aux remontées d'eau et des remontées d'eau dans le système péruvien d'upwelling à différentes échelles de temps.

Mots clés: Paléoclimatologie, Système d'Upwelling Péruvien, vent côtier, précipitations, ENSO, Heirch Stadial I.

Paleoclimatic variability and extreme events since the last deglaciation in Peru: sedimentary record and model simulations

Abstract:
Reconstructing precipitation and wind from the geological record could help to understand the potential changes in precipitation and wind dynamics in response to climate change in Peru. The objectives of this thesis were: 1) To reconstruct the millennial variability of fluvial and aeolian inputs and to infer changes in precipitation and surface wind in Peru during the last deglaciation. 2) Reconstruct the interannual variability of precipitation-dependent fluvial discharges and infer the variability of ENSO during the last deglaciation and 3) Reconstruct the millennial variability of aeolian inputs dependent of surface wind during the Holocene. For this purpose, grain-size distribution and end-member analysis were used to infer the sources of terrigenous material. In addition, the titanium concentration obtained by high-resolution XRF was used to infer ENSO variability. During the last deglaciation, our results suggest that variations in river discharge in the western margin of South America deglaciation were sensitive to Atlantic Meridional Overturning Circulation on millennial timescales. In addition, we find that the amplitude of ENSO events was 50 to 190 % larger during the deglaciation compared to the Late Holocene, which supports the hypothesis that ENSO in the Eastern Pacific is strengthened by ice sheet meltwater discharge. Concerning to surface wind, during the Holocene, our results suggest an increase in aeolian inputs linked to stronger surface wind during the Mid-Holocene. Although there remains uncertainty about the effects of current climate change on wind and upwelling dynamics in Peruvian Upwelling System, our results and previous studies suggest that a northern (southern) shift of the Intertropical Convergence Zone-South Pacific Subtropical High system may generate an intensification (weakening) of upwelling-favorable wind and upwelling in Peruvian Upwelling System at different times-scale.

Marco Yseki – Thèse de doctorat - 2022

Keywords: [Paleoclimatology, Peruvian Upwelling System, wind, precipitation, ENSO]